UNIVERSITÀ DEGLI STUDI DI MILANO

Dipartimento di Scienze Farmacologiche e Biomolecolari

CORSO DI DOTTORATO IN

Scienze Endocrinologiche e Metaboliche
Ciclo XXVIII

TESI DI DOTTORATO DI RICERCA

PROTEIN MISFOLDING IN KENNEDY'S DISEASES AND IN RELATED MOTOR NEURON DISEASES (MNDs)

Settori disciplinari: BIO/09, BIO/13, MED/13

DOTTORANDO: Dott. Riccardo M. Cristofani

Matricola: R10035

TUTOR: Chiar. mo Prof. Angelo Poletti

COORDINATORE DEL DOTTORATO: Chiar. mo Prof. Angelo Poletti

A.A. 2014/2015

TABLE OF CONTENTS

ABSTRACT **5**

INTRODUCTION **9**

Spinal and bulbar muscular atrophy (SBMA) 10

Androgen Receptor 16

Amyotrophic lateral sclerosis (ALS) 21

Superoxide dismutase 1 25

TARDBP 28

FUS 30

OPTN 30

VCP 31

C9ORF72 31

The protein quality control system 34

The chaperones 34

The proteasome 35

Autophagy 37

Misfolded proteins transport 44

AIMS AND OBJECTIVES **47**

MATERIALS AND METHODS **49**

RESULTS **63**

AR expression in quadriceps muscle and spinal cords of SBMA mouse model 64

Autophagic markers in muscle of SBMA male mice 67

Pro-autophagic chaperone and co-chaperone levels in muscle of SBMA male mice 69

Analysis of expression of proteins regulating autophagy in muscle of SBMA male mice 73

Autophagic response in spinal cord of SBMA male mice 75

HSPB8 prodegradative effect on ARpolyQ 77

Dynein silencing effect on NSC34 cells morphology, ARpolyQ aggregates and autophagy 79

Effects of dynein inhibition with EHNA on ARpolyQ clearance 82

Analysis of viability of NSC34 cells treated with EHNA 87

Pro-degradative effect of EHNA on ARpolyQ 89

Treatment with EHNA enhances UPS mediated degradation of misfolded proteins 91

The autophagic response in EHNA treated NSC34 cells 93

The effect of EHNA on chaperone and co-chaperones levels 96

BAG1 mediates ARpolyQ UPS degradation 99

EHNA effects on CMA markers 101

EHNA effects on fALS cell models 103

HSPB8 pro-degradative effect on C9ORF72 ALS cell model 106

EHNA effect on C9ORF72 ALS cell model 110

DISCUSSION **112**

REFERENCES **122**

ABSTRACT

Motor neuron diseases, like spinobulbar muscular atrophy (SBMA) and amyotrophic lateral sclerosis (ALS) are characterized by the presence of inclusions or aggregates of proteinaceous materials. In SBMA, inclusions are formed by testosterone dependent aggregates of mutant androgen receptor (AR) with an elongated polyglutamine tract (ARpolyQ), while in ALS inclusions contain several aggregated proteins including TDP43, ubiquilin, optineurin. Exceptions are familial ALS forms linked to superoxide dismutase 1 (SOD1) mutations, to mutated TDP43 and to C9ORF72 poly-dipeptides (DPRs), in which aggregates are mainly composed of mutant SOD1, mutant TDP43 or DPRs, respectively. In general, protein aggregation is due to generation of aberrant protein conformations (misfolding) combined to a failure, in neuronal cells, of the protein quality control (PQC) system, which may be insufficient to correctly remove the misfolded proteins. In other target tissue, such as the muscles, a different physiological PQC regulation may be helpful to remove misfolded proteins related to MNDs.

The PQC system requires the activities of chaperones, degradative systems ubiquitin-proteasome (UPS) and autophagy. After misfolded protein recognition by chaperones, the dynein motor complex plays a crucial role to efficiently remove these species via autophagy, transporting them to autophagosome and assisting autophagosome-lysosome fusion.

In this thesis, I have investigated the implications of protein misfolding in SBMA and in ALS. Taking advantage of a comparative analysis of misfolded proteins response in skeletal muscle and in spinal cord of SMBA mice, we proved that autophagy is dramatically perturbed in muscles. Indeed, we found the up-regulation of most

autophagic markers (Beclin-1, ATG10, p62/SQSTM1, LC3). In addition, the chaperon small Heat Shock Protein B8 (HSPB8) and its co-chaperone BCL2-Associated Athanogene 3 (BAG3), required for autophagy, were robustly up-regulated together with other specific HSPB8 interactors (HSPB2 and HSPB3). Interestingly, the BAG3:BAG1 ratio, increased in muscle, suggesting preferential misfolded proteins routing to autophagy rather than to proteasome. Misfolded proteins, recognized by HSPB8-BAG3 complex, are actively transport by dynein to MTOC to be inserted in autophagosome and degraded by autophagy,

Then, we analysed the role of dynein mediate transport in the autophagic removal of misfolded proteins. In immortalized motoneuronal NSC34 cells, we found that the reduction of dynein protein levels, obtained using a specific siRNA, resulted in autophagy inhibition and in unexpected testosterone dependent ARpolyQ aggregates reduction. Also, we found that pharmacological dynein inhibition, with erythro-9-(2-Hydroxy-3-nonyl) adenine hydrochloride (EHNA), in NSC34 cells expressing ARpolyQ, mutant SOD1, truncated TDP43 form or C9ORF72 DPRs, induced a great reduction of mutant protein aggregates, even in presence of an autophagy inhibitor (3-MA), but not of a proteasome inhibitor (MG132). By performing fractionation studies we found that EHNA increased the ARpolyQ levels in PBS and Triton-X100 fractions. Surprisingly, we found that ENHA effects were paralleled by an increased expression of BAG1, a co-chaperone which routes misfolded proteins to UPS, but not of BAG3 suggesting the prevalence of UPS functions. Indeed, when dynein activity was blocked, BAG3:BAG1 ratio was decreased, thus in favour of BAG1 expression, suggesting the involvement of the pro-degradative activity of BAG1 on ARpolyQ aggregates.

Collectively, these data show that mutant ARpolyQ induces a potent autophagic response in muscle cells. This may be useful to evaluate the SBMA progression.

In parallel, dynein blockage perturbs autophagy and modifies the response of PQC system to misfolded protein. This results in reduced aggregation of MNDs-related misfolded proteins, a phenomenon that may occurs via an increase in their solubility and the induction of UPS functions.

INTRODUCTION

Motor neuron diseases (MNDs) are a group of young and adult onset neurological disorders characterised by the loss of motor neuron which control essential voluntary muscle activity such as walking, speaking, swallowing and breathing. Motor neuron loss results in muscle weakness and atrophy that, with different progression rate, may lead to death. In MNDs, upper, lower or both motor neurons are affected. In fact, upper motor neurons localized in the brain and lower motor neurons localized in the brain stem and in the spinal cord are closely related in the control of movements. MNDs are classified according to their sporadic or inherited manifestations and to the localization of the neurons involved. In fact, some MNDs are inherited and finely associated with localization of involve neurons, but most MNDs have unknown causes and great differences between disease manifestations. Lower motor neurons are involved in Kennedy's disease, also referred to as spinal and bulbar muscular atrophy (SBMA), as well as in spinal muscular atrophy (SMA) and in progressive muscular atrophy (PMA); upper motor neurons are involved in primary lateral sclerosis (PLS) and in spastic paraplegias; both upper and lower motor neurons are normally affected in amyotrophic lateral sclerosis (ALS) and in progressive bulbar palsy (PBP)(Figlewicz & Orrell, 2003). In this thesis we will be discuss data obtained on the SBMA and ALS.

Spinal and bulbar muscular atrophy (SBMA)

SBMA was described in 1897 by Japanese neurologist, H. Kawahara (Kawahara, 1897), and has been known as Kennedy's disease since 1968, when W. Kennedy reported the clinical details related to the disease (Kennedy et al., 1968). SBMA patients normally show weakness and wasting of the facial, bulbar, and limb muscles, along with sensory

disturbances and endocrinological abnormalities (Katsuno et al., 2012; Parodi & Pennuto, 2011).

SBMA is an X-linked disease caused by abnormal CAG repeat expansion in the first exon of the androgen receptor (AR) gene, localized on chromosome Xq11-12, that is translated in poly-glutamine (polyQ) tract in AR protein. The CAG repeat ranges between 9 and 36 in normal individuals and is over 38 (up to 68) in patients (Grunseich et al., 2014a; La Spada et al., 1991). SBMA was the first to be identified in a series of nine different neurodegenerative diseases in which polyQ elongations in totally unrelated proteins have been identified. In fact, an abnormal polyQ tract is present in the huntingtin protein responsible for Huntington's disease (HD), in the ataxin-1, -2 and -3, in the Cav2.1 P/Q voltage-dependent calcium channel, in ataxin-7 and in TATA-binding protein (TBP) responsible respectively for spinocerebellar ataxia (SCA) type 1, 2, 3, 6, 7 and 17, and in atrophin-1 protein responsible for dentatorubral-pallidoluysian atrophy (DRPLA) (Tab. 1).

Table 1 – Polyglutammine-Associated Diseases, adapted from (Fan et al., 2014)

			Expanded CAG Repeats	
PolyQ Diseases	*Locus*	*Protein*	*Normal*	*Pathological*
SBMA	Xq11–q12	Androgen receptor	6–36	38–68
SCA1	6p23	Ataxin-1	6–39	41–83
SCA2	12q24	Ataxin-2	14–32	34–77
SCA6	19p13	CACNA1A	4–18	21–30
SCA7	3p21–p12	Ataxin-7	7–18	38–200
SCA17	6q27	TBP	25–43	45–63
MJD/SCA3	14q24–q31	Ataxin-3	12–40	62–86
HD	4p16.3	Huntingtin	6–35	36–121
DRPLA	12p13	Atrophin-1	3–38	49–88

polyQ, polyglutamine; SCA, spinocerebellar ataxia; HD, Huntington's disease; MJD, Machado–Joseph disease; DRPLA, dentatorubropallidoluysian atrophy; SBMA, spinal bulbar muscular atrophy; CACNA1A, calcium channel, voltage-dependent, P/Q type, a 1A subunit; TBP, thymine–adenine–thymine–adenine (TATA) box binding protein.

Similar to other polyQ diseases, in SBMA the age at onset of the disease has been inversely linked to the size of the CAG-repeat expansions (Atsuta et al., 2006), usually between 30 and 60 years old, but early nonspecific symptoms, such as tremor and muscle cramps, make it difficult to identify the precise time of onset. Also, SBMA patients may be misdiagnosed with other neuromuscular diseases; altogether the prevalence is 1-2 per 100.000 individuals.

Degeneration of lower motor neurons localized in the anterior horn of the spinal cord and in the brainstem characterizes SBMA. Subsequently, muscles innervated by these neurons are affected and patients show myopathy followed by muscle atrophy (Sorarù et al., 2008; Harding et al., 1982; Kennedy et al., 1968). Dorsal root ganglia (DRG) sensory neurons and cells involved in male reproductive functions are also known to be affected.

Recent data suggest that muscle tissues can be a player in the pathogenesis of SBMA. This evidence modifies the classical view of SBMA as a disease exclusively of the primary motor neuron and indicates that mutant AR plays its toxicity also in the muscle (Lieberman et al., 2014; Cortes et al., 2014). Indeed, skeletal muscle is one of the major targets of androgens and muscle degeneration may not only be a consequence of chronic denervation due to motor neuron loss. Previous studies show that: i) both myogenic and myopathic features are present in muscle biopsies of patients (Sorarù et al., 2008); ii) knock-in mutant AR male mice develop myopathy before the onset of spinal cord pathology (Yu et al., 2006a); iii) over-expression of muscle-specific insulin-like growth factor (IGF-1) or peripheral administration of IGF-1 mitigates SBMA symptoms in transgenic mice (Rinaldi et al., 2012; Palazzolo et al., 2009), supporting a

primary contribution of skeletal muscle in the disease pathogenesis. Moreover, abnormally increased levels of creatine kinase in the serum of SBMA patients are not usually expected when studying a neurogenic-only disorder (Mariotti et al., 2000). Collectively, these results suggest that AR toxicity can occur in muscles before motor neurons and that skeletal muscle structure and function alterations may be cell-autonomous. In conclusion, AR toxicity in skeletal muscles is sufficient to cause disease and lead to the denervation-induced atrophy (Monks et al., 2007). Accordingly, muscle degeneration in SBMA mouse models may be both intrinsic and/or motor neuron-dependent.

Although AR is expressed in other areas of the central nervous system, such as the cortex, cerebellum, hippocampus, hypothalamus and olfactory bulb, AR toxicity mainly affects lower motor neuron functions and targets (Rocchi & Pennuto, 2013; Roselli et al., 1989). The main clinical features are weakness, atrophy and fasciculation. Thus, SBMA progression (Fig. 1) starts from tremor of the hand, first noticed when patients used their hands, for example, when holding a glass. Gradually, SBMA patients noticed muscular weakness, predominantly in the lower extremities, leading to the need of a handrail when climbing stairs. Next, patients became affected by dysarthria, dysphagia and needed to use a walking stick, and subsequently a wheelchair. At the later stages, patients developed pneumonia due to aspiration and required in-hospital care (Atsuta et al., 2006). Therefore, the majority of SBMA patients do not die from motor neuron complications and have a normal life expectancy (Atsuta et al., 2006). Androgen insensitivity typically occurs variably during adolescence with testicular atrophy,

oligospermia/azospermia with reduced fertility and gynecomastia (Battaglia et al., 2003; Nagashima et al., 1988).

SBMA affects only adult males, even if females present subclinical disease manifestations when homozygous; then SBMA is sex dependent and well correlates with testosterone levels. This molecular mechanism is at the basis of the androgen-dependence of the disease and has been studied in mice models of SBMA. With these mice, it was found that male ARpolyQ mice subjected to chemicals or surgical castration ameliorate the disease phenotype, whereas female ARpolyQ mice treated with testosterone show SBMA symptoms and features (Yu et al., 2006a; Chevalier-Larsen et al., 2004; Katsuno et al., 2002).

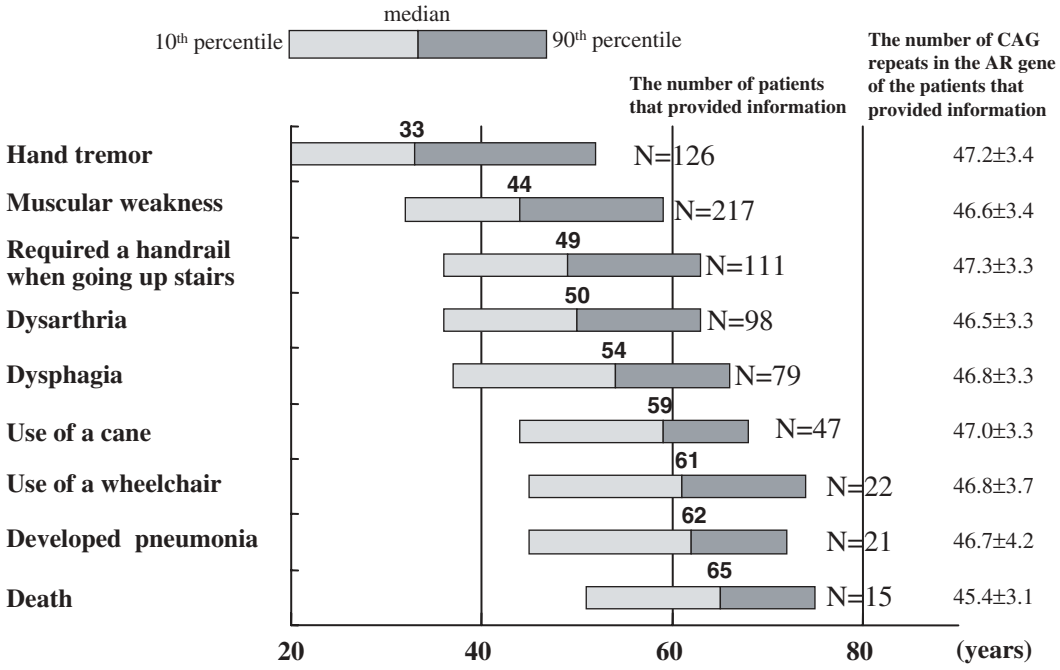

Figure 1 - Age distribution of ADL milestones for 223 SBMA patients. (from Atsuta et al., 2006)

Androgen Receptor

AR is a protein belonging to the nuclear receptor superfamily of transcription factors responsible for the biological actions of androgenic steroids. Like other nuclear receptors, AR is activated by ligand.

The human AR gene (Fig. 2) was cloned in 1988 (Chang et al., 1988; Trapman et al., 1988; Lubahn et al., 1988) and well characterized in the following years. Because AR gene is localized in the X-chromosome, females have two copies of the gene, while males only one, but in the first case one is inactivated by random X-inactivation. AR open reading frame (ORF) is composed by 8 exons encoding for approximately 919 amino acids, organized in different functional domains: i) The N-terminal transactivation domain, encoded by exon 1, contains the polyQ and other amino acid stretches (polyproline (polyP) and polyglycine (polyG) tracts); ii) the highly conserved DNA-binding domain, where exons 2 and 3 encode for two Zinc-fingers; iii) C-terminal ligand binding-domain encoded by exons 4 to 8, that contain the nuclear targeting sequence and the steroid binding domain (Brinkmann, 2001). The N-terminal region is highly polymorphic in polyQ tract and the elongated form is linked to SBMA. PolyQ functions are unknown, but it has been postulated that the Q-rich regions are involved in protein-protein interactions. Also, polyP and polyG tract functions are still unknown. N-term is also responsible of N/C interaction of AR that induces antiparallel AR dimerization. AR dimer protects the ligand in the LBD binding pocket and this results in AR stabilization. Expanded polyQ impairs N-term AR interaction with co-activators and/or other transcriptional components, resulting in mild repression of target gene transcription. Nevertheless, expanded polyQ leads to AR aggregation, and the

consequent reduction of the total amount of receptor protein able to promote transcription. In parallel, a large number of clinical and experimental observations suggest that AR loss-of-function explains only the endocrinological SBMA features (Neuschmid-Kaspar et al., 1996). In fact, in AR endocrine disorders, such as androgen insensitivity syndrome, no neurological signs are present. Instead, in SBMA, expanded ARpolyQ activation leads to motor neuron death, clearly showing the gain of new toxic function. Moreover, SBMA animal models expressing the expanded ARpolyQ showed motor neuron dysfunction even in the presence of the endogenous wild-type receptor. Finally, the expression of expanded ARpolyQ in neuronal cells alters several cell functions, leading to cell death. AR activation and toxicity are mediated by its ligands testosterone (T) and dihydrotestosterone (DHT). Indeed, inactive AR in cytoplasm is associated with the heat shock protein (Hsp) 70, Hsp90 and Hsp40 which maintain the correct protein folding of AR. After ligand interaction, AR is released from the cytoplasmic soluble complex and translocates into the nucleus, where it normally activates the transcription of target genes (Fig. 3).

The polyQ tract alters the structure of AR, which changes from its usual random coil to a parallel β-sheet that leads to a oligomeric fibrils structure, as the first step of aggregation (Wyttenbach, 2004).

The formation of toxic mutant AR oligomers or aggregates activates a series of events that lead to cell degeneration (Jochum et al., 2012; Muchowski & Wacker, 2005; Taylor et al., 2003).

The SBMA histopathological hallmark is the presence of nuclear inclusions containing ARpolyQ in motor neurons and brainstem, as well as in non-neuronal tissues (Yu et al.,

2006a; Li et al., 1998). AR aggregates were also observed in the cytoplasm of sensory neurons where they seem to be associated with axonal degeneration (Suzuki et al., 2008). Although several studies show that inclusions prevent mutant protein toxicity by sequestering them into an aggregate structure that initially contributes to their degradation. Next, accumulation of misfolded proteins seems to play a role in SBMA neurodegeneration (Miller et al., 2011; Rusmini et al., 2007). In fact, the sequestration of molecular chaperones and proteasome subunits suggests that motor neurons are unable to fold and degrade mutant AR, resulting in aggregates accumulation.

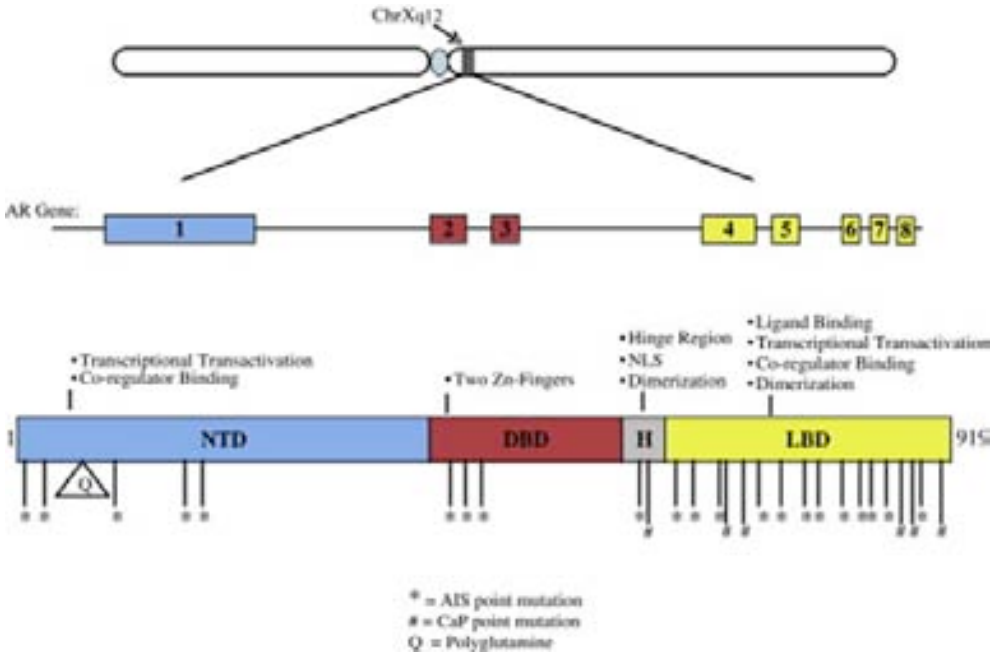

Figure 2 - Schematic representation of AR gene. (from La Spada et al., 2008)

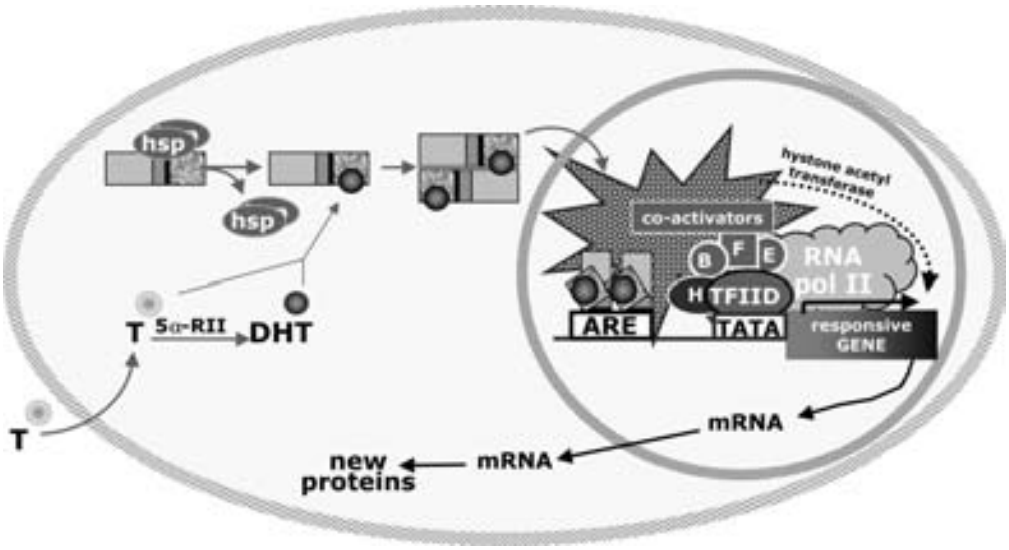

Figure 3 - Mechanism of action of the androgen receptor. (from Poletti, 2004)

Different studies show the different roles of AR aggregates in impairing of neuronal cell functions. Three types of aggregates have been identified because of different localization and functions: cytoplasmic, neuropil and nuclear. i) Cytoplasmic aggregates formed in cell culture are partially soluble, detectable in SDS-PAGE and redistributed in cytoplasm by removing the ligand; this confirms that cells might use aggregates to prevent polyQ toxic functions. ii) In cell culture neuropil aggregates are present in few cells (4-6% of total transfected cells), but they could play an important role in the morphological modification observed in neurites of SBMA cell models. In fact, these aggregates could alter neurite functions by blocking the organelle transport along the microtubules. iii) Nuclear aggregates are typically present in the brain of SBMA patients and in transgenic animals. Usually, in the transfected cell model, only a few neurons present aggregates. Additionally, nuclear inclusions are rare and observed only when a very long polyQ tract (more than 90Q) is present. In nuclear compartment, AR aggregates sequester the steroid receptor co-activator 1 (SRC1) and the CREB-binding protein (CBP) with consequent alteration of transcription. These aggregates are insoluble and are usually detectable in WB since they are retained in staking gel on SDS-PAGE.

It is clear that polyQ tract alters the folding of AR leading to misfolded proteins formation. The cells try to active protective pathway in order to prevent the formation of potentially toxic misfolded species, as well as their accumulation. This protection is exerted mainly by the protein quality control (PQC) system management of misfolded proteins. PQC system could not be sufficient to remove misfolded AR in post-mitotic

cells such as motor neurons, particularly in aged cells were the activity of the PQC is normally decreased.

Amyotrophic lateral sclerosis (ALS)

ALS or Lou Gehrig's disease covers a spectrum of syndromes characterized by motor neurons degeneration described by Jean Matin Charcot in 1869 as a progressive adult onset disease. Most upper and lower motor neurons are involved in this disease, only motor neurons involved in eyes and bladder control are not affected (Majoor-Krakauer et al., 2003). The degeneration of motor neurons leads to loss of ability to initiate and control voluntary movements in the muscle. Patients may lose the ability to speak, eat, move and breathe. ALS progression is uncontrollable and patients die in a few years from early symptoms (3,5 +/-3 years) because of respiratory muscle failure, with great variations in relation to the age of onset (Eisen et al., 1993). Generally, ALS onset age is 60-70 and occurs in western nations with an incidence of 1-2 case every 100.000 people/year and a prevalence of 4-6 patients every 100.000 people. In Italy there are ca. 6.000 patients (25.000 in USA). Young onset of disease is also found. Disease occurs in both sexes with higher prevalence in male (1,5:1 ratio), probably due to hormonal protection in women and a greater exposure among men to supposed risk factors (Orsini et al., 2015; Pasinelli & Brown, 2006).

Neurologists' early studies did not consider the genetic contribution to ALS, but was included after the first description of ALS families. These cases account for approximately 10% of the total ALS incidence and are named familial ALS (fALS). Usually, fALS is inherited as an autosomal dominant mutation. A high number of genes

and mutations have been linked to fALS, and even more (about 100 genes) have been associated with ALS since 2006 (Lattante et al., 2015). These genes were classified for penetrance and risk and considered “major” or “minor” genes if they were particularly related to one geographic cohort. “Major” genes (Fig. 4) responsible for fALS are the Cu/Zn superoxide dismutase-1 (SOD1) gene in 13%, the TAR DNA binding protein (TARDBP) gene in 3%, the fused in sarcoma (FUS) gene in 5% and the C9ORF72 in 30-50% of cases. Other mutations occur in VAMP (vescicle-associated membrane protein)-associatetd protein B (VAPB) gene, sentaxin (SETX) gene, optineurin gene, matrin-3 gene, dynactin gene and others (Johnson et al., 2014; Pokrishevsky et al., 2012; Maruyama et al., 2010; Pasinelli & Brown, 2006). In sporadic ALS (sALS) only few mutations have been identified to contributing to the disease, but recently the C9orf72 exanucleotide expansion has been linked to a great numbers of sALS, fALS and ALS with frontotemporal dementia (FTD) symptoms (named ALS/FTD) (Renton et al., 2011; DeJesus-Hernandez et al., 2011).

The proteins responsible for ALS have very different functions and the type of mutations in the gene sequence are numerous. More than 150 missense mutations have been reported in SOD1 gene and 40 mutations in TARDBP gene (Tortelli et al., 2013; Gendron et al., 2013). These mutations contribute in different ways to ALS; in fact mutations are scattered in wide portion of gene and may exacerbate different ALS type. ALS related proteins have different functions but acquire aberrant conformations (misfolded) that lead to aggregate formation. Otherwise, mutations alter structure and functions of proteins responsible for the misfolded proteins response. In any case, in this condition, the impairment of degradative pathways leads to protein aggregation.

Notably, the C9ORF72 exanucleotide expansion may encode (by a peculiar type of translation (see below)) for long dipeptides (DPRs) (polyGP, polyGA, polyGR, polyPA and polyPR) which may also lead to aggregate formation (Mori et al., 2013).

The presence of misfolded protein species and aggregates is also responsible for other neurodegenerative disorders such as Huntington's, Parkinson's and Alzheimer's diseases.

-

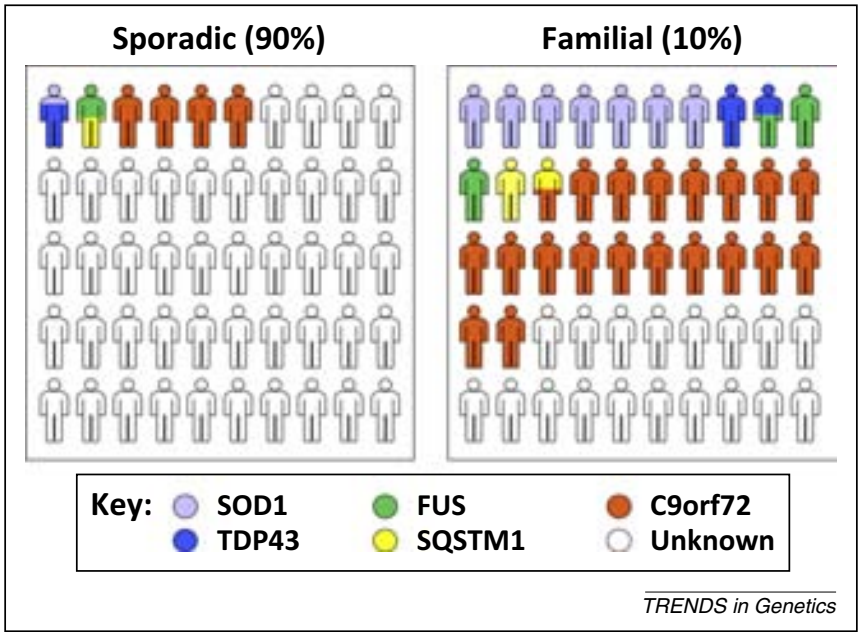

Figure 4 - Major genetic causes in familial and sporadic ALS (from Lattante et al., 2015)

-

Superoxide dismutase 1

SOD1 gene (Fig. 5) is the first fALS gene and was identified by Rosen in 1993 (Rosen et al., 1993). Its discovery offered the first insight into the study of the molecular mechanisms at the basis of ALS. Subsequently to SOD1 identification, many groups produced different ALS models based on different SOD1 mutations, to study the mechanisms and progression of ALS. Most of these models are still widely used.

SOD1 gene is highly conserved during evolution. The protein is *ubiquitously* expressed and may reach 1-2% of the total proteins of central nervous system (Pardo et al., 1994). SOD1 is an antioxidant enzyme localized in cytosol, where it converts superoxide to molecular oxygen and hydrogen, to prevent oxidative damage mediated by oxygen radicals. However, this is not only function of SOD1, in fact yeast studies have shown that less than 1% of total SOD1 is required to exert its primary function, opening the possibility that SOD1 enzyme may play other still unknown, but equally important functions (Reddi & Culotta, 2013; Corson et al., 1998). In parallel, clear evidence has shown that SOD1 loss of function plays a secondary role in disease, but it is clear that in ALS patients SOD1 acquires an undefined new toxic function (Saccon et al., 2013). This is well examined in SOD1-fALS and many functions have been proposed to possibly explain the role of mutated SOD1 in ALS pathology.

The majority of SOD1 mutations destabilize the native protein folding and structure (Shaw & Valentine, 2007; Furukawa & O'Halloran, 2005; Rodriguez et al., 2005) and because of this, mutant SOD1 associates into aggregates. Aggregates of SOD1 have been observed post-mortem in motor neurons of ALS patients and the mutations that increase instability also increase aggregation, which is correlated with a decrease of

survival time (Byström et al., 2010; Wang et al., 2008). SOD1 aggregates are also observed in motor neurons of sALS patients, suggesting that they could be a common ALS feature. Recently, different authors proposed other toxic mechanisms of SOD1 in ALS: a) mutant SOD1 expressing glia cells (astrocytes and microglia) are toxic to motor neurons; b) SOD1 is a zinc sensor able to activate ER stress and mutations in SOD1 resulting in chronic ER stress and ERAD dysfunction; c) mutant SOD1 may results in abnormal autophagy; d) SOD1 can be a transcription factor and regulate transcription; e) SOD1 can bind mRNAs and play a role in their stabilization; f) SOD1 can be considered as a signalling molecule able to integrate signals from oxygen and glucose (reviewed by Bunton-Stasyshyn et al., 2014).

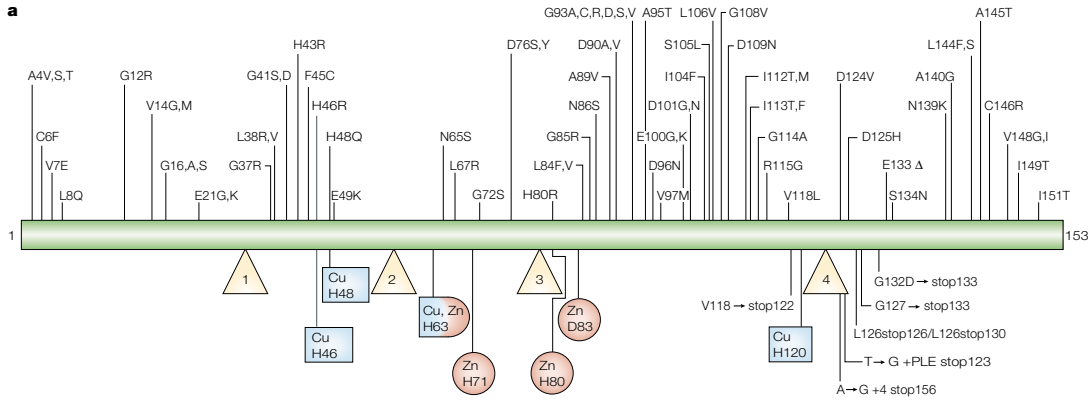

Figure 5 - Schematic representation of mutations in the SOD1 gene

TARDBP

TARDBP gene (Fig. 6) was identified in 2006 by two groups that observed the TDP-43 protein (encoded by TARDBP gene) in ubiquitinated neuronal cytoplasmic inclusions of sALS and fALS patients (Arai et al., 2006; Neumann et al., 2006). Almost all mutations are localized in the C-terminal glycine-rich region and are responsible for the presence of a classical ALS phenotype, which however, can be sometime associated with dementia. TDP-43 is an RNA-binding protein involved in microRNA biogenesis, pre-mRNA splicing and stability of mRNA (Iguchi et al., 2013). TDP-43 normally localizes into the nuclei, but in TDP-43 pathology is redistributed in cytoplasm and forms aggregates in affected neuronal and glial cells (Arai et al., 2006; Neumann et al., 2006). Also, animal models overexpressing wild type or mutated TDP-43 clearly develop spastic paralysis and neuronal inclusions, characteristic of ALS. Interestingly, not only the described single point mutations have been associated with ALS but also the characteristic 25-kDa C-terminal fragment (CTFs) was observed to be correlated with disease development and progression (Swarup & Julien, 2011; Wils et al., 2010; Wegorzewska et al., 2009).

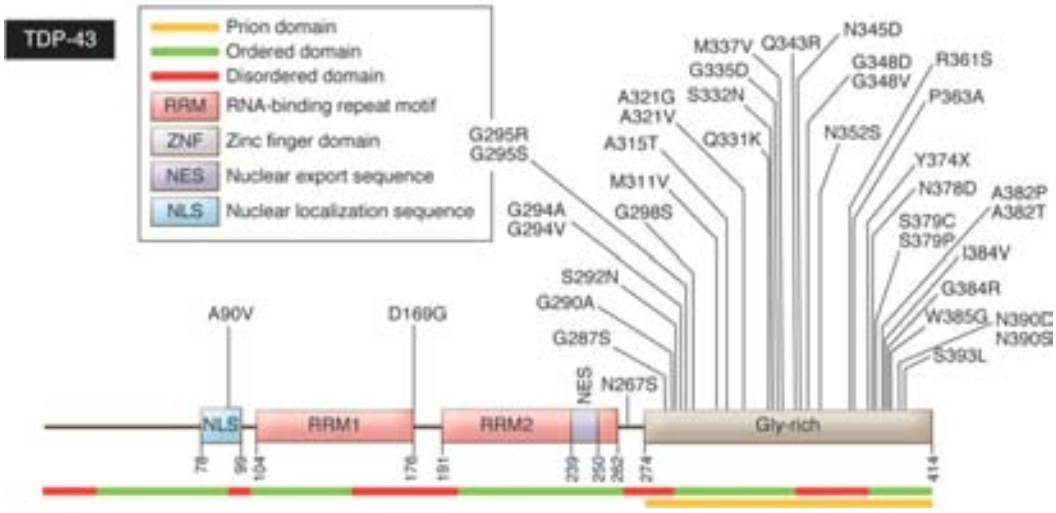

Figure *6* - Schematic *representation of mutations in the TDP-43* gene

FUS

FUS gene mutations responsible for 4% of fALS were identified in 2009 by Kwiatkowski et al. (Kwiatkowski et al., 2009). FUS mutations are localized in the C-terminus in the nuclear localization signal (NLS) sequence. The mutations cause aberrant cytoplasmic distribution of FUS protein (Kwiatkowski et al., 2009). Patients exhibit classical ALS phenotype without cognitive impairment and with different progressions even among carriers of the same mutations (Iguchi et al., 2013). FUS shares structures and functions with TDP-43, in fact both proteins regulate alternative pre-mRNA splicing and transcription (Lagier-Tourenne et al., 2012), although they have different mRNA targets. FUS was observed in neuronal cytoplasmic inclusions positive for GRP78/BiP, p62/SQSTM1 and ubiquitin (Seelaar et al., 2010). Interestingly, mutated FUS is not co-localized with TDP-43, but some studies show that wtFUS is present in TDP-43 aggregates of sALS (Deng et al., 2010).

Animal models of FUS related ALS, that overexpress mutant FUS proteins, exhibit pathological phenotype like ALS, but also wt FUS over-expression results in progressive motor neuron degeneration (Iguchi et al., 2013).

OPTN

OPTN gene mutations correlates with fALS in 1-4% of cases. OPTN was first observed mutated in Japanese families; other dominant and recessive mutations were later identified. Optineurin encoded by OPTN gene negatively regulates TNFα-induced nuclear factor kappa B (NF-κB) activation. OPTN ALS-causative mutations abolish the inhibition of activation of NF-κB (Maruyama et al., 2010). Other functions of optineurin

are correlated with autophagy, since it may act as an autophagic receptor and because it is involved in the maintenance of Golgi morphology (Sahlender et al., 2005). Optineurin is also present in ubiquitinated neuronal cytoplasmic inclusions of sALS (Osawa et al., 2011).

VCP

Mutations in Valosin-containing protein (VCP) gene were first described in patients suffering of inclusion body myopathy (IBM) correlated with FTD (Badadani et al., 2010; Watts et al., 2004). Recently, in 2010, VCP mutations have been identified in 1-2% of autosomal dominant fALS cases (Johnson et al., 2010). VCP is involved in several cellular pathways responsible for protein degradation, such as ubiquitin proteasome system (UPS), autophagy and endosomal sorting (Meyer et al., 2012). ALS related VCP mutations disrupt autophagosome maturation and block the autophagic pathway (Ju et al., 2009). VCP mutation carriers exhibit heterogeneous phenotypes with the same mutations. VCP-ALS patients present ubiquitinated TDP-43 inclusions in the affected motor neurons. This is confirmed also in mutant VCP knock-in mice, that develop age related motor dysfunction characterized by abnormal TDP-43 inclusions in the brain, spinal cord and muscles (Badadani et al., 2010).

C9ORF72

In 2009, the major ALS locus was identified on chromosome 9p21 (van Es et al., 2009). The C9ORF72 gene was then associated to ALS thanks to the identification of large GGGGCC exanucleotide repeat expansion (from 700 to 1,600 copies) within a C9ORF72

non coding region (DeJesus-Hernandez et al., 2011; Renton et al., 2011). C9ORF72 expansion was observed in up to 80% of fALS/FTD cases, 20%-50% of fALS cases and 5%-20% of sALS and it is considered the most common cause of ALS and FTD (Ling et al., 2013). Clinically, C9ORF72 ALS patients have a higher incidence of earlier and bulbar onset with rapid disease progression compared to patients without expansion (Chiò et al., 2012). The pathogenic mechanism of C9ORF72 expansion seems to be related to three different possible mechanisms: a) the loss of function of C9ORF72 gene (haploinsufficiency), b) the gain of toxic function of new mutated proteins, c) the gain of new RNA toxicity caused by mutated RNA (Fig. 7) (La Spada & Taylor, 2010). Moreover, bi-directional transcription and ATG independent translation (RAN translation), directly correlated with RNA secondary structure of long repeated sequence, lead to two different possible toxic RNAs and five different long di-peptides: poly-(glycine-proline, GP), poly-(glycine-alanine, GA), poly-(glycine-arginine, GR), poly-(proline-alanine, PA), poly-(proline-arginine, PR) (Fig. 8). Differently from other ALS-related proteins, the long DPRs produced by GGGGCC expansion in C9ORF72 gene do not have specific functions (Mori et al., 2013). In addition, the alternative combination of these mechanisms may lead to disease.

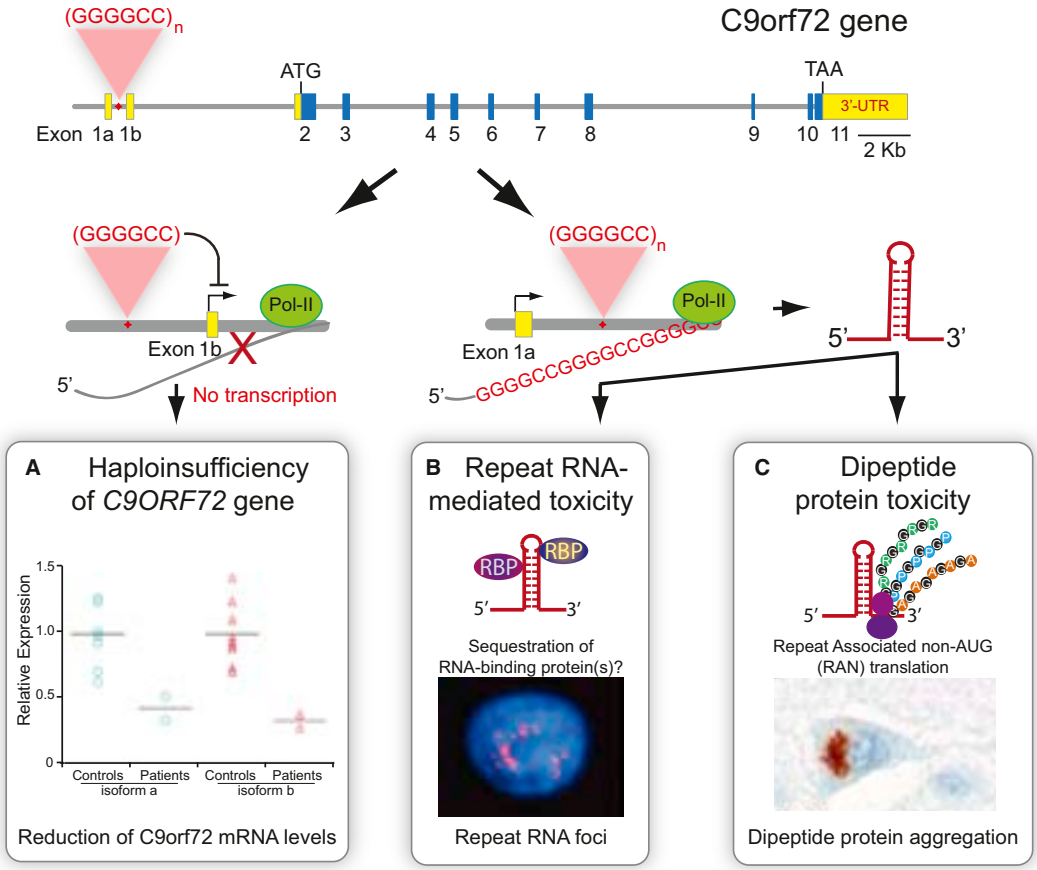

Figure *7* - Schematic *representation toxic mechanisms* of *C9ORF72 exanucleotide expantion*

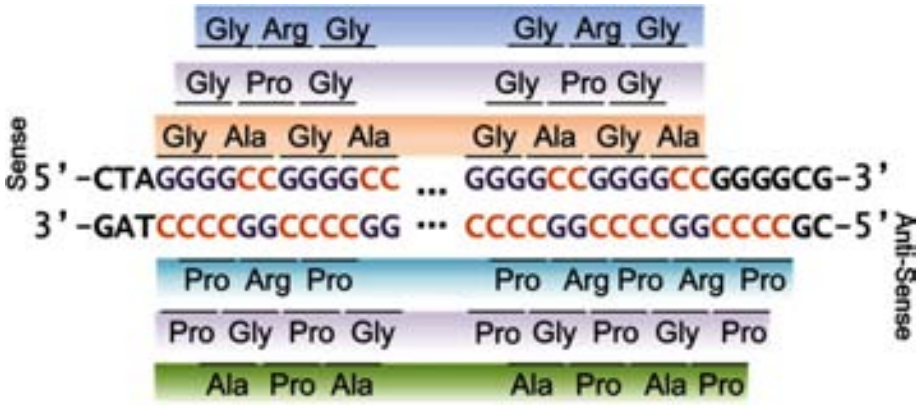

Figure 8 - Schematic rappresentation of protein generated by RAN translation of expanded GGGGCC and CCCCGG. From (Gendron et al., 2015)

The protein quality control system

In healthy cells, the misfolded proteins are managed by protein quality control (PQC). Unfortunately, in some pathological conditions, PQC may be overwhelmed and this would result in misfolded protein accumulation. This occurs in ALS and in SBMA, where mutant ALS-related proteins and inactive mutant AR are rapidly cleared by proteasome, that consequently reduces its ability to process proteasome substrates. Indeed, we already proved that over-expression of mutant ALS-related proteins in motor neuronal cells reduces the proteasome degradation of GFPu proteins. Similarly, we showed that only the soluble and cytoplasmic inactive mutant AR reduces the proteasome activity analysed by GFPu reporter protein. In fact, testosterone treatment activates AR nuclear translocation and aggregation that leads to the reduction of GFPu levels. This is because AR is now partially localized in the nucleus to play its functions, and partially sequestered in aggregates, which may prevent proteasome saturation.

Next, SBMA will be used to describe the PQC mechanisms and functions in the maintenance of protein homeostasis to prevent misfolded protein accumulation and cell death.

The chaperones

Several families of HSPs represent the first defence of PQC. HSPs recognize and stabilize misfolded proteins with their chaperone activity. It has been proven that different chaperones increase the ARpolyQ clearance, accumulation and aggregation in SBMA cell models (Adachi et al., 2009). In fact, enhancing the HSPs levels by heat

shock response mediated by heat shock factor 1 (HSF-1), ARpolyQ aggregation is reduced (Kondo et al., 2013). Several HSPs prevent ARpolyQ aggregation, such as HSP70, HSP40 and HSP90. The complex interaction between HSPs and ARpolyQ has been well reviewed in Pratt et al., 2014 (Pratt et al., 2014), where the authors described the interaction between ARpolyQ and HSP90, possibly, as a start of aggregation. Moreover, the ability of molecular chaperons to prevent ARpolyQ aggregation changes based in the types and interactions between HSPs involved.

HSP70 interacts with the C-terminus of Heat shock cognate (HSC) protein 70-interacting protein (CHIP), that ubiquitinates misfolded protein by its E3 ubiquitin ligase activity and subtracts ARpolyQ from folding machinery to PQC degradation. CHIP over-expression in SBMA neuronal models show a great reduction of ARpolyQ accumulation. In parallel, CHIP over-expression in SBMA transgenic mice shows a clear reduction of SBMA symptoms and AR nuclear accumulation (Adachi et al., 2007).

We also proved that the chaperone HSPB8, a small ATP-independent HSPs, is an inhibitor of ARpolyQ aggregation (Rusmini et al., 2013). HSPB8 acts in a complex with BCL2-associated athanogene 3 (BAG3), HSC70 and CHIP to route misfolded proteins resistant to HSPs-dependent refolding toward autophagic degradation (Rusmini et al., 2013; Gamerdinger et al., 2011; Crippa et al., 2010b).

The proteasome

If chaperones fail to refold, specific proteins target toxic species to degradative pathway: the ubiquitin proteasome system (UPS) (Fig. 9) and the autophagy. Regarding UPS degradation, misfolding proteins recognized by HSP70/HSP40 complex are

ubiquitinated by CHIP and directed to the 20S proteasome subunit. Then, wt and mutant AR are efficiently degraded by UPS and accumulate in neuronal and non-neuronal cells after UPS inhibition (Dossena et al., 2014; Rusmini et al., 2013; Rusmini et al., 2010). Different equilibrium between UPS and autophagy power is observed in different cells and may imply the differences in ARpolyQ processing (Crippa et al., 2013b; Onesto et al., 2011). Recently, it has been proven that ARpolyQ tends to form insoluble species prevalently in neuronal cells compared to other types. In fact, in iPSCs derived from SBMA patients, ligand induced ARpolyQ aggregates can be detected in filter retardation assay (FRA) only when cells are differentiated to motor neurons and not in undifferentiated iPSCs or fibroblast (Nihei et al., 2013). Previous studies, with the proteasome reporter YFPu, investigated the role of the UPS after ligand-induced ARpolyQ aggregation. These studies clearly showed that the UPS pathway is impaired in absence of ARpolyQ aggregates (untreated ARpolyQ is cleared by UPS), but ARpolyQ aggregate formation is correlated with normal UPS activity. These observations confirm that aggregates protect UPS from an overwhelming of misfolded protein excess. In parallel, aggregates may be massively handled by autophagy for degradation.

Autophagy

Autophagy (meaning "self-eating"), in particular macroautophagy (normally named autophagy), is a degradative pathway responsible for the digestion and recycling of nutrients via autophagosome. Autophagosome engulfs proteins and organelles and delivers them to lysosome for degradation. Other autophagy pathways contribute at protein homeostasis: i) microautophagy is an unspecific degradative process similar to macroautophagy, but the lysosomal membrane encases directly cytosolic components (Li et al., 2012). ii) chaperone mediated autophagy (CMA) is a form of lysosome degradation in which the substrates are delivered directly to the lysosome without autophagosome formation. CMA recognizes a pentapeptide sequence KFERQ and HSC70 and lysosome-associated membrane protein type 2 (LAMP-2A) is involved in recognition and lysosome internalization (Fig. 10) (Kaushik & Cuervo, 2012).

Autophagy was found to be altered in different MNDs, including SBMA and ALS. In addition, mutations in proteins involved in autophagy pathway have been linked to diseases (Menzies et al., 2015). Autophagy (Fig. 11) is a multi-step process that starts with initiation, when the fusion of different membrane sources forms a phagophore. This structure surrounds portions of cytoplasm until the two edges are fused together to form an autophagosome. In this step various autophagy (ATG) proteins are involved. In particular, ATG5 –ATG12 – ATG 16L1, ATG7, ATG9, ATG 10 and ATG 14 contribute to phagophore expansion and closure. Moreover, the cleavage of microtubule-associated protein 1 light chain 3 (LC3) by ATG4B to form LC3-I and the following conjugation with phosphatidyletanolamine by ATG7 and ATG3 to form LC3-II are necessary steps to complete the autophagosome biogenesis (see Menzies et al., 2015 for review). Then,

autophagosomes are trafficked by dynein to the perinuclear region, where the fusion with lysosome occurs. This step is regulated by VAMP7, VAMP8 and VT11B belonging to the family of SNARE proteins. Overall, correct acid lysosomal pH and functional degrading enzymes are necessary conditions for efficient autophagy. Moreover, there must be sufficient lysosomes available, because the autophagy process consumes lysosomes. Recently, lysosome biogenesis has been observed to be regulated by the transcription factor EB (TFEB), the master regulator for lysosomal biogenesis. For this reason, TFEB plays an important role in autophagy regulation.

ARpolyQ is recognized by p62/SQSTM1, which interact with LC3-II to target AR toward autophagy. Misfolded proteins are directed to the microtubule organization centre (MTOC), where misfolded proteins can interact and form aggresomes, in order to facilitate the insertion into nascent autophagosomes (Johnston et al., 2002). While UPS is responsible for wt and mutant ARpolyQ degradation in basal condition, autophagy is essential when UPS is overwhelmed. In fact, the accumulation of ARpolyQ insoluble species may be linked to a defect in autophagy. In support of this hypothesis it was proven that depletion of p62/SQSTM1 results in an increase of insoluble ARpolyQ in affected cells and an earlier disease onset in SBMA mice models (Doi et al., 2013). In parallel, p62/SQSTM1 over-expression reduces the soluble and insoluble fractions of ARpolyQ (Doi et al., 2013). In this condition, autophagy is essential for PQC system functions (Rusmini et al., 2013; Carra et al., 2012; Rusmini et al., 2010).

Autophagy is controlled by specific chaperones, such as the HSPB8, which responds to proteasome inhibition (Crippa et al., 2010a; Crippa et al., 2010b). In addition, re-routing from proteasome to autophagy is also mediated by the co-chaperone BAG3,

that interacts with HSPB8 and BAG1, respectively responsible for autophagy or proteasome clearance (Gamerdinger et al., 2011). Then, the increasing HSPB8 level, promoted by transcriptional activation of HSPB8 promoter, results in a higher number of HSPB8-BAG3 complex (2:1 ratio) that interacts with HSC70-CHIP and misfolded proteins. We have already proven that HSPB8 decreases ARpolyQ aggregation via the increase of the ARpolyQ solubility (Rusmini et al., 2013). In motor neurons, HSPB8 prevents ARpolyQ aggregation without modifying p62-SQSTM1 and LC3 expression, but it is able to reduce p62 bodies formation and restore a normal autophagic flux, which is impaired in SBMA cell models after testosterone treatment (Rusmini et al., 2013). Because of this, HSPB8-BAG3 interaction and their relative levels are important in the removal of misfolded proteins and for a normal viability of motor neurons. HSPB8 levels decrease with age in mice, but the protective effects of HSPB8 on motor neuron are confirmed by the high HSPB8 levels observed in ALS mice motor neurons that survive at the end-stage of the disease (Crippa et al., 2010b). Notably, the K141N and K141E missense mutations in HSPB8 α-crystalline domain have been linked to Charcot-Marie-Tooth type 2L disease and in hereditary distal motor neuropathy type II. The expression of these mutant HSPB8 proteins shows neurite degeneration only in primary motor neuronal cells culture (reduction in number and in average length of the neurites). Although the mechanism through which mutant HSPB8 leads to a specific motor neuron disease is currently unknown, these data show the important role of HSPB8 in the maintenance of efficient motor neurons (Irobi et al., 2010; Fontaine et al., 2006).

PQC and autophagy are important targets to modulate in order to counteract misfolded protein toxicity. In our laboratory, we observed that autophagy facilitation by HSPB8 induction or by trehalose treatment drastically reduced misfolded protein aggregation also in ALS models. Autophagy modulation seems to be a target to counteract misfolded protein toxicity in MNDs (Rusmini et al., 2013; Crippa et al., 2013a; Onesto et al., 2011; Rusmini et al., 2010; Crippa et al., 2010b).

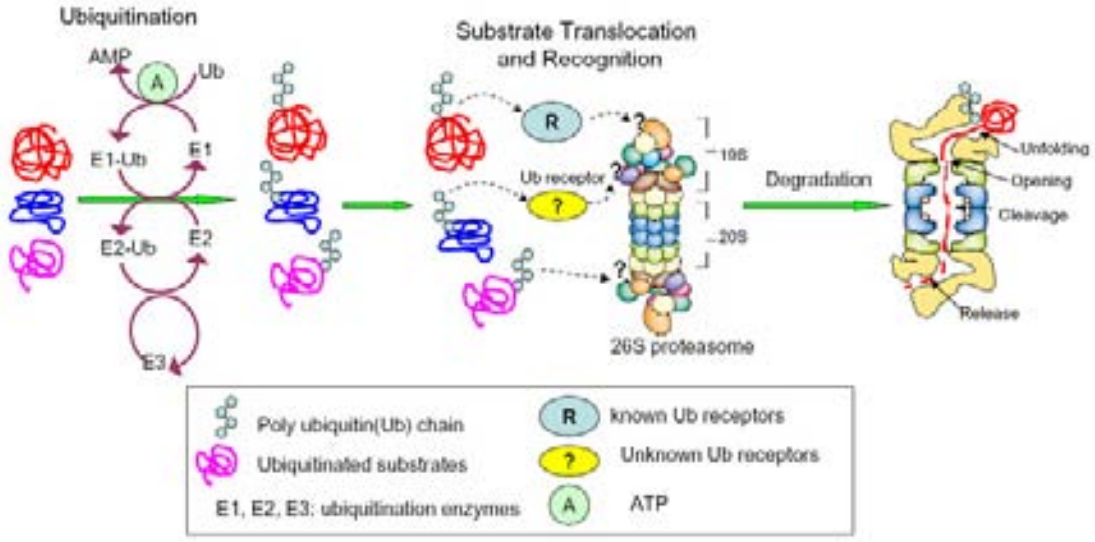

Figure 9 - Schematic Diagram of ubiquitin proteasome pathway.
From Huang Laboratori at University of California Irvine

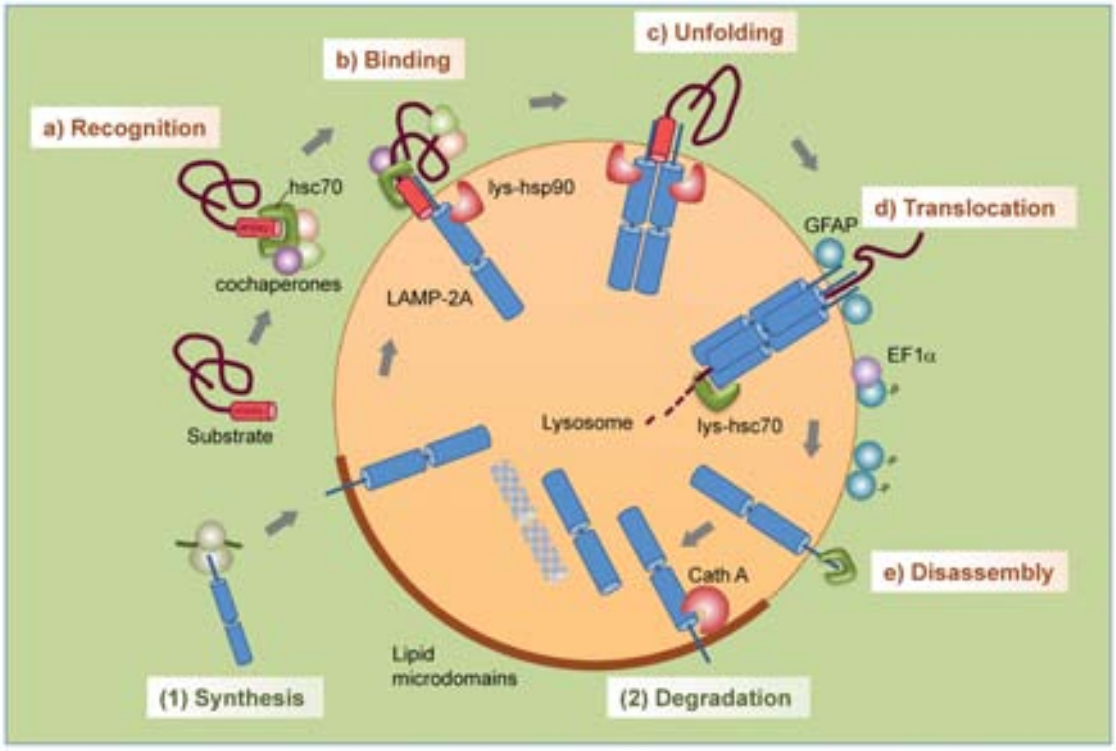

Figure 10 - Steps and regulation of CMA. Steps: (a) Recognition of substrate proteins by hsc70/ cochaperones; (b) binding of substrate-chaperone complex to LAMP-2A; (c) unfolding of the substrate; (d) LAMP-2A multimerization, substrate translocation and subsequent degradation; (e) disassembly of LAMP-2A multimer/translocon. Regulation of levels of LAMP-2A at the lysosomal membrane is attained through (1) de novo synthesis and (2) degradation in specialized microdomains at the lysosomal membrane (from Kaushik et al., 2012).

-

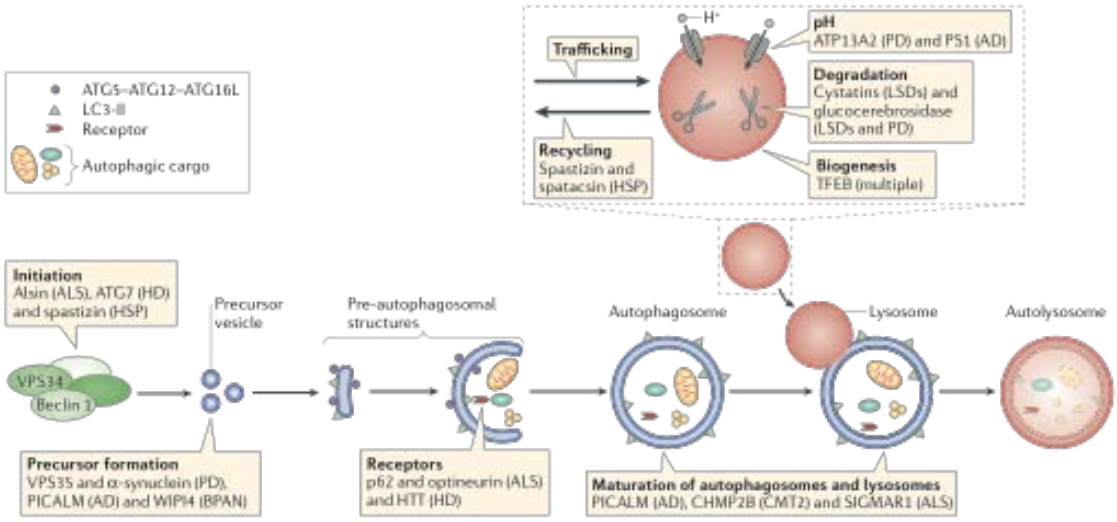

Figure 11 - Overviewoftheautophagypathwayandthesitesofactionofdisease-associatedproteins. This diagram shows a simplified version of autophagy (from Menzies et al., 2015).

-

Misfolded proteins transport

To efficiently remove misfolded proteins, autophagy requires the functions of dynein motor protein. In fact, cytoplasmic dynein binds directly or indirectly to Rab GTPases and drives: i) autophagy substrates at autophagosome nucleation site (Gamerdinger et al., 2011); and ii) autophagosome to lysosome fusion (Jahreiss et al., 2008). Cytoplasmic dynein binds the BAG3 that interacts with HSPB8-HSC70-CHIP and recognizes misfolded proteins to concentrate them at the MTOC (Crippa et al., 2010b; Johnston et al., 2002). These observations support the key role of cytoplasmic dynein to enable autophagy in the clearance of MND-related misfolded proteins. Furthermore, also BAG3 plays an essential role in the delivery of misfolded proteins to MTOC and autophagosomes. In fact, BAG3 contains the proline-rich (PXXP) repeat motif that specifically interacts with the 14-3-3 proteins, acting as a bridge between HSC70 substrate and the dynein complex. Subsequently, dynein and the associated factors move on the microtubule toward the MTOC, where aggresomes are formed (Dul et al., 2001). Thus, BAG3/HSC70 complex recognizes HSPB8, CHIP and misfolded proteins and by BAG3 PXXP domain are specifically routed by dynein to form the aggresome (Gamerdinger et al., 2011). The BAG3-mediated routing via HSC70 is involved in a selective autophagy, in which ubiquitination might occur at later stages, mediated by CHIP. Interestingly, in aggresomes, several misfolded proteins are not ubiquitinated (García-Mata et al., 1999), and BAG3-assisted aggresome targeting of misfolded proteins can also be independent from their ubiquitination status (Gamerdinger et al., 2011). It has been proposed that BAG3 mediates the recruitment of misfolded proteins to be ubiquitinated by CHIP, while an alternative pathways

involved in aggresome formation is controlled by histone deacetylase 6 (HDAC6), that it is also an interactor of the dynein motor complex (through the dynactin/p150Glued). This apparently occurs only after CHIP-mediated ubiquitination of substrates escaping UPS degradation (Muñoz-Moreno et al., 2015; Kraft et al., 2010; Sha et al., 2009; Dompierre et al., 2007). Thus, both aggresome pathways require dynein to concentrate misfolded proteins at MTOC (Johnston et al., 2002). Notably, mutations in the gene DYNC1H1 coding for dynein (cytoplasmic 1, heavy chain 1), the essential subunit of the cytoplasmic dynein complex, have been found in several neuronal diseases (e.g.: spinal muscular atrophy with lower extremity dominance (SMA-LED), intellectual disability with neuronal migration defects, malformations of cortical development, and Charcot-Marie-Tooth disease, type 2O) (Strickland et al., 2015; Scoto et al., 2015; Sau et al., 2011; Moore et al., 2009; Ravikumar et al., 2005; Hafezparast et al., 2003; LaMonte et al., 2002). At the same time, in transgenic mice models of fALS (SOD1 G93A mice) characterized by anterograde and retrograde transport alterations (Bilsland et al., 2010; Williamson & Cleveland, 1999), dysfunctional dynein was able to improve motor function and to extend survival (El-kadi et al., 2010; Teuchert et al., 2006; Kieran et al., 2005).

Even though the axonal transport deficit occurs in other MNDs, like Huntington's disease (HD) and Alzheimer's disease, altered axonal transport does not seem to play a role in SBMA disease initiation or progression (Malik et al., 2011).

Collectively, all these observations indicate that misfolded protein transport plays a central role in MNDs. Several questions on the role of dynein in the clearance of misfolded proteins remain open. In particular, it remains to be determined at which

stage monomeric misfolded species collapses into oligomeric and aggregated forms that initially produce aggresomes and later mature to insoluble inclusions not sufficiently removed by (and capable of blocking the) autophagic flux.

AIMS AND OBJECTIVES

The aims of this work was to investigate the implications of protein misfolding in SBMA and in ALS. In the first part of the thesis, I characterized the response to misfolded ARpolyQ protein in skeletal muscle and spinal cord tissues during disease progression in SBMA, by analysing both AR expression levels and selected genes involved in the of PQC degradative pathways in quadriceps muscle and in spinal cords of SBMA transgenic mice model. By RT-qPCR and western blot analysis, I studied the expression of proteins responsible for autophagic recognition of misfolded proteins. I also evaluated the existence of differences in the response of the two tissues to misfolded proteins.

In the second part of the thesis, I focused my attention on the role of dynein in autophagic removal of misfolded proteins responsible for MNDs. First of all, I confirmed that HSPB8 exterts a pro-degradative activity on ARpolyQ aggregates. By using dynein modulators, I deeply investigated the role of dynein on autophagic flux and on the levels of ARpolyQ, G93A SOD1 and TDP-43 ΔC misfolded proteins responsible for SBMA or fALS. Moreover, I analysed the levels of chaperones and co-chaperones involved in misfolded proteins degradation in order to measure the equilibrium between different PQC degradative pathways (UPS, Autophagy and CMA) after the inhibition of dynein-mediated transport. Finally, I evaluated the pro-degradative effect of HSPB8 and the role of dynein mediated transport in motor neuron cells expressing C9ORF72 expanded products recently correlated with fALS and sALS.

MATERIALS AND METHODS

Chemicals

Erythro-9-(2-Hydroxy-3-nonyl) adenine hydrochloride (EHNA), Z-Leu-Leu-Leu-al (MG-132) and trehalose have been obtained from Sigma-Aldrich (St. Louis, MO, USA), 3-Methyladenine (3-MA) have been obtained from Selleckchem (Houston, TX, USA).

Generation and maintenance of AR113Q knock-in mice

Animal care and experimental procedures were conducted in accordance with the Italian Institute of Technology and the University of Trento ethical committees and were approved by the Italian Ministry of Health. Generation and genotyping of mice containing androgen receptor with 113 CAG repeats in exon 1 was described previously (Yu et al., 2006a; Yu et al., 2006b). Mice genetic background was C57Bl/6J. Females carrying one copy of AR113Q in the X chromosome were crossed with C57Bl/6J mice to maintain the colony. Mice were genotyped by PCR on tail DNA, using REDExtract-N-Amp Tissue PCR kit (Sigma-Aldrich, St Louis, MO, USA) according to manufacturer's instructions. The mice were housed in filtered cages in a temperature-controlled room with a 12-hour light/12-hour dark cycle with ad libitum access to water and food. Quadriceps muscles and spinal cord were rapidly collected after the sacrifice, snap frozen in liquid nitrogen, and conserved at −80°C until RNA and protein extraction.

Plasmids & siRNA

The plasmid coding for AR.Q46, GFP-AR.Q48, and pCI-HSPB8 are routinely used in our laboratory and they have been previously described (Giorgetti et al., 2015; Rusmini et

al., 2013; Carra et al., 2005; Simeoni, 2000). pcDNA/HA-Bag1 coding for the protein Bag1 was obtained from prof. Harm H. Kampinga, University of Groningen, Groningen, The Netherlands (Nollen et al., 2001; Nollen et al., 2000). The plasmid expressing the proteasome function reporter GFPu was obtained from prof. Ron Kopito, Stanford University, Stanford, CA, USA (Bence et al., 2001). The pCMV-β plasmid, encoding for β-galactosidase (Clontech Lab., Mountain View, CA, USA), was used to evaluate the protein expression levels after EHNA treatment. pcDNA3-wtSOD1 and pcDNA3-G93A-SOD1 expressing human wtSOD1 or mutant G93A-SOD1 were obtained from Dr. Caterina Bendotti, Mario Negri Institue, Milano, Italy (Tortarolo et al., 2004). pFLAG-FL TDP-43, and pFLAG-ΔC TDP-43, expressing FLAG-tagged wt full-length human TDP-43 and a C-terminus truncated form, respectively, were obtained from Dr. Emanuele Buratti, International Centre for Genetic Engineering and Biotechnology, Trieste, Italy (Ayala et al., 2008a; Ayala et al., 2008b). pAG3 C9orf72 Nested 2 Rpt and pAG3 C9orf72 Nested 66 Rpt encoding for 2 or 66 GGGGCC repeats without ATG, without stop codon and tagged with one peptide-tag per frame (polyGA-HA; polyGP-Myc; polyGR-FLAG) was obtained from Prof. Leonard Petrucelli, Mayo Clinic, Jacksonville, Florida, USA. pCMV-Flag-polyGP-V5-His encoding for polyGP di-peptide was obtained from Prof. Daisuke Ito, Keio University School of Medicine, Tokio, Japan (Yamakawa et al., 2015). pcDNA3 was used to normalize for transfected plasmid DNA amount.

pcDNA5/TO-GFPAR.Q39 was used to obtain stable and inducible SBMA cell model and was constructed by cloning the sequence coding for GFPARQ.39 into NheI and XbaI sites of pcDNA5/TO (Life Technologies Corporation, Carlsbad, CA, USA) previously modified with insertion of BamHI and NheI sites.

To silence endogenous proteins, we have used: a) cytoplasmic dynein 1 heavy chain 1 custom siRNA duplex (5'-GGG UAA AGC UAG AGA GAA UUU-3' (sense) 5'-AUU CUC UCU AGC UUU ACC CUU-3' (antisense)); b) HSPB8 custom siRNA duplex (5'- CGG AAG AGC UGA UGG UAA AUU-3' (sense) 5'- UUU ACC AUC AGC UCU UUC CGU U-3' (antisense)) (Dharmacon, Thermo Scientific Life Sciences Research, Waltham, MA, USA).

Cell culture and transfection

The immortalized motoneuronal cell line NSC34 (Durham et al., 1993; Cashman et al., 1992) is routinely used in our laboratory and has been transfected with Lipofectamine (Life Technologies Corporation, Carlsbad, CA, USA)/transferrin (Sigma-Aldrich), as previously described (Marron et al., 2005; Piccioni et al., 2002; Simeoni, 2000), using 0.6 μg of plasmid DNA, 4 μL of transferrin solution and 2 μL of Lipofectamine (amount for one well of 12-wells multiwell plate). siRNA transfection was performed with Lipofectamine 2000 (Life Technologies), using 40 pmol of target RNA and following manufacturer's instructions.

Inducible stably transfected NSC34-GFPAR.Q39 cell line was obtained by transfecting pcDNA5/TO-GFPAR.Q39 into TR4 NSC34 cell line stably transfected with pcDNA6/TR encoding for tetracycline repressor, kindly provided from Dr. Enrico Garattini, Mario Negri institute, Milan, Italy (Locatelli et al., 2012).

Rat adrenal pheochromocytoma (PC12) cells stably transfected with the plasmid encoding AR.Q112 express AR under the control of a Tet-On promoter responsive to 1 μg/mL of doxycycline. PC12-AR.Q112 have been produced and kindly provided by prof.

Diane Merry, TJU, Philadelphia, PA, USA (Walcott & Merry, 2002).

iPS cells from fibroblast of SBMA patients (SB6MP2 clone) generated by Oct4, Klf4, Sox2 and c.Myc transfection were kindly provided by dr. Christopher Gruniseich and dr. Kennet Fischbeck, NIH, Betesta, USA. iPS cells were cultured in Essential 8 medium (Life Technologies) and differentiated into motor neurons as described by Grunseich et al, 2014 (Grunseich et al., 2014b). Briefly, iPSCs were grown to 80% confluency, then digested with collagenase IV (Life Technologies), scraped off of the dish, and cells were re-plated into low adherence dishes (Corning, Corning, NY) in KSR (Life Technologies) based media with 20 ng/ml FGF (ORF genetics, Kopavogur, Iceland), 20 µM ROCK-I (Selleckchem), 10 µMSB431542 (Stemgent, Lexington, MA, USA), and 0.2 µM LDN193189 (Stemgent), to allow embryo bodies (EBs) formation. EBs were transitioned to a KSR free medium at day 3. 1 µM retinoic acid (Sigma) was added at day 5 to direct cells differentiation into rostral spinal cord phenotype. 1 µM smoothened agonist (Merck Millipore, Darmstadt, Germania). and 0.5 µM purmorphamine (Ann Arbor, MI, USA) were added at day 7 to ventralize the differentiating population. The EBs were dissociated at day 14 and plated at 150.000 cells/well on 12-well multiwell plates coated with poly-D-lysine (Life Technologies) and laminin (Sigma). Differentiated-motor neurons were allowed to growth for an additional 14 days in neurobasal media (Life Technologies) with 25 µM glutamate (Euroclone), 0.4 µg/ml ascorbic acid (Sigma), 10 ng/ml GDNF (PeproTech, Rocky Hill, NJ, USA), 10 ng/ml CNTF (PeproTech), 1 µg/ml laminin (Sigma), B-27 (Life Technologies), N2 (Life Technologies), non-essential amino acids (Euroclone), and pen/strep/glutamine (Euroclone). Motoneuronal cells were treated with 10nM

testosterone and/or 100μM EHNA for last 48 hours.

Stably transfected NSC34-wtSOD1 and NSC34-G93A-SOD1 cell lines have been produced and kindly provided by Prof. Maria Teresa Carrı`, Università Roma Tor Vergata, Roma, Italy. These cell lines express myc-tagged human wtSOD1 or G93A-SOD1 and were routinely maintained as described by Ferri et al. (Ferri et al., 2006).

In the experiments involving steroid hormone treatments, the serum was replaced with charcoal-stripped serum, to eliminate endogenous steroids (Pozzi et al., 2003; Piccioni et al., 2002; Poletti et al., 2001).

RNA and protein extraction

NSC34 cells were plated at 180.000 cells/well in six-well multiwell plates and treated with 100 μM EHNA. After 48 hours, cells were harvested and centrifuged 5 min at 100 x g at 4°C; the pellets were lysate by 10 passages through a 21-gauge needle in TRI Reagent (Sigma-Aldrich). Frozen spinal cord and muscle were suspended in TRI-Reagent (Sigma-Aldrich) and homogenized with Tissue-Lyser (QIAGEN, Valencia, CA, USA). Then, RNA was extracted following the TRI-REAGENT Manufacturer's protocol. After homogenization, 1-bromo-3-chloropropane was added to ensure complete dissociation of nucleoprotein complexes and then the samples were centrifuged to obtain the phase separation. The aqueous phase, containing RNA was isolated and purified. Briefly, aqueous phase was washed with 2-propanol and subsequently with ethanol both to remove the residual phenol and to precipitate RNA, respectively. The RNA pellet was dis- solved in RNase-free water (30μL). RNA quantification was carried out by absorbance at 260 nm. The proteins were precipitated from the organic phase

with propanol and then the pellets were washed with 0.3M guanidine hydrochloride/95% ethanol solution (3 times). After the three washes, ethanol was added and the pellets were re-suspended using 1% SDS- 8M Urea in Tris HCl pH8.0 solution (100μL).

mRNA expression analysis

Total RNA (1 μg) was treated with DNAse (Sigma-Aldrich), and reverse transcribed into cDNA using the High-Capacity cDNA Archive Kit (Life Technologies) according to the manufacturer's protocol. All primers for real-time PCR were designed using the program Primer 3. The primers were synthesized by MWG Biotech (Ebersberg, Germany) with the following sequence: mAR: 5'-ATC CCA GTC CCA CTT GTG TC-3'(forward), 5'-GGT CTT CTG GGG TGG AAA GT-3' (reverse); mouse ATG10: 5'-TTC ACA GCA GAT AGG CGA TG -3' (forward), 5'-TGC AGG TCT CGT CAC TTC AG-3' (reverse); mouse Beclin1: 5'-TGA AAT CAA TGC TGC CTG GG-3' (for- ward), 5'-CCA GAA CAG TAT AAC GGC AAC TCC -3' (reverse); mouse HSPB2: 5'-GCT CAG TGA AGG CAA GTT CC -3' (forward), 5'-CAG GAC ATA GGT GCG ACA GA-3'(reverse); mouse HSPB2: 5'-GCT CAG TGA AGG CAA GTT CC -3' (forward), 5'-CAG GAC ATA GGT GCG ACA GA-3'(reverse) mouse HSPB3: 5'-CAT CAT CAT CCA GAC CTT CG -3' (forward), 5'-ACT TCC ACC ACC AAG ATT CC-3' (reverse) mMAP-LC3-B: 5'-CGT CCT GGA CAA GAC CA-3' (forward), 5'-CCA TTC ACC AGG AGG AA-3' (reverse); mP62/SQSTM1: 5'-AGG GAA CAC AGC AAG CT-3' (forward), 5'-GCC AAA GTG TCC ATG TTT CA-3' (reverse); mGAPDH: 5'-CCA GAA CAT CAT CCC TGC AT-3' (forward), 5'-CAG TGA GCT TCC CGT TCA-3' (reverse); mRplPO: 5'-GGT GCC ACA CTC CAT CAT CA-3' (forward), 5'-AGG CCT TGA CCT TTT CAG TAA GT-3'

(reverse); mHSPB8: 5'-ATA CGT GGA AGT TTC AGG CA-3' (forward), 5'-TCT CCA AAG GGT GAG TAC GG-3' (reverse); mBAG3: 5'-ATG GAC CTG AGC GAT CTC A-3' (forward), 5'-CAC GGG GAT GGG GAT GTA-3'(reverse); mBAG1: 5'-GAA ACA CCG TTG TCA GCA CT-3' (forward), 5'-GCT CCA CTG TGT CAC ACT C-3'(reverse); mLamp2A: 5'-GCA GTG CAG ATG AAG ACA AC-3' (forward), 5'-AGT ATG ATG GCG CTT GAG AC-3' (reverse); mHSC70: 5'-CCT CGG AAA GAC CGT TAC CA-3' (forward), 5'-TTT GTT GCC TGT CGC TGA GA-3' (reverse); mβ-actin: 5'-GTC GAG TCG CGT CCA CC-3' (forward), 5'-GTC ATC CAT GGC GAA CTG GT-3' (reverse); hHSPB8: 5'- AGA GGA GTT GAT GGT GAA GAC C-3' (forward), 5'-CTG CAG GAA GCT GGA TTT TC-3' (reverse); hBAG1: 5'-TTT AGA GCA GCC CGA GTG AT-3' (forward), 5'- GAC AGC AGA CAG CCA ACA AA-3' (reverse); hBAG3: 5'-GGG TGG AGG CAA AAC ACT AA-3' (forward), 5'-AGA CAG TGC ACA ACC ACA GC-3' (reverse); hP0: 5'-GTG GGA GCA GAC AAT GTG GG-3' (forward), 5' -TGC GCA TCA TGG TGT TCT TG-3' (reverse).

The evaluated efficiency of each set of primers was close to 100% for both target and reference genes. Real-time PCR was performed using the CFX 96 Real-Time System (Bio-Rad, Hercules, CA, USA) in a 10 μL total volume, using the iTaq SYBR Green Supermix (Bio-Rad), and with 500 nM primers. PCR cycling conditions were as follows: 94°C for 10 min, 40 cycles at 94°C for 15 s and 60°C for 1 min. Melting curve analysis was performed at the end of each PCR assay as a control for specificity. Data were expressed as C_t values and used for the relative quantification of targets with the $\Delta\Delta C_t$ calculation (Rusmini et al., 2015; Crippa et al., 2013a). To exclude potential bias due to averaging data transformed through the equation $2^{-\Delta\Delta Ct}$ to give N-fold changes in gene expression, all statistics were performed with ΔC_t values. Each experiment was

carried out with four independent samples.

Western blot (WB) analysis and filter retardation assay (FRA)

NSC34 or PC12 cells were plated in 12-well plates at 80.000 cell/well, transfected as previously described or induced with 1 μg/mL doxycycline. AR activation is induced by 10 nM testosterone treatment for 48 hours. Inhibition of dynein ATPase activity is performed by 100 μM EHNA for 48 hours. In experiments involving autophagy blockage or induction, 10 mM 3-MA or 100 mM trehalose were added to the cells for the last 48 hours. Proteasome inhibition was performed by 10 μM MG132 treatment for the last 16 hours (overnight treatment). 48 hours after plating, cells were harvested and centrifuged 5 min at 100 x g at 4°C; the cell pellets were re-suspended in PBS (added of the protease inhibitor cocktail, Sigma-Aldrich) and homogenized using slight sonication as previously described (Rusmini et al., 2007; Poletti et al., 2001). Total proteins were determined with the bicinchoninic acid method (BCA assay, Euroclone). Protein concentration, of spinal cord and quadriceps samples, was determined using Pierce 660nM protein assay reagent with Ionic Detergent Compatibility Reagent (IDCR) (Thermo-Fisher Scientific). WB analysis were performed using 10 and 15% SDS-polyacrylamide gel electrophoresis. WB was performed on 10%, 12% or 15% SDS – polyacrylamide gel electrophoresis loading 15 μg or 20 μg of total proteins. Samples were then electro-transferred to nitrocellulose (Bio-Rad) or PVDF (polyscreen transfer membrane, Amersham, GE Healthcare Wauwatosa, WI, USA, USA) using a semi-dry transfer apparatus (Trans-Blot^{w} Turbo^{TM} Transfer System, Bio-Rad). The membranes were treated with a blocking solution containing 5% nonfat dried milk powder

(EuroClone, MI, Italy) in Tris buffered saline with Tween 20 (0,01%) for 1 hour and then incubated with one of the following primary antibodies: (a) rabbit polyclonal AR-H280 (dilution 1:3.000) to detect wtAR and ARpolyQ (Santa Cruz Biotchnology, Texas, USA); (b) rabbit polyclonal anti-LC3 (dilution 1:4.000, Sigma-Aldrich); (c) rabbit polyclonal anti-P62/SQSTM1 (dilution 1:4.000, Abcam, UK); (d) rabbit polyclonal anti-dynein heavy chain (dilution 1:1.000, Santa Cruz); (e) rabbit polyclonal anti-GFP HRP conjugated (dilution 1:15.000 Vector Laboratories, Burlingame, CA, USA); (f) rabbit polyclonal anti-HA (dilution 1:1.000, Santa Cruz); (g) rabbit polyclonal anti-LAMP2A (dilution 1:1.000, Abcam); (h) mouse monoclonal Anti-Hsc70 antibody [13D3] (dilution 1:3.000, Abcam); (i) home-made rabbit polyclonal anti-BAG3 (kindly provided by Prof. Serena Carra, Università degli studi di Modena e Reggio Emilia, Italy; 1:6000); (l) rabbit polyclonal anti-BAG1 (Santa Cruz, Dallas, TX, USA, 1:500); (m) home-made rabbit polyclonal anti-HSPB8 (provided by Dr. J. Landry, Quebec, Canada; 1:1000); (n) mouse monoclonal anti-FLAG (Sigma, 1:1000); (o) rabbit polyclonal anti-MYC (Santa Cruz, 1:1000); (p) monoclonal anti-α-tubulin (Sigma-Aldrich, 1:4.000); (q) anti-β-actin (Sigma-Aldrich, 1:2.000); (r) rabbit polyclonal anti-GAPDH (1:4.000, Santa Cruz). Immunoreactivity was detected using the following secondary peroxidase-conjugated antibodies: goat anti-rabbit (dilution 1:20.000, Santa Cruz); goat anti-mouse (dilution 1:20.000, Santa Cruz). Signals were revealed by chemiluminescence detection kit reagents (Clarity™ Western ECL Blotting Substrate, Bio-Rad). The same membranes were subsequently processed with different antibodies to detect the levels of different proteins in the same sample, after stripping for 20 min at room temperature (StripABlot, EuroClone).

FRA was performed using a Bio-Dot SF Microfiltration Apparatus (Bio-Rad). 6 µg of the total proteins were filtered through a 0.2 µm cellulose acetate membrane (Whatman, GE Healthcare). Slot-blots were probed as described for WB to detect AR.Q46, GFP-AR.Q39, AR.Q112, and with (a) rabbit polyclonal ADI-SOD-100-F (1:1000, Enzo Life Science, NY, USA) to detect SOD1; (b) mouse polyclonal anti-flag (dilution 1:1000, Sigma-Aldrich) to detect FL, ΔC-TDP-43 and polyGP.

A ChemiDoc XRS System (Bio-Rad) was used for the image acquisition of WB and FRA. Optical intensity of samples assayed with WB or FRA was detected and analyzed using the Image Lab software (Bio-Rad).

Protein Fractionation

Protein fractionation of NSC34 transfected with AR.Q46 was modified from Koyama et al. (Koyama et al., 2006). The cells were harvested and centrifuged 5 min at 1.200 rpm at 4°C, re-suspended in PBS (containing protease inhibitor cocktail, Sigma) and homogenized using slight sonication. The homogenates were centrifuged at 16.000 g for 10 min at 4°C. The resultant supernatants were collected as the PBS-soluble fraction. The pellets were extracted by slight sonication in 1% Triton X-100 (TX)/PBS. After centrifugation at 16.000 g for 10 min at 4°C, the supernatants were considered the TX-soluble fraction. The pellets were extracted by slight sonication in 5% SDS/PBS. After centrifugation at 16.000 g for 10 min at 4°C, the supernatants were considered the SDS-soluble fraction. Protein concentrations of PBS and TX fraction were measured by a BCA protein assay (Pierce) and analysed in Western blot as described above.

Microscopy analyses on NSC34 cells

NSC34 cells were plated in 12-well multiwell plates containing coverslips at 70.000 cells/well density, transiently transfected with the plasmid coding for GFP-ARQ.48 or hHSPB8 or with DYNC1H1 siRNA as previously described. AR activation is induced by 10 nM testosterone treatment for 48 hours, inhibition of dynein ATPase activity is performed by treatment with 100 μM EHNA for 48 hours. In experiments involving autophagy induction, 100mM trehalose was added to the cells for the last 48 hours. Then, the cells were fixed and processed as previously described (Sau et al., 2007). The following primary antibodies were used to analyze LC3 and p62/SQSTM1 protein distributions: rabbit polyclonal anti-LC3-B antibody (1:500, Sigma-Aldrich) in 5% nonfat milk, and rabbit polyclonal anti-P62/SQSTM1 antibody (1:500, Abcam) in 5% nonfat milk. Secondary antibodies were: Alexa 488 anti-rabbit and Alexa 594 anti-rabbit (1:1000, Life Technologies) in 5% nonfat milk. Cells were stained with DAPI to visualize the nuclei. An Axiovert 200 microscope (Zeiss Instr., Oberkochen, Germany) equipped with FITC/TRITC/DAPI and combined with a Photometric Cool-Snap CCD camera (Ropper Scientific, Trenton, NJ, USA) was used. Phase contrast image was used to evaluate the morphology. Images were processed using the Metamorph software (Universal Imaging, Downing- town, PA, USA).

Proteasome activity

Proteasome chymotryptic assay was performed as described by Allen et al. (Allen et al., 2003). NSC34 cells were plated in 6-well multiwell plates at 180.000 cells/well. Cells were washed with ice-cold PBS and then harvested and centrifuged at 100 x g for 5

min, at 4°C. Pellets re-suspended in 0.3 mL of proteasome extract buffer (20 mM Tris/ HCl, pH 7.4, containing 0.1 mM EDTA, 1 mM 2-mercaptoethanol, 5 mM ATP, 20% v/v glycerol, and 0.04% v/v Nonidet P-40) were homogenized by 10 passages through a 21-gauge needle, and then centrifuged at 12.000 x g for 15 min at 4°C, saving the supernatant. Total proteins were determined with BCA protein assay (Pierce). Proteasome assay reaction mixtures consisted of 50 mM HEPES/KOH, pH 8.0, containing 5 mM EGTA, 100 μg of cell protein extract per mL of assay reaction. Chymotryptic proteasome substrate conjugated with amidomethylcoumarin (AMC), the peptide Suc-LLVY-AMC, was added to the mix at 50 μM and incubated at 37°C for 45 min. The resulting fluorescence was measured at 340 nm excitation and 460 nm emission using a plate spectrofluorimeter (Enspire, Perkin Elmer, MA, USA).

Cell viability assay

The 3-(4,5-dimethyl-2-thiazolyl)-2,5 diphenyl-2H-tetrazolium bromide (MTT)-based cell proliferation assay (MTT assay) was carried out on NSC34 cells 24 or 48 hours after treatment with EHNA 100 μM, and performed, in 24-well multiwell plates at 45.000 cells/well. MTT solution was prepared at 1.5 mg/mL in DMEM without phenol red and was filtered through a 0.2 μm filter. Then, the culture medium was removed from the plate and 300 μL of MTT solution was added into each well. Cells were incubated for 30 min at 37°C with 5% CO2, 95% air and complete humidity. After 30 min, 500 μL of 2-propanol was added into each well and the precipitates were suspended. The optical density (OD) of the wells was determined using a plate reader at a wavelength of 550 nm.

β-galactosidase assay

NSC34 cells were plated in 24-well multiwell plates at density of 40.000 cells/well and transfected with 0.4 μg of pCMV-βgal plasmid. 24 hours after transfection the cells were lysated in 250 μL of lysis buffer (Promega) and 100 μL of samples were added to 750 μL of assay buffer ($Na_2HPO_4*7H_2O$ 60 mM, NaH_2PO_4*H2O 40 mM, KCl 10 mM, $MgSO_4$ 1mM, β-mercaptoethanol 50 mM, pH 7.0), in presence of 4 mg/mL of β-galactosidase substrate o-nitrophenyl-β-D-galactopyraniside (ONPG, Sigma) and incubated at 37°C until yellow color appearance. Then, 500 μL of 1M Na_2CO_3 were added and 200 μL of the final solution were transferred into a 96-well plate and 420 nm absorbance was evaluated using Enspire plate spectrofluorimeter (PerkinElmer).

Statistical analysis

Statistical analysis has been performed using Student's t-test for two group comparisons and two-way ANOVA for more group comparisons using the PRISM software (GraphPad Software, La Jolla, CA, USA).

RESULTS

AR expression in quadriceps muscle and spinal cords of SBMA mouse model

Muscle tissue was recently considered as a possible primary target of ARpolyQ toxicity in SBMA pathogenesis. In order to understand the role of ARpolyQ in muscle tissue we first analysed the expression of AR in muscle and in spinal cord of SBMA male mice and age-matched controls. We collected quadriceps muscle from male non-transgenic (Wt) mice and from male ARQ113 transgenic (SBMA) mice at 9 (corresponding to pre-symptomatic stage) or 24 (corresponding to symptomatic stage) weeks of age. We also used 24 week-old female mice as negative control. As it is clearly shown in the graph in Fig. 12A, AR expression levels are comparable in control and SBMA mice. Also, no differences are observed between pre-symptomatic and symptomatic SBMA male mice. Moreover, female control mice show the same expression levels observed in SBMA mice. This indicates no apparent negative selective pressure associated to atrophy of muscle fibers expressing high levels of ARpolyQ, suggesting that the loss of muscle cells induced by ARpolyQ toxicity does not cause modification in the overall levels of AR expression in muscles. In parallel, we analysed the AR expression levels in spinal cord because in this tissue AR expression is confined to anterior horn motor neuron (affected in SBMA patients) (Marron et al., 2005; Poletti, 2004; Pozzi et al., 2003). Interneuron and glial cells expresses very low levels of AR (Matsumoto et al., 2013; Matsumoto, 1997; Matsumoto et al., 1988). The graph in Fig. 12B demonstrates that AR expression remains unchanged in spinal cord in all conditions analysed, possibly supporting the notion that in the mouse model selected for this study there is no relevant loss on motor neuron in the spinal cord, the exclusive target of ARpolyQ neurotoxicity in this structure. Collectively, these data also show that AR expression

levels in SBMA mice are very similar to those found in control mice both in muscle and spinal cord, at all age tested.

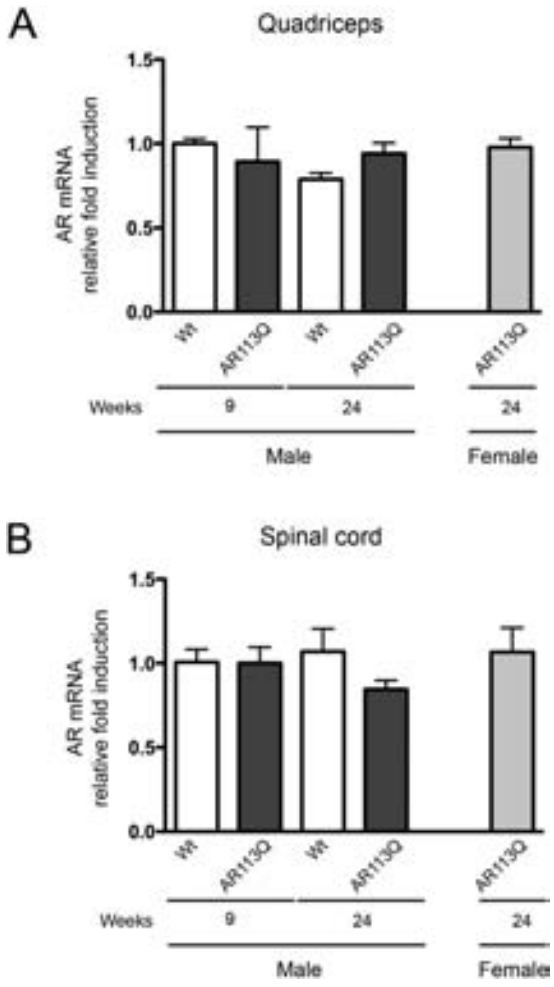

Figure 12 - Expression of AR in quadriceps muscle and spinal cords of SBMA mouse model. RT-qPCRs were performed on total RNA extracted from quadricep muscles (**A**) or whole spinal cords (**B**) of male non-transgenic (Wt) mice, and of AR113Q mice at 9 (corresponding to presymptomatic stage) or 24 (corresponding to symptomatic stage) weeks of age. As additional control, quadriceps muscles of female AR113Q mice at 24 weeks were used (n = 5). Data have been normalized to the amount of GAPDH mRNA, expressed relative to the levels determined in Wt mice at 9 weeks taken as internal reference, and expressed as fold changes. Data are means ± SD of three independent replicates for Wt and AR113Q mice at 9 weeks, and of five independent replicates for Wt and AR113Q mice at 24 weeks. (**A**) RT-qPCR on AR mRNA expression levels in quadricep muscles. (**B**) RT-qPCR on AR mRNA expression levels in spinal cords.

Autophagic markers in muscle of SBMA male mice

Next, we analysed the gene expression of selected mRNA coding for proteins involved in PQC system in skeletal muscle of symptomatic SBMA male mice. To better understand the possible correlation between PQC regulation and symptoms onset we analysed the expression of autophagic markers in quadriceps because it has been proven that the autophagic master regulator gene product TFEB is up-regulated in these mice at symptoms onset (Chua et al., 2014). We analysed, by RT-qPCR, the expression of four genes that encode for essential autophagic proteins:

i) Bleclin 1 (ATG6 ortholog) and ii) ATG10 which are both critical for autophagosome assembly; iii) p62/SQSTM1 and LC3 which are both regulated by TFEB and are typically considered autophagy markers. As it shows in Fig. 13, we found that all autophagic markers analysed are clearly and specifically up-regulated in muscle of symptomatic SBMA male mice; no differences were found between all other mice groups studied.

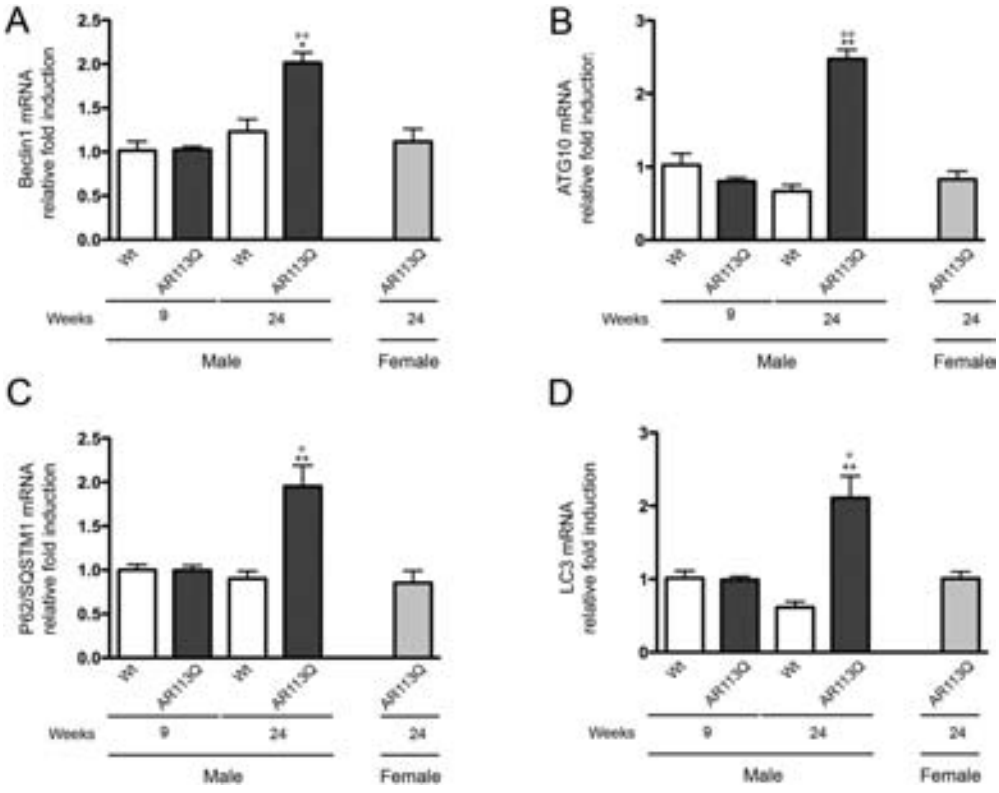

Figure 13 - Expression of autophagic markers in quadriceps muscle of SBMA mouse model. RT-qPCRs were performed on total RNA extracted from quadricep muscles of male non-transgenic (Wt) mice, and of AR113Q mice at 9 (corresponding to presymptomatic stage) or 24 (corresponding to symptomatic stage) weeks of age. As additional control, quadriceps of female AR113Q mice at 24 weeks were used (n = 5). All animals were age-matched. Data have been normalized to the amount of GAPDH mRNA, expressed relative to the levels determined in Wt mice at 9 weeks taken as internal reference, and expressed as fold changes. Data are means ± SD of three independent replicates for Wt and AR113Q mice at 9 weeks, and of five independent replicates for Wt and AR113Q mice at 24 weeks. (A) RT-qPCR on Beclin1 mRNA expression levels in quadricep muscles. *p<0.05 vs. 24 weeks Wt mice; °°p<0.001 vs. 9 weeks AR113Q mice.
(B) RT-qPCR on ATG10 mRNA expression levels in quadricep muscles. **p < 0.001 vs. 24 weeks Wt mice; °°p < 0.001 vs. 9 weeks AR113Q mice. (C) RT-qPCR on P62/SQSTM1 mRNA expression levels in quadricep muscles. **p<0.001 vs. 24 weeks Wt mice; °p<0.05 vs. 9 weeks AR113Q mice. (D) RT-qPCR on LC3 mRNA expression levels in quadricep muscles. **p<0.001 vs. 24 weeks Wt mice; °p<0.05 vs. 9 weeks AR113Q mice.

Pro-autophagic chaperone and co-chaperone levels in muscle of SBMA male mice

We had already proven that autophagy promotion by HSPB8 over-expression (also confirmed in this study in Fig. 18; see above) or by the HSPB8 inducer-trehalose result in a clear reduction of testosterone induced misfolded and insoluble species of ARpolyQ in motoneuronal cells. Thus, here we investigated the levels of expression of HSPB8, a pro-degradative chaperone involved in autophagic degradation of SBMA and ALS related proteins. Indeed, HSPB8 expression is increased by UPS blockage to facilitate autophagy like in ALS affected motor neuron and muscle cells. RT-qPCR analysis of SBMA muscle tissue (Fig. 14A) shows that HSPB8 gene is transcriptionally up-regulated only in symptomatic SBMA male mice, while it is unchanged in all other conditions analysed. This suggests that HSPB8 may contribute to counteract ARpolyQ toxicity in muscle tissue. We also tested the levels of HSPB2, that directly interacts with HSPB8, and the levels of HSPB3 that interacts with HSPB2. Interestingly, HSPB3 was found to be mutated in an axonal type of motor neurophaty (Kolb et al., 2010). HSPB2 and HSPB3 are both highly expressed in skeletal muscle (Carra et al., 2012) where they are involved in myogenic differentiation (den Engelsman et al., 2009; Sugiyama et al., 2000). RT-qPCR analysis of SBMA muscle tissue (fig. 14B,C) shows that HSPB2 and HSPB3 genes are transcriptionally up-regulated only in symptomatic SBMA male mice, while they remained unchanged in all other conditions analysed. Moreover, to efficiently exert its pro-degradative activity, HSPB8 must associate to the co-chaperone BAG3; once the complex is formed and the misfolded protein recruited, these proteins interact with HSC70 and CHIP. Now misfolded proteins become ubiquitinated by CHIP and they are recognized by p62/SQSTM1 for their insertion into

autophagosomes. Alternately, when the co-chaperone BAG1 is up-regulated or when low levels of BAG3 are present, the HSC70-CHIP complex can interact with BAG1 which re-route misfolded proteins to UPS, rather than to autophagy. In this context, BAG3 levels, BAG1 levels and their ratio are essential to understand which pathway is preferred to clear misfolded proteins in a given cell type. Expression levels of BAG1 and BAG3 in SBMA muscle male mice were analysed by RT-qPCR. Fig. 15 shows that both co-chaperones are induced only in muscle of symptomatic SBMA male mice. However, the ratio measured is dramatically increased only in favour of BAG3 in symptomatic SBMA male mice. Collectively, these data clearly show that autophagy is preferentially activated in response to mutant ARpolyQ in muscle tissue of SBMA male mice.

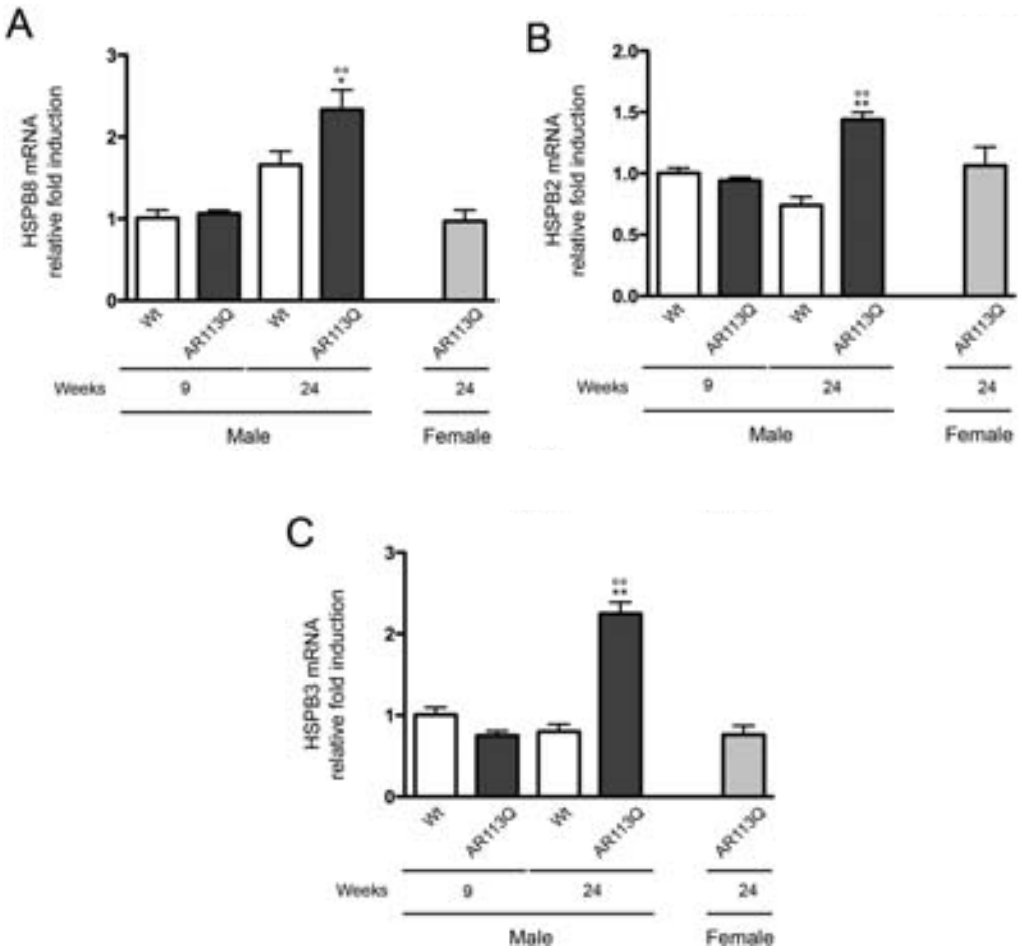

Figure 14 - Expression of pro-autophagic chaperones in quadriceps muscle of SBMA mouse model. RT-qPCRs were performed on total RNA extracted from quadricep muscles of male non-transgenic (Wt) mice, and of AR113Q mice at 9 (corresponding to presymptomatic stage) or 24 (corresponding to symptomatic stage) weeks of age. As additional control, quadriceps of female AR113Q mice at 24 weeks were used (n = 5). All animals were age-matched. Data have been normalized to the amount of GAPDH mRNA, expressed relative to the levels determined in Wt mice at 9 weeks taken as internal reference, and expressed as fold changes. Data are means ± SD of three independent replicates for Wt and AR113Q mice at 9 weeks, and of five independent replicates for Wt and AR113Q mice at 24 weeks. (A) RT-qPCR on HSPB8 mRNA expression levels in quadricep muscles. *$p<0.05$ vs. 24 weeks Wt mice; °°$p<0.001$ vs. 9 weeks AR113Q mice. (B) RT-qPCR on HSPB2 mRNA expression levels in quadricep muscles. **$p < 0.001$ vs. 24 weeks Wt mice; °°$p < 0.001$ vs. 9 weeks AR113Q mice. (C) RT-qPCR on HSPB3 mRNA expression levels in quadricep muscles. **$p<0.001$ vs. 24 weeks Wt mice; °°$p<0.001$ vs. 9 weeks AR113Q mice.

-

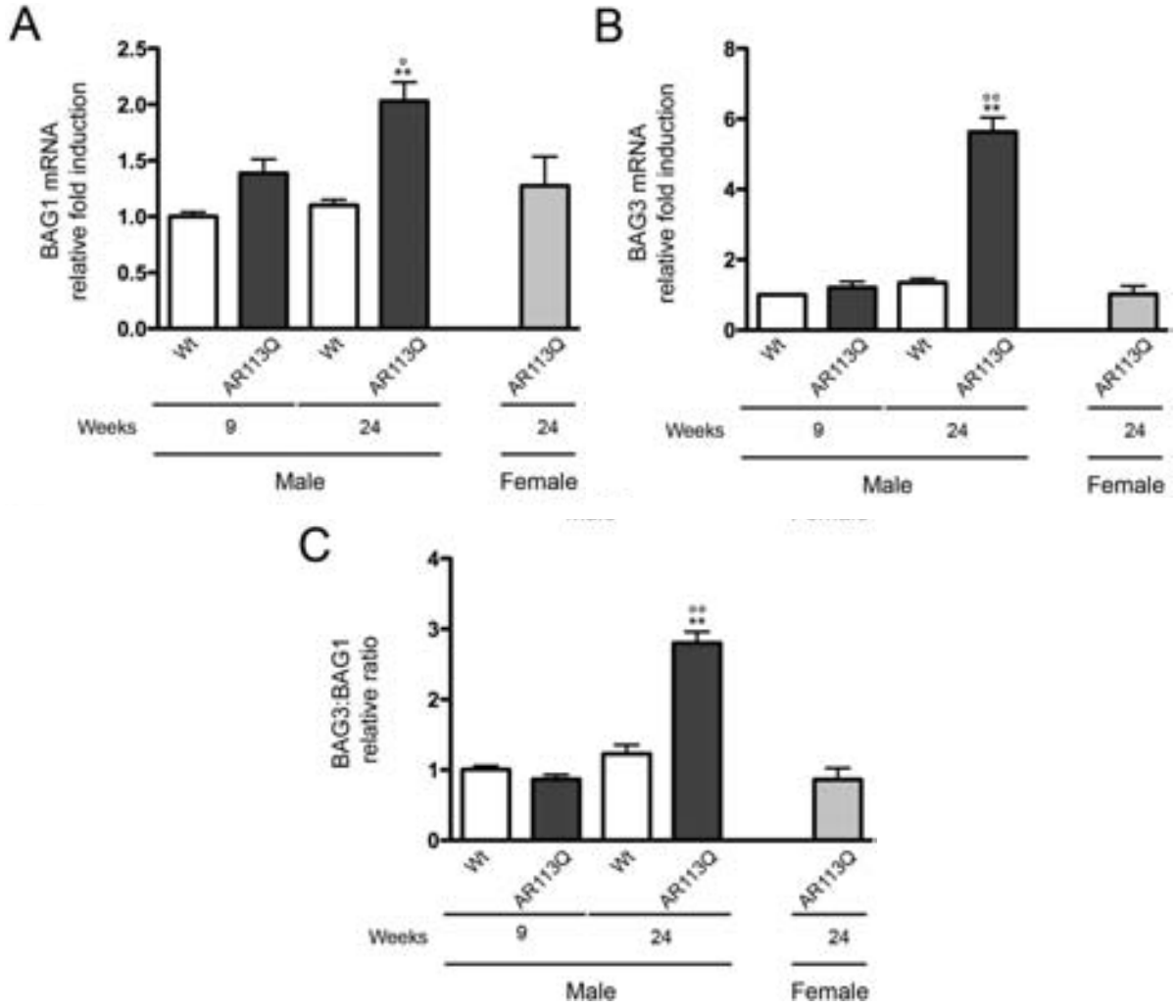

Figure 15 - Expression of BAG1 and BAG3 co-chaperones in quadriceps muscle of SBMA mouse model. RT-qPCRs were performed on total RNA extracted from quadricep muscles of male non-transgenic (Wt) mice, and of AR113Q mice at 9 (corresponding to presymptomatic stage) or 24 (corresponding to symptomatic stage) weeks of age. As additional control, quadriceps of female AR113Q mice at 24 weeks were used (n = 5). All animals were age-matched. Data have been normalized to the amount of GAPDH mRNA, expressed relative to the levels determined in Wt mice at 9 weeks taken as internal reference, and expressed as fold changes. Data are means ± SD of three independent replicates for Wt and AR113Q mice at 9 weeks, and of five independent replicates for Wt and AR113Q mice at 24 weeks. (A) RT-qPCR on BAG1 mRNA expression levels in quadricep muscles. **p<0.001 vs. 24 weeks Wt mice; °p<0.05 vs. 9 weeks AR113Q mice. (B) RT-qPCR on BAG3 mRNA expression levels in quadricep muscles. **p < 0.001 vs. 24 weeks Wt mice; °°p < 0.001 vs. 9 weeks AR113Q mice. (C) BAG3:BAG1 relative ratio of mRNA expression levels in quadricep muscles. Data represent variations of the relative levels of BAG3 and BAG1 normalized over the relative BAG3 and BAG1 levels of age-matched 9 weeks Wt mice. **p < 0.001 vs. 24 weeks Wt mice; °°p<0.001 vs. 9 weeks AR113Q mice.

-

Analysis of expression of proteins regulating autophagy in muscle of SBMA male mice

Next, we evaluated whether the expression modulation observed in HSPB8 related autophagic genes is reflected in variations of proteins levels. Western blot (WB) analysis showed that LC3-I drastically decrease in symptomatic SBMA male mice (Fig. 16 A,C) and that p62/SQSTM1 does not change between the analysed groups (Fig. 16 A,B), indicating that autophagy is activated in SBMA muscle tissue and that although p62/SQSTM1 mRNA is induced, p62/SQSTM1 is well cleared by autophagy. Also WB analysis (Fig. 16 A,D-G) showed that the levels of HSPB8, BAG3 are increased in symptomatic SBMA male mice while BAG1 levels are equal in all the groups analysed as observed in mRNA analysis. In addition, the BAG3:BAG1 ratio (Fig. 16 H) is confirmed as increased also in protein levels.

-

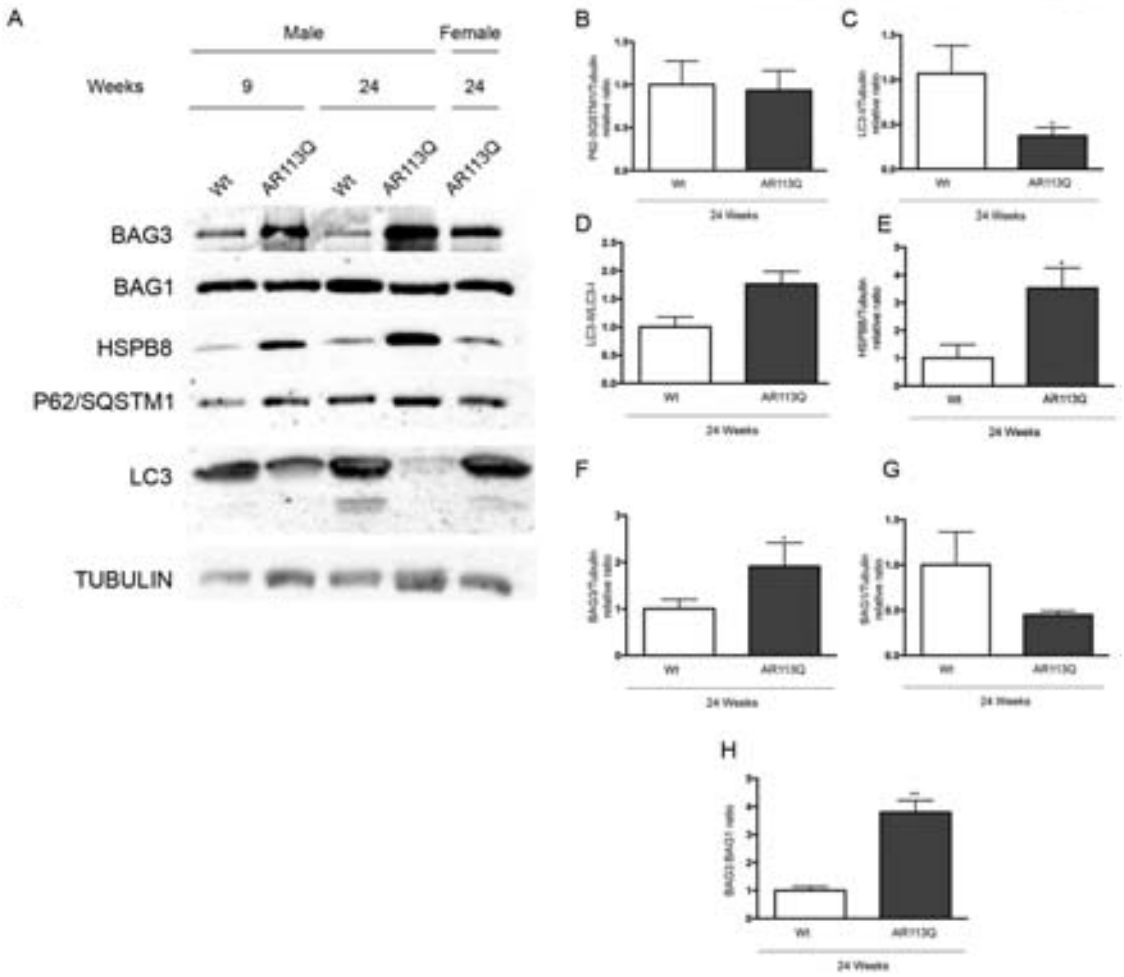

Figure 16 - Evaluation of the levels of proteins regulating autophagy and HSPB8-mediated response in skeletal muscle of symptomatic AR113Q male mice. (A) Western blot analysis perfomed on quadriceps of male wt and AR113Q mice at 9 and 24 weeks. As additional control, quadriceps of female AR113Q mice at 24 weeks were used. (B) Quantification of p62/SQSTM1 protein expression levels in in wt (n = 3) and AR113Q (n = 3) male mice at 24 weeks. The p62/SQSTM1 protein levels were normalized using tubulin as control. (C) Quantification of LC3-I protein expression levels in in wt (n=3) and AR113Q (n=3) male mice at 24 weeks. The LC3-I protein levels were normalized using tubulin as control. *p < 0.05 vs. 24 weeks Wt mice. (D) Quantification of the LC3-II/LC3-I ratio in wt (n=3) and AR113Q (n=3) male mice at 24 weeks. (E) Quantification of HSPB8 protein expression levels in in wt (n=3) and AR113Q (n=3) male mice at 24 weeks. The HSPB8 protein levels were normalized using tubulin as control; *p < 0.05 vs. 24 weeks Wt mice. (F) Quantification of BAG3 protein expression levels in in wt (n=3) and AR113Q (n=3) male mice at 24 weeks. The BAG3 protein levels were normalized using tubulin as control; *p < 0.05 vs. 24 weeks Wt mice. (G) Quantification of BAG1 protein expression levels in in wt (n=3) and AR113Q (n=3) male mice at 24 weeks. The BAG1 protein levels were normalized using tubulin as control. (H) Quantification of the ratio between BAG3 and BAG1 protein levels in wt (n=3) and AR113Q (n=3) male mice at 24 weeks; **p<0.001 vs. 24 weeks Wt mice.

-

Autophagic response in spinal cord of SBMA male mice

We then evaluated whether changes in PQC markers are also present in the spinal cords of the AR113Q mice at the pre-symptomatic and at the symptomatic stages. As is shown in Fig. 17 the expression analysis of Beclin-1, p62/SQSTM1, LC3, HSPB8, HSPB2, HSPB3, BAG1 and BAG3 (Fig. 17 (A–H), respectively) did not show detectable variation in the different groups tested, including symptomatic (24wks) AR113Q male mice. We only observed variation in the relative BAG3:BAG1 ratio (Fig. 8(i)), which in symptomatic AR113Q male mice is in favour of the BAG3 expression, suggesting the preferred activation of the autophagic pathway over the UPS pathway also in the spinal cord.

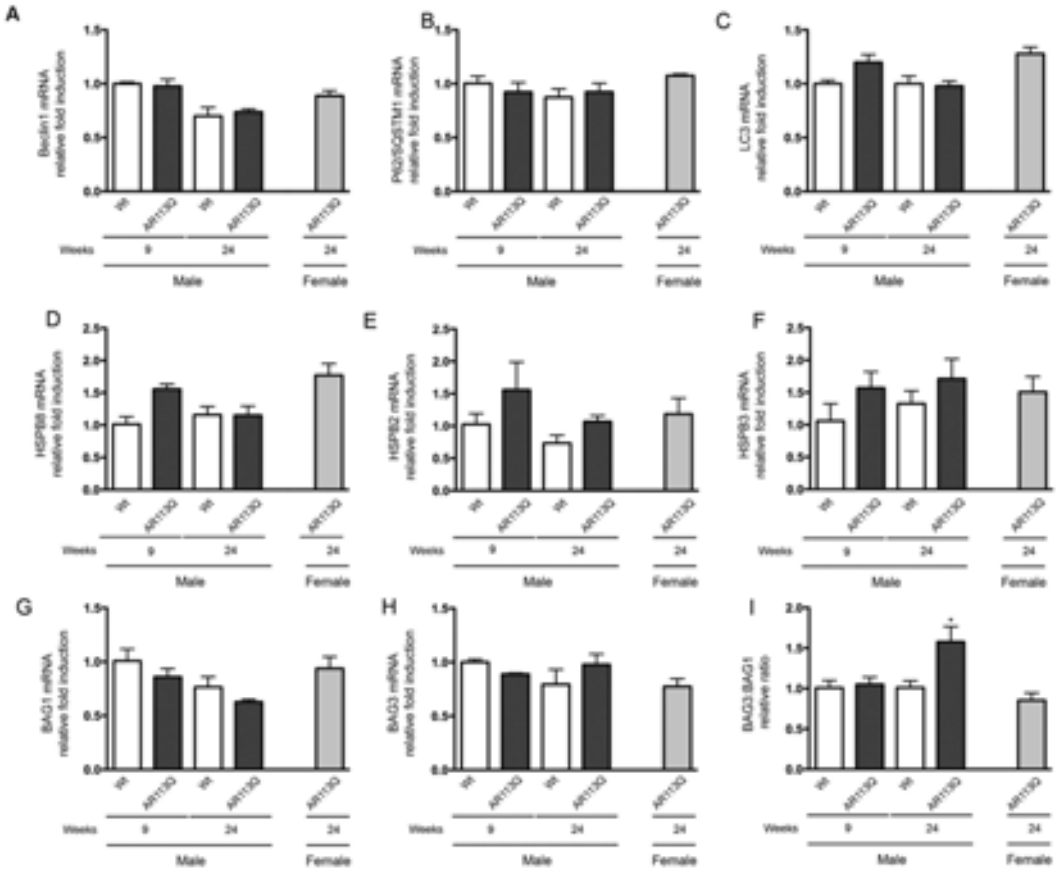

Figure 17 - Expression of autophagic markers, chaperones, and co-chaperones in spinal cords of SBMA mouse model. RT-qPCRs were performed on total RNA extracted from whole spinal cord of male non-transgenic (Wt) mice, and of AR113Q mice at 9 weeks (corresponding to presymptomatic stage) or 24 weeks (corresponding to symptomatic stage). As additional control, spinal cord of female AR113Q mice at 24 weeks were used (n = 5). All animals were age-matched. Data have been normalized to the amount of GAPDH mRNA, expressed relative to the levels determined in Wt mice at 9 weeks taken as internal reference, and expressed as fold changes. Data are means ± SD of three independent replicates for Wt and AR113Q mice at 9 weeks, and of five independent replicates for Wt and AR113Q mice at 24 weeks. (A) RT- qPCR on Beclin1 mRNA expression levels in spinal cord. (B) RT-qPCR on P62/SQSTM1 mRNA expression levels in spinal cord. (C) RT-qPCR on LC3 mRNA expression levels in spinal cord. (D) RT-qPCR on HSPB8 mRNA expression levels in spinal cord. (E) RT-qPCR on HSPB2 mRNA expression levels in spinal cord. (F) RT-qPCR on HSPB3 mRNA expression levels in spinal cord. (G) RT-qPCR on BAG1 mRNA expression levels in spinal cord. (H) RT-qPCR on BAG3 mRNA expression levels in spinal cord. (I) BAG3:BAG1 relative ratio of mRNA expression levels in whole spinal cord. Data represent variations of the relative levels of BAG3 and BAG1 normalized over the relative BAG3 and BAG1 levels of age-matched 9 weeks Wt mice. *p<0.05 vs. 24 weeks Wt mice.

HSPB8 prodegradative effect on ARpolyQ

We next confirmed that HSPB8 has a potent prodegradative effect on ARpolyQ soluble and insoluble species promoted by testosterone activation in NSC34 motoneuronal cells. As clearly show in high resolution immunofluorescence microscopy (HRFM) analysis (Fig. 18), the mutant ARpolyQ is localized in the cytoplasm of cells without testosterone. Subsequently, testosterone treatment induces ARpolyQ translocation into the nucleus. In addition, incomplete translocation resulted in aggregate formation in the perinuclear zone of 30-35% cells. These are visible as inclusions in IF analysis. The Heat Shock Protein (HSP) B8 over-expression, by facilitating autophagy, counteracts the misfolded ARpolyQ aggregation. In immunofluorescence (IF) analysis we showed that HSPB8 drastically reduces ARpolyQ inclusions induced by 10nM testosterone. We also evaluated the PBS-insoluble fraction of mutant ARpolyQ in filter retardation assay (FRA) with the cellulose acetate membrane that hold only proteins bigger than 0,2μm. FRA analysis (Fig. 18) revealed that testosterone induces mutant ARpolyQ retention on cellulose acetate confirming the presence of aggregates and PBS-insoluble mutant ARpolyQ species. Also, as is shown in IF analysis HSPB8 over-expression completely removes mutant ARpolyQ aggregates. Moreover, the evaluation of HSPB8 effect by western blot (WB) analysis showed the reduction of the total soluble ARpolyQ protein (Fig. 18).

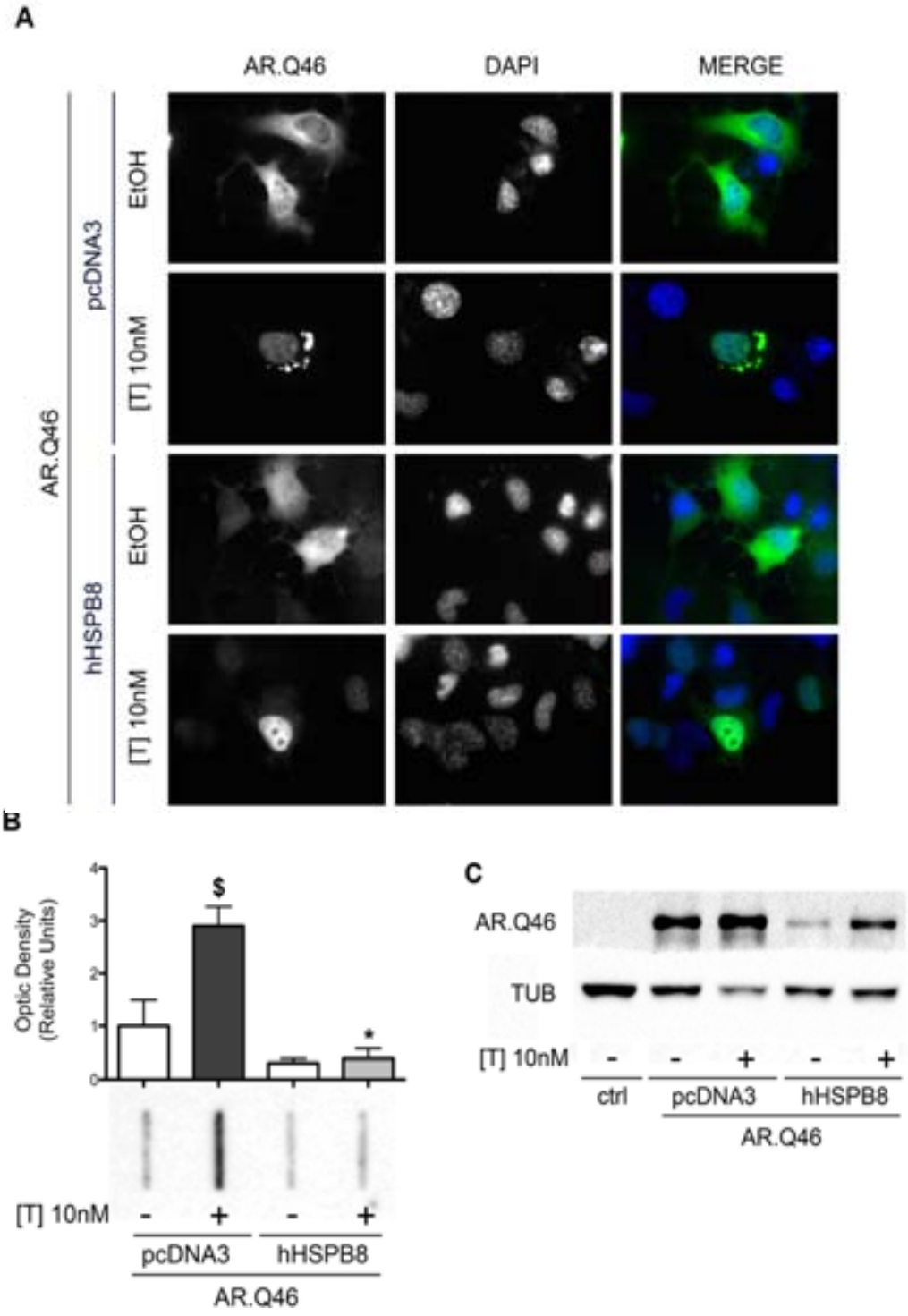

Figure 18 - Autophagic clearance of ARpolyQ. NSC34 cells transfected with AR.Q46 alone or with hHSPB8 treated with veichle (ethanol, EtOH) or 10 nM testosterone (T), for 48h. (A) High resolution immunofluorescence microscopy (HRFM) analysis (63x magnification) of AR (green); Nuclei stain with DAPI (blue). (B) Filter retardation assay (FRA) showed AR.Q46 insoluble fraction accumulation after 10 nM T treatment and reduction after HSPB8 over-expression. Histograms represent the densitometric analysis of three replicates for each sample ($=P<0,05 vs. EtOH; *=p<0,05 vs. T). (C) WB analysis of AR.Q46 soluble fraction, β-tubulin was used as loading control.

Dynein silencing effect on NSC34 cells morphology, ARpolyQ aggregates and autophagy

HSPB8 recognizes misfolded proteins and target them to autophagy. This process is mediated by misfolded proteins and HSPB8-BAG3-HSC70-CHIP complex formation that may transport misfolded proteins at MTOC for the subsequent insertion into autophagosome. The transport is mediated by dynein motor proteins that with 14-3-3 proteins interacts with BAG3 and indirectly with misfolded proteins. Thus, dynein mediated this retrograde transport and it is essential for autophagic degradation of misfolded proteins. However, if autophagy is overwhelmed, dynein may contribute to concentrate misfolded proteins to MTOC where they can normally interact to form aggregates. To test the role of dynein we designed a specific siRNA recognizing the heavy chain 1 of cytoplasmic dynein1 (DYNC1H1 siRNA) in order to worsen the autophagy and the overall ARpolyQ clearance.

As is shown in the phase contrast microscopy and in the HRFM (Fig. 19 A), DYNC1H1 siRNA reduces the dynein cytoplasmic levels and induces a mild change in cell morphology. After DYNC1H1 siRNA transfection, the dynein level reduction is also confirmed in WB analysis (Fig. 19 B) where dynein protein almost disappears. The densitometric analysis clearly shows a reduction of approximately 80%. Next, we analysed the effect of dynein silencing on aberrant biochemical properties of mutant ARpolyQ. We silenced dynein in immortalized motoneuronal cell line (NSC34 cells) stably transfected with inducible GFP-tagged AR.Q39. Unexpectedly, dynein silencing reduces the levels of PBS insoluble species of mutant ARpolyQ evaluated by FRA (Fig.

19 C). Densitometric analysis clearly shows the reduction of testosterone induced mutant ARpolyQ retained on the cellulose acetate membrane.

We then analysed the consequence of dynein perturbation on autophagy by the localization of LC3 and p62/SQSTM1 proteins responsible for autophagosome formation. As expected, the dynein silencing resulted in an impaired autophagy as showed by the HRFM of LC3 and p62/SQSTM1 autophagic markers that clearly shows the accumulation on LC3 and p62/SQSTM1 into large autophagosome and p62/SQSTM1 bodies (Fig. 19 D) confirming perturbed autophagy without functional dynein transport.

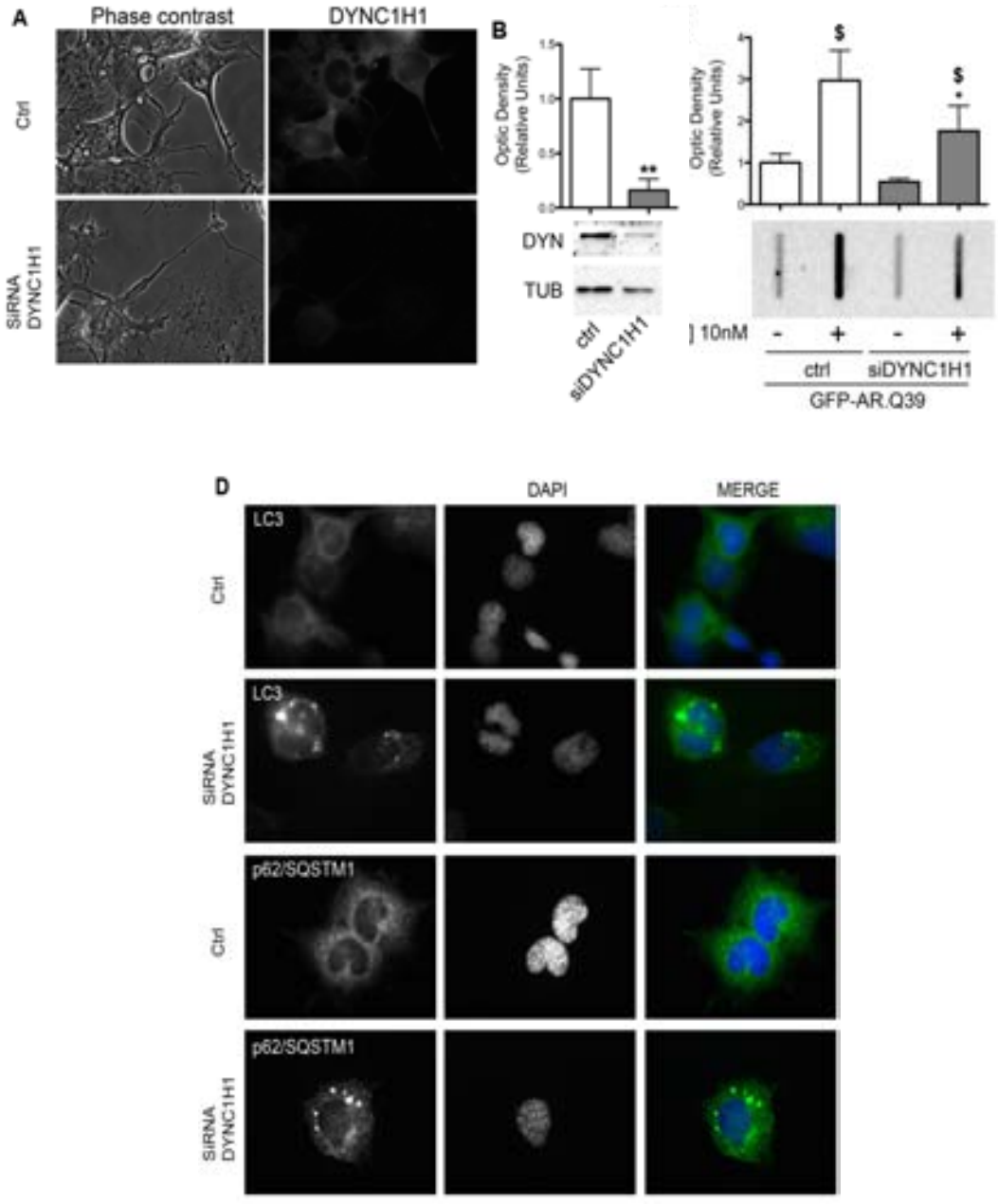

Fig. 19 - Effect of dynein silencing on autophagy and ARpolyQ clearance.

(A) Phase contrast and HRFM performed on NSC34 cells transfected with dynein 1 heavy chain 1 (DYNC1H1) siRNA shows cell morphology and dynein distribution. (B) WB analysis of NSC34 cells transfected with DYNC1H1 siRNA shows the levels of dynein heavy chain; β-tubulin was used as loading control. Histogram represents the densitometric analysis of three replicates for each sample (**=p<0,01 vs. control) (C) FRA of NSC34 stably expressing GFP-AR.Q39 and transfected with DYNC1H1 siRNA shows AR.Q39 PBS insoluble fraction accumulation after 10 nM T treatment and reduction after dynein silencing. Histogram represents the densitometric analysis of three replicates for each sample ($=p<0,05 vs. relative EtOH; *=p<0,05 vs. T); (D) HRFM performed on NSC34 cells transfected with DYNC1H1 siRNA shows sequestosome 1 (p62/SQSTM1) or Microtubule-associated proteins 1A/1B light chain 3A (LC3) distribution (green); nuclei were stained with DAPI (blue) (63x magnification).

Effects of dynein inhibition with EHNA on ARpolyQ clearance

Dynein silencing efficiency is mediated by the number of cells that receive the siRNA during transfection. Although we have obtained a great silencing efficiency (Fig. 19 B) not all cells picked up siRNA at the same amount.

In order to avoid this and to more deeply analyse the role of dynein motor function impairments in the clearance of mutant ARpolyQ we also used pharmacologic inhibitors of dynein activity. This approach allowed us to inhibit dynein activity in all treated cells. Among the two small molecules generally used as dynein inhibitors, vanadate and erythro-9-[3-2-(hydrosynonyl)]adenine (EHNA), only the latter is highly specific for the ATP binding site of dynein. EHNA inhibits the ATPase and motor activities of cytoplasmic dynein thus blocking the microtubule-based transport toward the MTOC. We treated the cell with 100 μM of EHNA.

Thus, we confirmed our previously data obtained in dynein-silenced cells. In FRA, EHNA greatly reduced the accumulation of testosterone-induced PBS insoluble misfolded ARpolyQ (AR.Q46; Fig. 20 A) in transiently transfected NSC34 cells.

In parallel, we demonstrated that in WB analysis (Fig 20 B) the effect of EHNA was not mediated by a reduction of the overall content of soluble ARpolyQ, but EHNA clearly shows a shift between the PBS and/or Triton insoluble fraction (possibly responsible for inclusion appearance in IF and aggregation in FRA) to the PBS soluble fraction of ARpolyQ (Fig. 20 C). In addition, EHNA treatment lead to a dramatic reduction of the overall amount of SDS-insoluble ARpolyQ species, normally present in large amounts in the stacking gels of EHNA-untreated ARpolyQ samples (Fig. 20 C). Next, we examined the effects of dynein inhibition on the formation of inclusion of misfolded ARpolyQ in

NSC34 cells expressing mutant AR.Q46. The immunofluorescence microscopy analysis shows that EHNA treatment lead to the complete clearance of cytoplasmic aggregates of ARpolyQ induced by testosterone (Fig. 20 D).

-

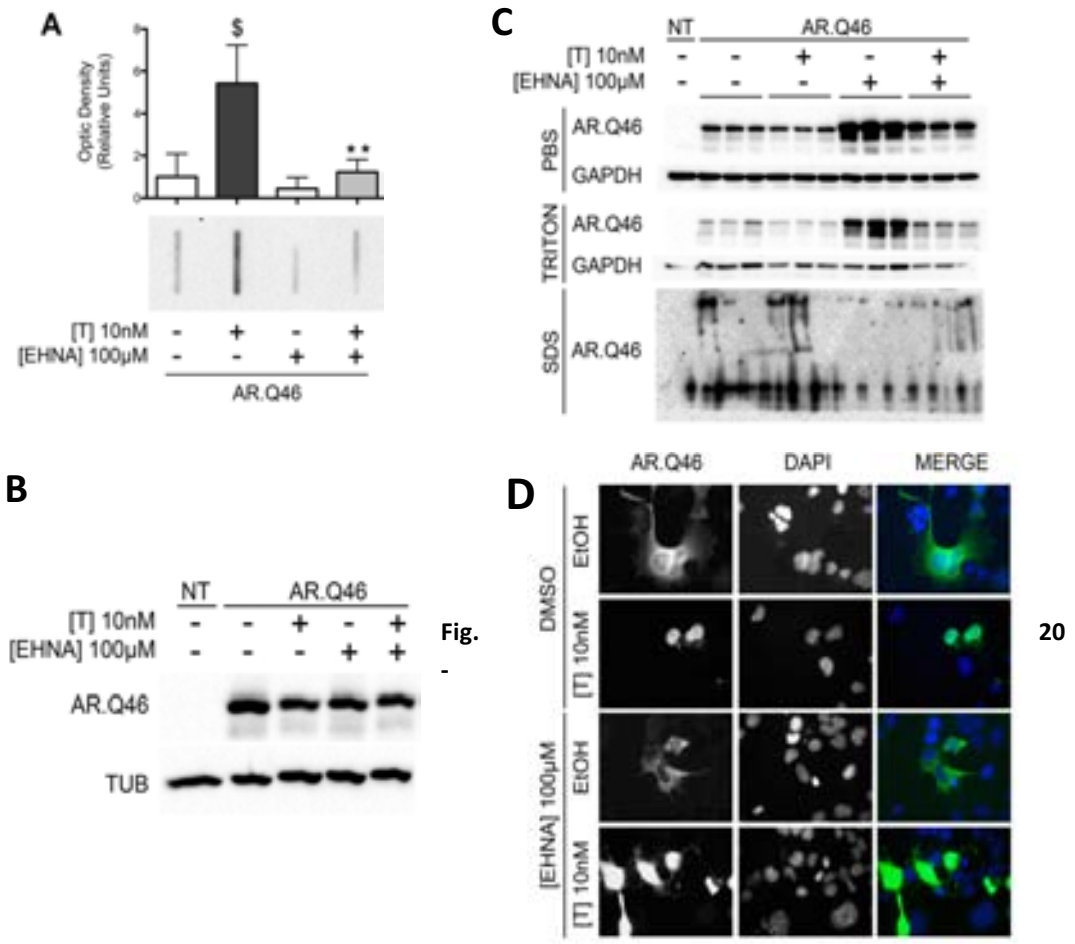

Fig. 20 -

Effect of dynein ATPase activity inhibition on AR.Q46 clearance.

NSC34 cells transfected with ARQ.46 and treated with ethanol (EtOH) or 10 nM testosterone (T) and/or EHNA 100 M for 48 hours. (A) Filter retardation assay (FRA) shows ARpolyQ PBS insoluble fraction ($=p<0.05 vs. EtOH; *=p<0.05 vs. T); (B) WB analysis on NSC34 cells transfected with AR.Q46 and treated with 10 nM T or EtOH and 100 μM EHNA or DMSO for 48 hours shows AR.Q46 soluble fraction, α-tubulin was used as loading control; (C) WB analysis on PBS, Triton X100 and SDS lysates fraction of NSC34 cells transfected with AR.Q46 and treated with 10nM T or EtOH and 100 μM EHNA or DMSO for 48 hours, GAPDH was used as loading control (D) HRFM performed on NSC34 cells transfected with AR.Q46 and treated with 10 mM T or EtOH and 100 μM EHNA or DMSO for 48 hours, AR was stained with AR H280 antibody (green), nuclei were stained with DAPI (blue) (63x magnification).

-

In order to validate the prodegradative effect of EHNA treatment observed in overexpressed ARpolyQ SBMA cell model, we extended our analysis to two alternative inducible and stable models of SBMA: i) the NSC34 motoneuronal cells expressing the GFP-AR.Q39 and ii) the PC12 neuronal-like expressing the AR.Q112. The NSC34 cells were developed to normalized the ARpolyQ levels in every cells. FRA in Fig. 21 A shows that the PBS insoluble mutant ARpolyQ levels observed in NSC34 expressing GFP-AR.Q39 are testosterone dependent and also increase when PQC degradative pathways are inhibited with 3-MA and MG132 compound to block autophagy and proteasome chimotryptic activity respectively. Notably, also in this case, EHNA treatment reverted the accumulation of most of the misfolded PBS insoluble species of ARpolyQ. In parallel, in PC12/AR.Q112 SBMA (developed by Dr. Diane Merry (TJU, Philadelphia, PA, USA)) inducible model characterized by an extremely long polyQ highly prone to intra-nuclear aggregates, we similarly observed the effects shown in Fig. 21 B.

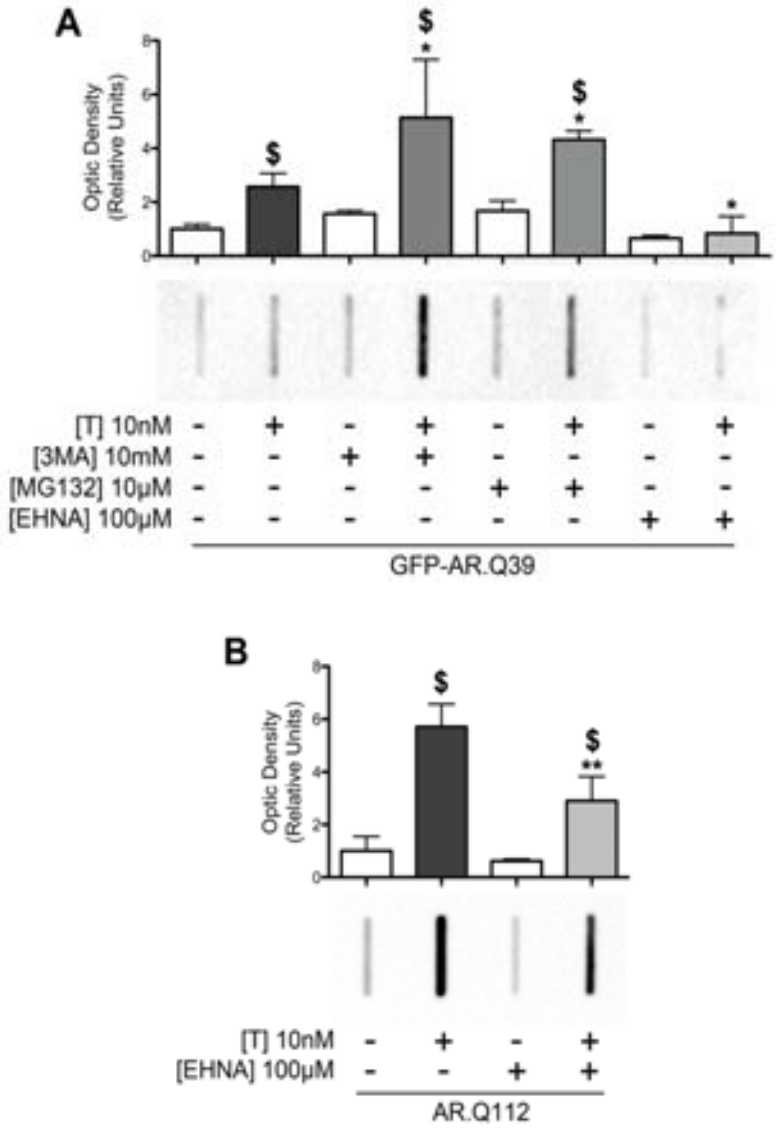

Figure 21 - Effect of dynein ATPase activity inhibition on ARpolyQ (Q.39 and Q.112) clearance.
Filter retardation assay (FRA) shows ARpolyQ insoluble fraction of: (A) NSC34 cells stably transfected with GFP-ARQ.39 induced with 1 μg/mL doxycycline for 72 hours and treated with 10 nM testosterone and/or 100 μM EHNA and/or 10 mM 3-MA for last 48 hours and/or 10 μM MG132 for last 16 hours ($=p<0.05 vs. relative EtOH; *=p<0.05 vs. T); (C) PC12 cells stably transfected with AR.Q112 induced with 1 μg/mL doxycycline for 72 hours and treated with 10 nM testosterone and/or 100 μM EHNA for last 48 hours ($=p<0.05 vs. relative EtOH**=p<0.01 vs. T). Histograms represent the densitometric analysis of three replicates for each sample.

Analysis of viability of NSC34 cells treated with EHNA

In order to confirm the specific pro-degradative effect of dynein ATPase activity inhibition, we tested EHNA possible interference with cells viability and/or transfected protein over-expression. First, to exclude toxic effect of EHNA treatment we performed a MTT assay to measure the viability of NSC34 cells after EHNA treatment. MTT assay is a colorimetric assay that measures the cell metabolic activity and, in a certain condition, evaluates the number of viable cells in the sample. Thanks to NADPH dependent oxidoreductase enzymes, that catalyse the reduction of the tetrazolium dye MTT to its insoluble and purple coloured formazan, we can evaluate the enzymatic activity and then the viability of the cells. Fig. 22 shows the spectrophotometric quantification of formazan of six independent replicates for each condition analysed. It is clear that EHNA treatment does not influences the viability of used cell model. Next to exclude the interference with transfected protein over-expression, we performed the classical β-galactosidase assay. The result is shown in Fig. 22 and represents the colorimetric analysis of 6 independent replicates for each condition analysed. Even in this case, EHNA treatment does not alter the expression of transfected β-galactosidase protein. Collectively, these experiments exclude that EHNA effect on misfolded ARpolyQ is not caused by toxic unspecified effect or by interference with disease cell models.

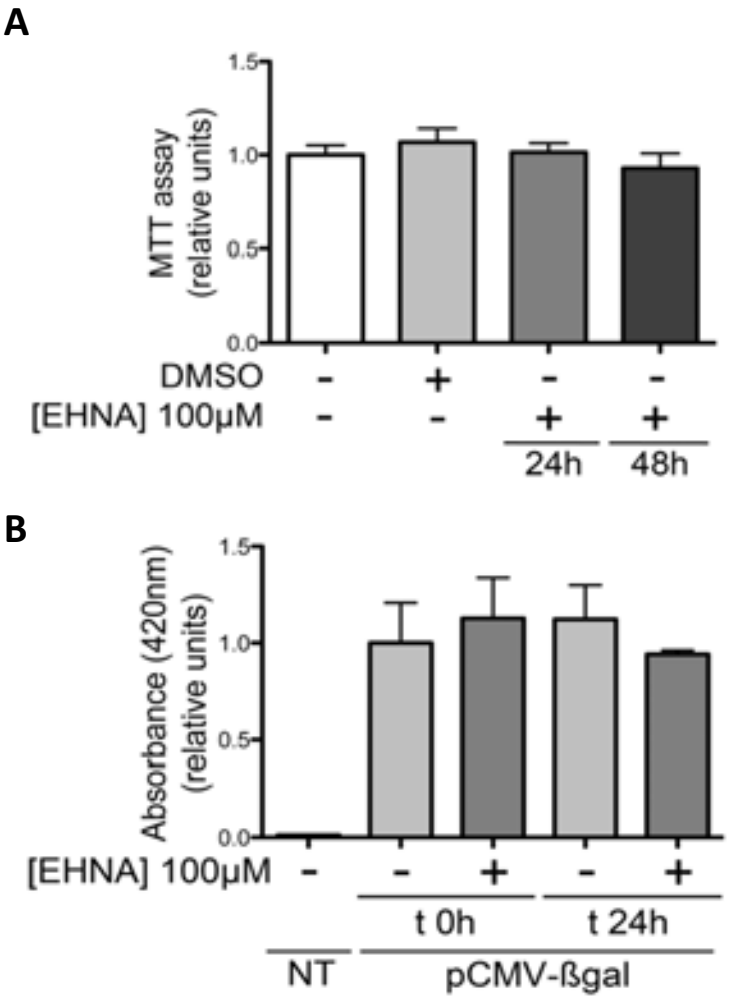

Figure 22 - Viability of NSC34 cells EHNA treated. (A) MTT assay performed on NSC34 cell treated with DMSO or 100 μM EHNA for 24 or 48 hours. (B) β-galactosidase assay performed on NSC34 cells transfected with pCMV-β and treated with DMSO or 100 μM EHNA for 24 or 48 hours after transfection; Histograms represent the analysis of six replicates for each samples.

Pro-degradative effect of EHNA on ARpolyQ

To evaluate which pathway is mainly involved in the enhanced solubility of testosterone-induced misfolded ARpolyQ species after inhibition of the dynein-mediated transport to MTOC, we selectively blocked the two major pathways of degradation. As is shown in Fig. 23, both the inhibition of autophagy with 3-MA and of the proteasome with MG132 resulted in a significant increase of insoluble misfolded ARpolyQ species in FRA. These species are considerably more abundant after 3-MA than MG132 treatment. However, dynein inhibition with EHNA is still able to reduce insoluble misfolded ARpolyQ species when autophagy is blocked with 3-MA, but not when proteasome is inhibited by MG132. These data strongly indicate that proteasome and not autophagy, is required to clear insoluble misfolded ARpolyQ species that cannot be transported and concentrated at MTOC to form the aggresomes.

-

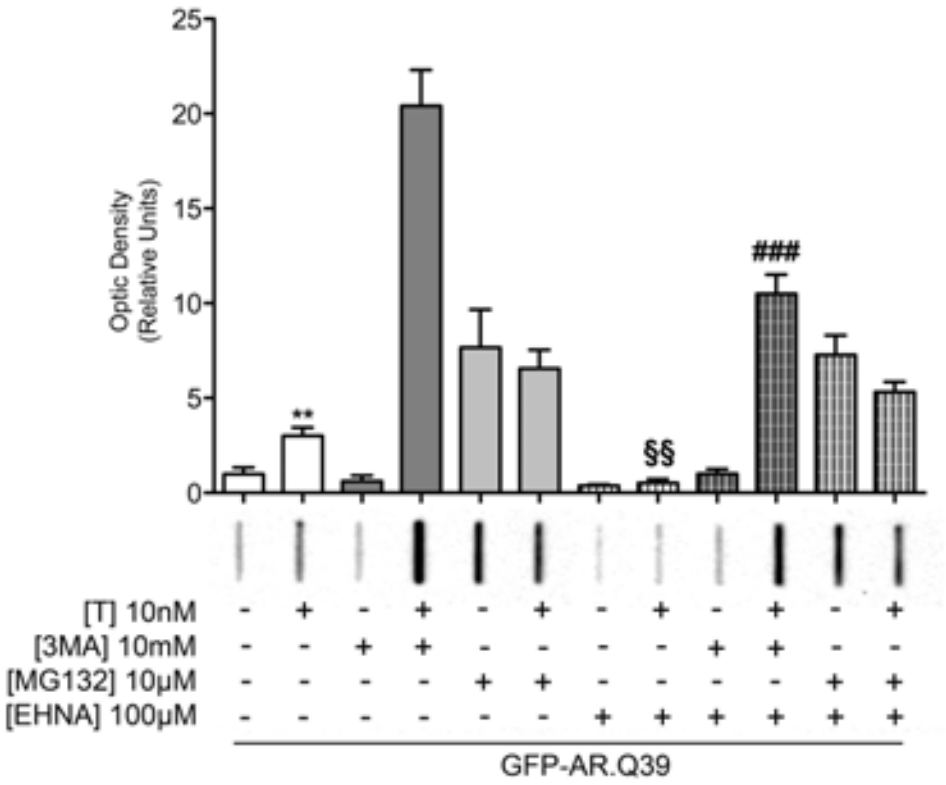

Figure 23 - Dynein ATPase activity inhibition promotes ARpolyQ clearance via UPS.

NSC34 stably transfected with GFP-AR.Q39 treated with 10 nM testosterone, 10 mM 3-MA and/or 100 M EHNA for last 48 hours and/or 10 M MG132 for last 16 hours. FRA shows ARpolyQ insoluble fraction (**=p<0.01 vs. EtOH; §§=p<0.01 vs. T; ##=p<0.01 vs. T/3MA); Histograms represent the densitometric analysis of three replicate for each samples .

-

Treatment with EHNA enhances UPS mediated degradation of misfolded proteins

To test whether UPS degradation is promoted by EHNA, we used the proteasome reporter GFPu, which consists of the GFP protein tagged with a short degron (CL1) capable to target the protein to proteasome for degradation (Rusmini et al., 2007; Sau et al., 2007; Bence et al., 2001). Any condition which perturb the proteasome activity will result in GFPu accumulation into the cells (Giorgetti et al., 2015; Rusmini et al., 2013; Rusmini et al., 2011; Rusmini et al., 2010). With this system, we confirmed our previous data showing that the formation of testosterone-inducible insoluble misfolded ARpolyQ species correlates with proteasome desaturation. Indeed, as is shown in Fig. 24 A, GFPu accumulates in NSC34 cells expressing the mutant AR (in its soluble form) in absence of testosterone, but it is rapidly cleared by the same cells after testosterone treatment (which induces ARpolyQ aggregation). Interestingly, dynein inhibition with EHNA resulted in a better clearance of GFPu when UPS was partially impaired, suggesting that the blockage of misfolded protein transport does not impair the proteasome activity even if the proteasome has to deal with larger fraction of proteins to be processed. We also confirmed that, in immortalized motoneuronal NSC34 cells, EHNA treatment has no direct effects (neither positive, nor negative) on the chimotryptic activity of the proteasome (Fig. 24 B).

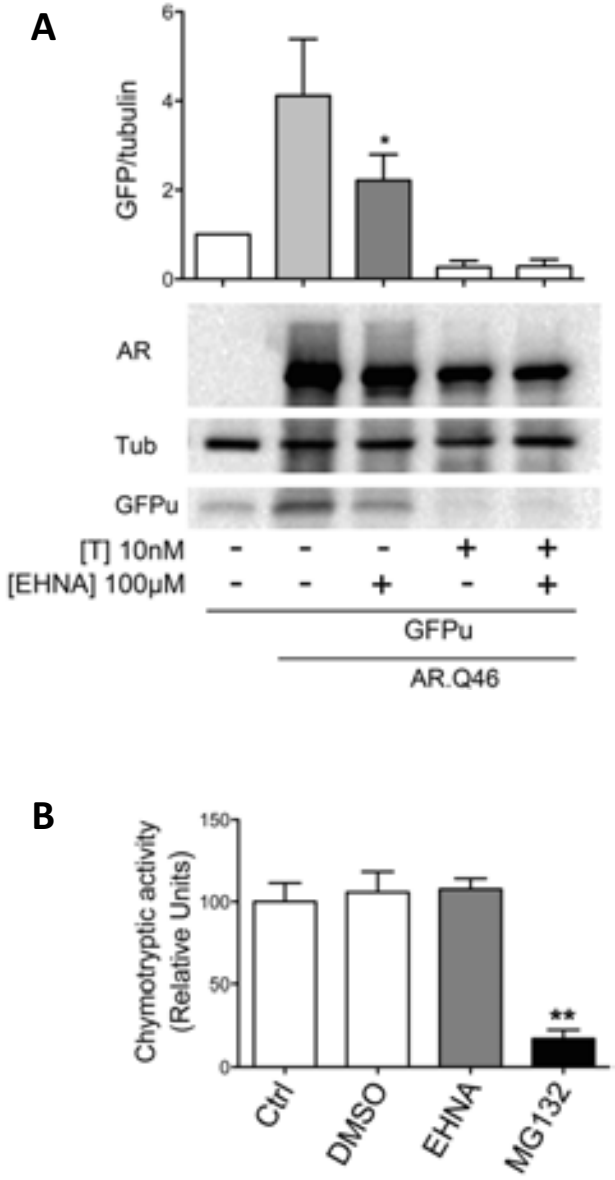

Figure 24 - Proteasome response in EHNA treated NSC34 cells.

(A) NSC34 cells transfected with GFPu reporter and/or ARpolyQ and treated with 10nM T and/or 100 μM EHNA. WB shows ARpolyQ and GFPu bands (*=p<0.05 vs. EtOH). β-tubulin was used as loading control; (B) Proteasome chimotryptic activity was performed on NSC34 treated with DMSO or 100 μM EHNA and 10 μM MG132 as negative control (**=p<0.01 vs. ctrl).

The autophagic response in EHNA treated NSC34 cells

In cells treated with EHNA, mutant ARpolyQ may be degraded more efficiently via the proteasome as a consequence of impaired autophagy. We then studied whether EHNA affected autophagy flux in basal conditions and upon stimulation with trehalose, a well-known mTOR-independent autophagy activator (Giorgetti et al., 2015; Zhang et al., 2014; Rusmini et al., 2013; Sarkar et al., 2007; Tanaka et al., 2004). First of all, EHNA alone has no effects on p62/SQSTM1 or on LC3 protein (Fig. 25 A, upper and middle insets, respectively; quantification in Fig. 25 B and Fig. 25 C, respectively) and mRNA (Fig. 25 D and 25 E, respectively) even if a mild, but not significant, increase of the levels of these transcripts can be detected in RT-qPCR analysis. In addition, EHNA does not significantly alter the LC3-II/LC3-I ratio measured by western blot (Fig. 25 C). We observed only subtle changes in the LC3 distribution (from LC3-I diffuse to LC3-II punctate distribution) and a mild increase of p62/SQSTM1 levels, with few p62/SQSTM1 bodies after EHNA treatment (Fig. 25 F). Thus, dynein inhibition with EHNA does not significantly affects autophagy in basal conditions. As expected, 3-MA treatment increased the LC3-II/LC3-I ratio, but this effect was partially counteracted by EHNA. Trehalose was able to significantly increase the LC3-II/LC3-I ratio (Fig. 25 C), which suggests an enhanced conversion of LC3 from its diffuse to its lipidated, authophagosome associated form (as also clearly evidenced and confirmed by the IF analysis in Fig. 25 F), a conversion required to start the initial autophagic steps. The effect of trehalose on the LC3-II/LC3-I ratio was significantly, even if not completely, inhibited by EHNA, and this was accompanied by a significant increase in the number and size of p62/SQSTM1 bodies (Fig. 25 F).

Collectively, these observations strongly suggest that EHNA prevents the lipidation of LC3 (to LC3-II) induced by trehalose and its association to nascent autophagosomes, and further suggests that, under our experimental conditions, the decreased levels of aggregated misfolded ARpolyQ is not due to increased degradation via autophagy

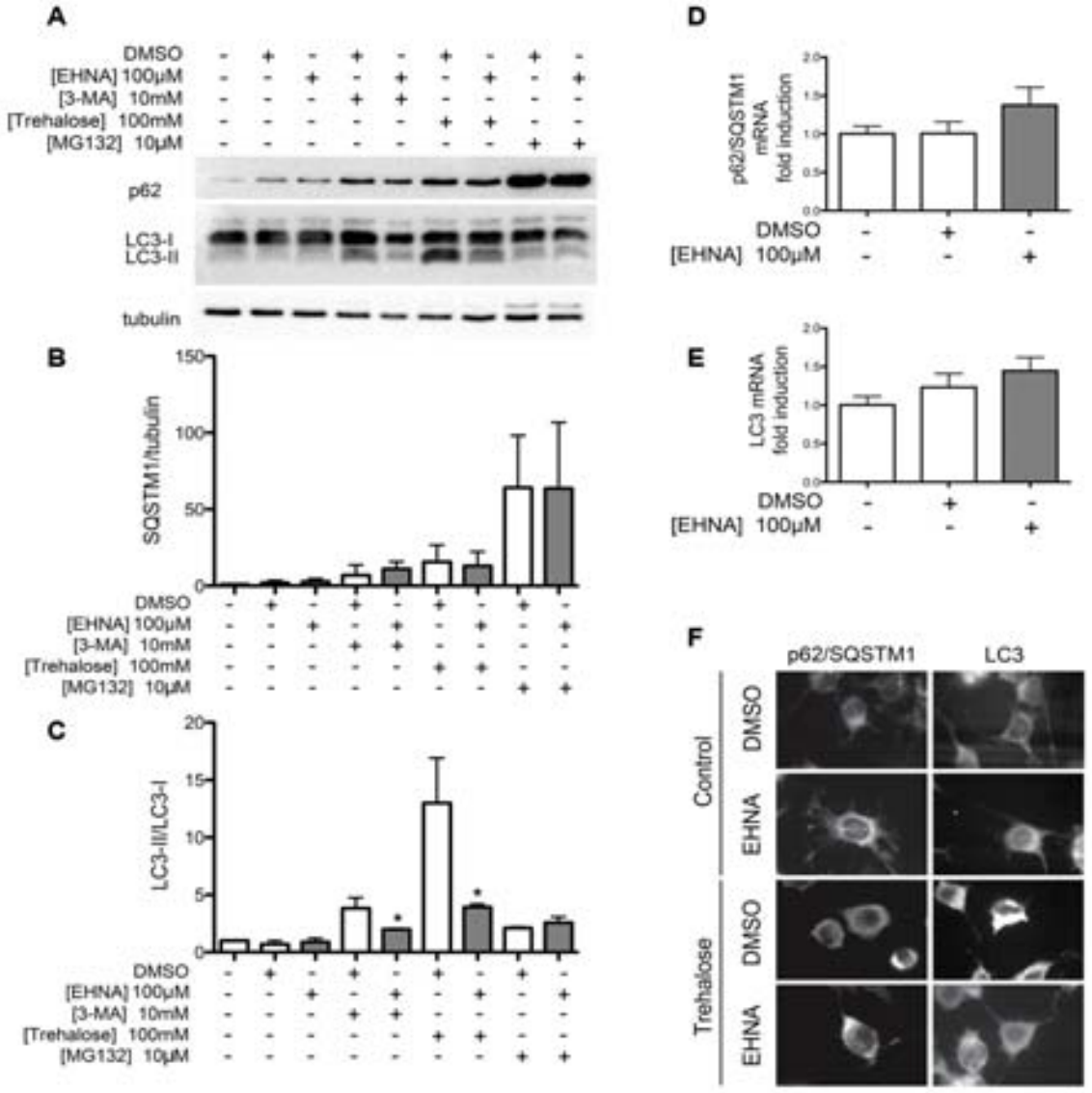

Figure 25 - Autophagy modulation by EHNA treatment.

NSC34 cells treated with DMSO, 100 M EHNA, 10 mM 3-MA, trehalose and/or 10 M MG132 for 48 hours; (A) WB analysis show p62-SQSTM1, LC3 levels; -tubulin was used as loading control; the histograms represent densitometric quantification of three replicates for each sample of p62-SQSTM1 (B) and LC3II/LC3I ratio (C) (*=p<0.05 vs. 3-MA or trehalose); (D,E) the histogram represents p62-SQSTM1 and LC3 mRNA levels normalized with RplP0 mRNA levels. Analysis was conducted on four samples (F) HRFM shows p62-SQSTM1 and LC3 localization (63x magnification).

The effect of EHNA on chaperone and co-chaperones levels

As previous results describe, chaperone and co-chaperone levels are essential to control the PQC removal of misfolded ARpolyQ and misfolded proteins in general. Here HSPB8 and BAG3 are necessary to target autophagic substrates to autophagy and BAG1 is necessary to target proteasome substrates to UPS. Here the BAG3:BAG1 ratio is an indicator of preponderant degradative pathway. Here we analysed by RT-qPCR the HSPB8, BAG3 and BAG1 mRNA levels in NSC34 cells treated with EHNA. Fig. 26 shows the analysis results where EHNA increased only BAG1 mRNA levels without alteration in HSPB8 and BAG3 levels.

We also extended our analysis on human SBMA iPSCs differentiated to motor neuron. After 14 days to obtain embryo bodies and 12 days in motoneuronal medium we treated our culture with testosterone and/or EHNA. Then, by RT-qPCR we analysed the mRNA levels of HSPB8, BAG3 and BAG1. As is shown in Fig. 27: i) HSPB8 level is equal in all conditions analysed (Fig. 27 A), ii) BAG3 is significantly increased when motor neuron culture is treated with testosterone and EHNA, but it slightly increased also in absence of EHNA (Fig. 27 B). Interestingly, EHNA drastically increases BAG1 mRNA level of motor neuron culture treated with testosterone and in their controls (Fig. 27 C). In conclusion, BAG1 expression analysis, in NSC34 cells and testosterone-treated MN iPSCs, strongly support our working hypothesis.

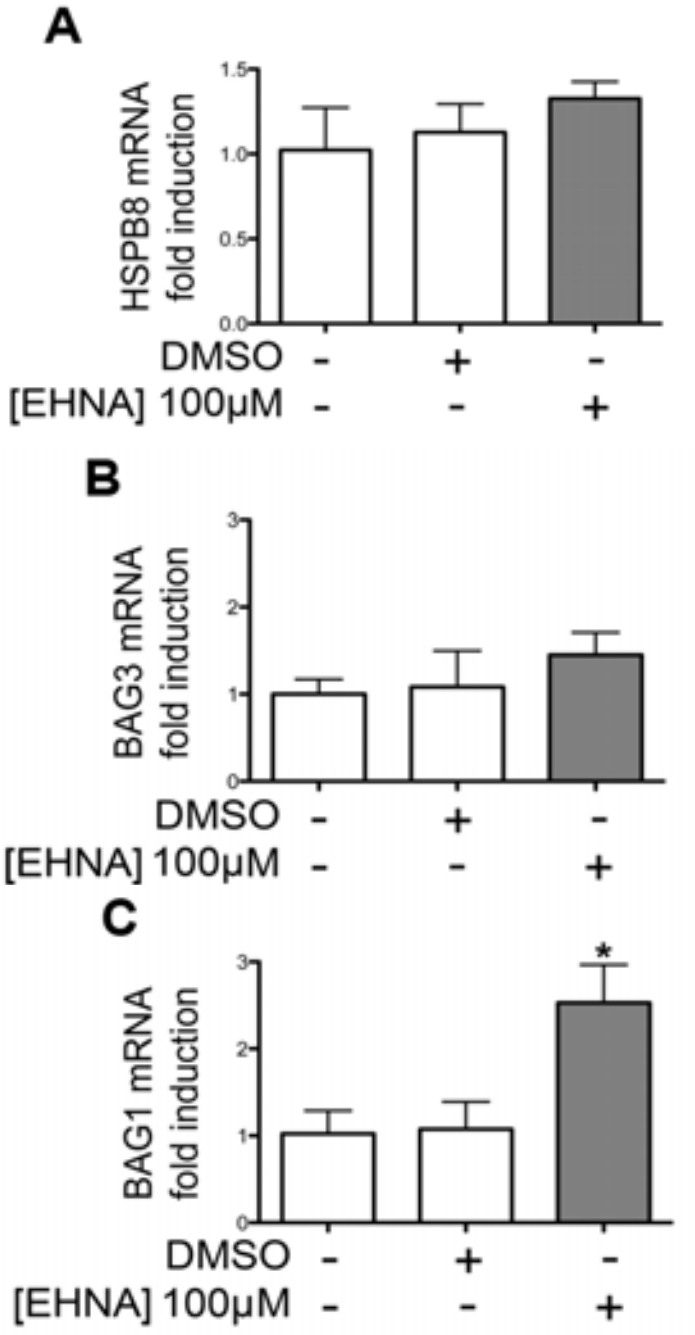

Figure 26 - Chaperones levels of EHNA treated NSC34 cells

NSC34 cells treated with DMSO or 100 µM EHNA for 48 hours. The histograms represent HSPB8, BAG3 and BAG1 mRNA levels normalized with RplP0 mRNA levels, four samples for each condition were analysed (*=p<0.05 vs. DMSO).

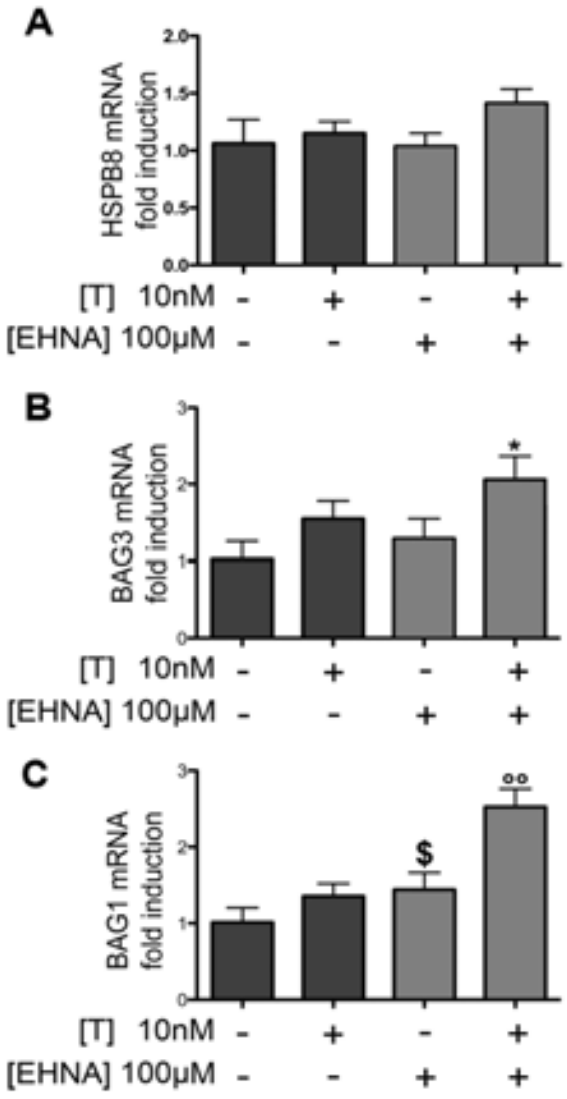

Figure 27 - Chaperones levels of EHNA treated motoneuronal differentiated iPS cells

MNs obtained from Kennedy's patients iPS cells treated with 10 nM testosterone (T) and/or 100 μM EHNA for 48 hours. The histograms represent HSPB8, BAG3 and BAG1 mRNA levels normalized with RplP0 mRNA levels, four samples for each condition were analysed (*=p<0.05 vs. T; $=p<0.05 vs. EtOH; °°=p<0.01 vs. T);

BAG1 mediates ARpolyQ UPS degradation

We then tested the functional significance of BAG1 up-regulation on misfolded ARpolyQ clearance upon inhibition of dynein-mediated transport. As expected, the FRA analysis (Fig. 28 A) shows that BAG1 over-expression completely prevents the accumulation of ARpolyQ retained on the cellulose acetate membrane. We also checked the BAG1 over-expression by WB analysis (panel 28 A lower inset). The reduction of misfolded ARpolyQ confirms the pro-degradative effect of BAG1.

Next, we wondered whether the pro-degradative function of BAG1 was dependent on a functional proteasome. FRA in Fig. 28 B shows that the proteasome inhibition, by MG132 o/n treatment, fully prevents the pro-degradative activity of BAG1 on testosterone-inducible insoluble misfolded ARpolyQ species in NSC34 cells. These data confirm that by preventing the HSPB8/BAG3(14-3-3) dynein-directed accumulation of misfolded ARpolyQ at the MTOC, the cells allow an optimized BAG1 recognition and proteasome degradation of the monomeric misfolded ARpolyQ species.

-

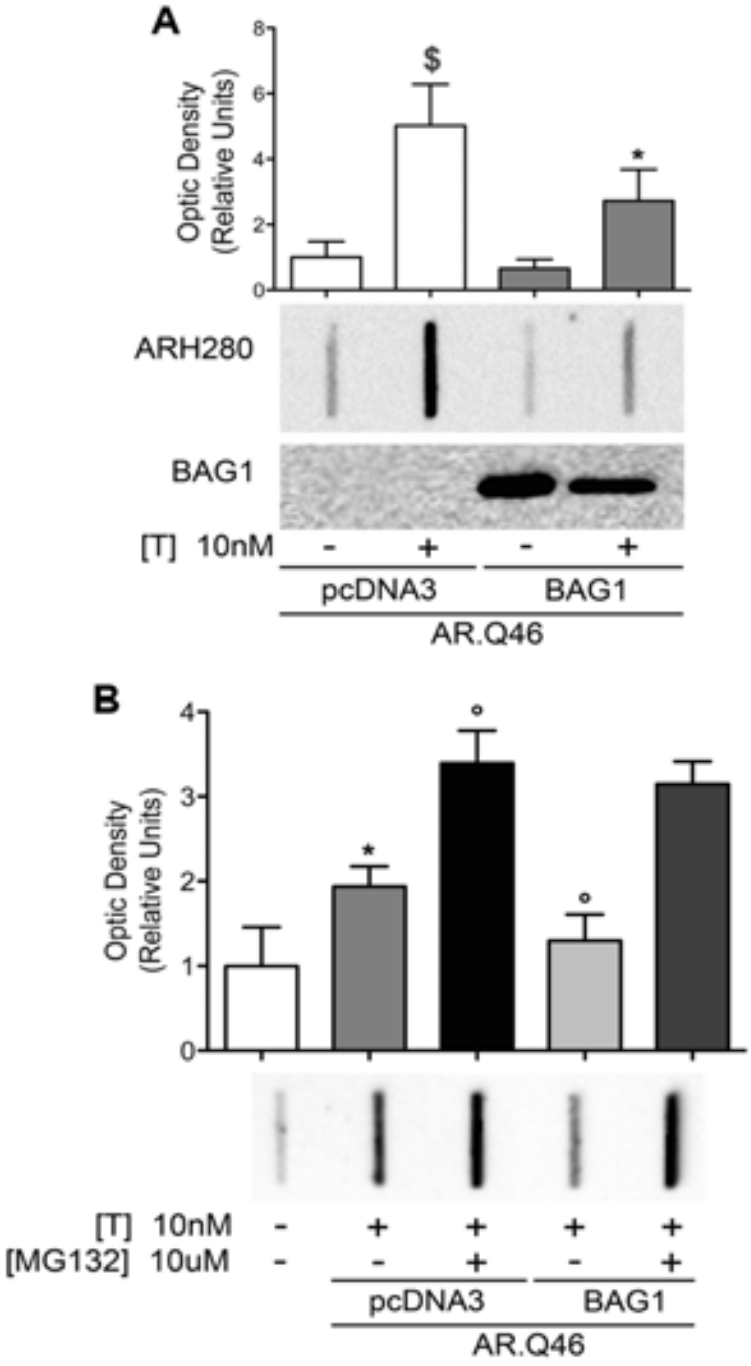

Figure 28 - BAG1 up-regulation reduces ARpolyQ accumulation.

(A) NSC34 cells expressing AR.Q46 and or BAG1 and treated with testosterone for last 48 hours; FRA shows PBS insoluble AR-polyQ levels (upper panel), histograms represent the densitometric analysis of three replicates for each sample ($=p<0.05 vs EtOH; *=p<0.05 vs. T), WB (lower panel) shows BAG1 protein level; (B) NSC34 cells expressing AR.Q46 and or BAG1 and treated with 10 nM testosterone for last 48 hours and/or 10 μM MG132 for last 16 hours; FRA shows PBS insoluble AR-polyQ levels, histogram represents densitometry analysis of three replicates for each sample (*=p<0.05 vs. EtOH; °=p<0.05 vs. T).

-

EHNA effects on CMA markers

BAG1 in association with HSC70 can also route misfolded proteins to CMA, which is however restricted to proteins bearing the KFERQ motif. Therefore, in collaboration with Prof. Carlo Ferrarese, Università degli Studi - Milano Bicocca, Milano, Italy, we analysed whether EHNA dynein inhibition may modulate the expression of key player required for CMA, such as HSC70 and lysosomal-associated membrane protein 2A (Lamp2A), a membrane glycoprotein required to protect and maintain lysosomes, and that serves as specific receptor for CMA. We performed a WB analysis (Fig. 29 A) and RT-qPCR (Fig. 29 D,E) on EHNA treated NSC34 cells. While EHNA treatment did not affect the mRNA nor the protein levels of the HSC70 (Fig. 29 A, 29 B and 29 D), it significantly increased both the mRNA and protein levels of Lamp2A. These increased expression levels of CMA markers confirm that the impairment of dynein transport and then of autophagic flux may be balanced also by CMA.

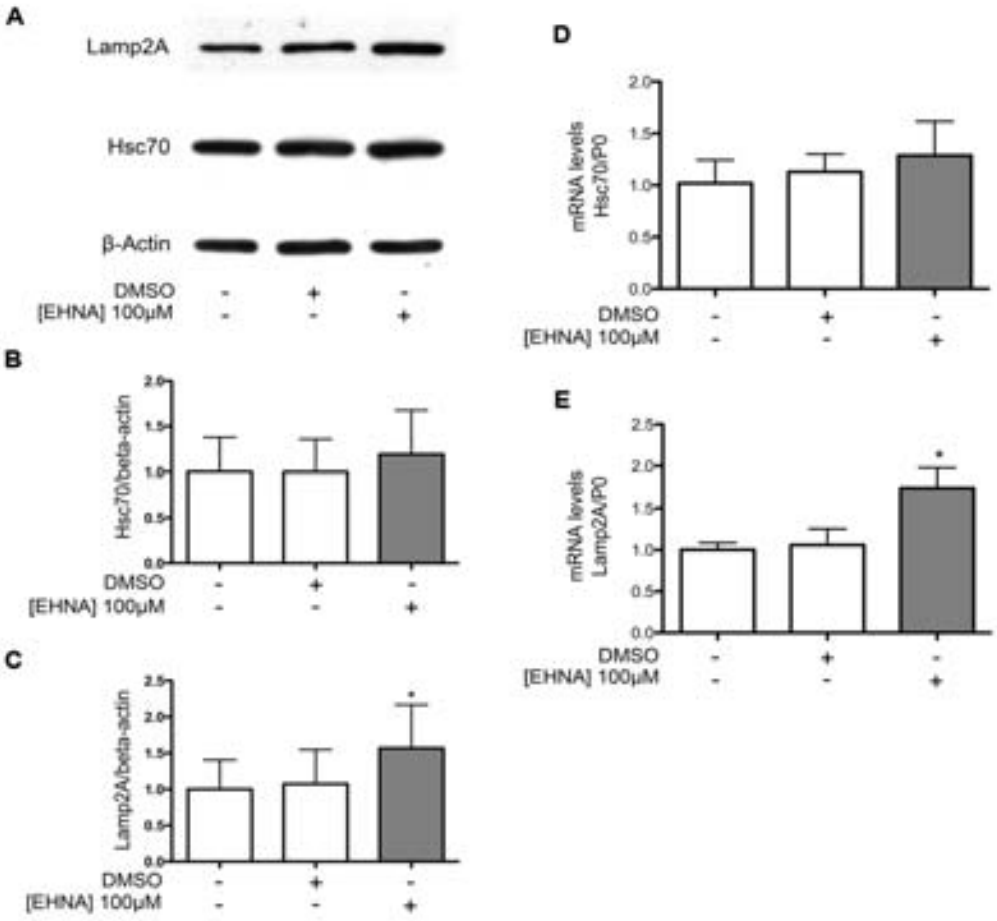

Figure 29 - EHNA effects on chaperone mediated autophagy (CMA).
NSC34 cells treated with DMSO or 100 μM EHNA for 48 hours, (A) WB analysis shows Lamp2A and Hsc70 protein levels, β-actin was used as loading control; (B, C) histograms represent densitometric analysis of nine samples (*=p<0.05 vs. ctrl); (D, E) RT-qPCR analysis of Hsc70 and Lamp2A mRNA levels normalized with RplP0 mRNA levels; histograms represent the analysis of 4 samples (*=p<0.05 vs. DMSO).

EHNA effects on fALS cell models

ALS-related proteins are misfolded and aggregated. Here we want to investigate whether the effects of dynein inhibition described above would exert its pro-degradative activities also on other mutant proteins responsible for ALS. We selected two proteins that have been associated to ALS: i) the enzyme superoxide dysmutase 1 (SOD1), which has been found mutated in approximately 20% of the familial forms of ALS (fALS), ii) a truncated form of TDP-43 (TDP-43 ΔC) which has been found in few cases of fALS. The mutant G93A SOD1 and the TDP-43 ΔC misfold and accumulate into cytoplasmic aggregates; as shown for ARpolyQ their autophagic clearance can be enhanced by the HSPB8/BAG3 complex. We thus evaluated whether also in these cases dynein inhibition resulted in increased solubility and/or degradation of the aggregates of misfolded proteins. FRA clearly shows that in two different models of ALS, G93A SOD1 transiently (Fig. 30 A) or inducible stably transfected (Fig. 30 B) motoneuronal NSC34 cells, EHNA treatment results in a massive reduction of the total amount of insoluble misfolded mutant SOD1. Similarly, it shows in the TDP-43 ΔC ALS model (Fig. 31 A), proving that dynein inhibition reduces insoluble species of the truncated fragment of TDP-43. We then analysed if EHNA pro-degradative effect was mediated PQC degradative pathway. As in the case of ARpolyQ, EHNA requires a functional proteasome activity to prevent the aggregation of mutant SOD1 (Fig. 30 C) and TDP-43 ΔC (Fig. 31 B); conversely, autophagy inhibition with 3-MA does not impair the pro-degradative effects exerted by EHNA on these two ALS-associated proteins (Fig. 30 C and 31 B).

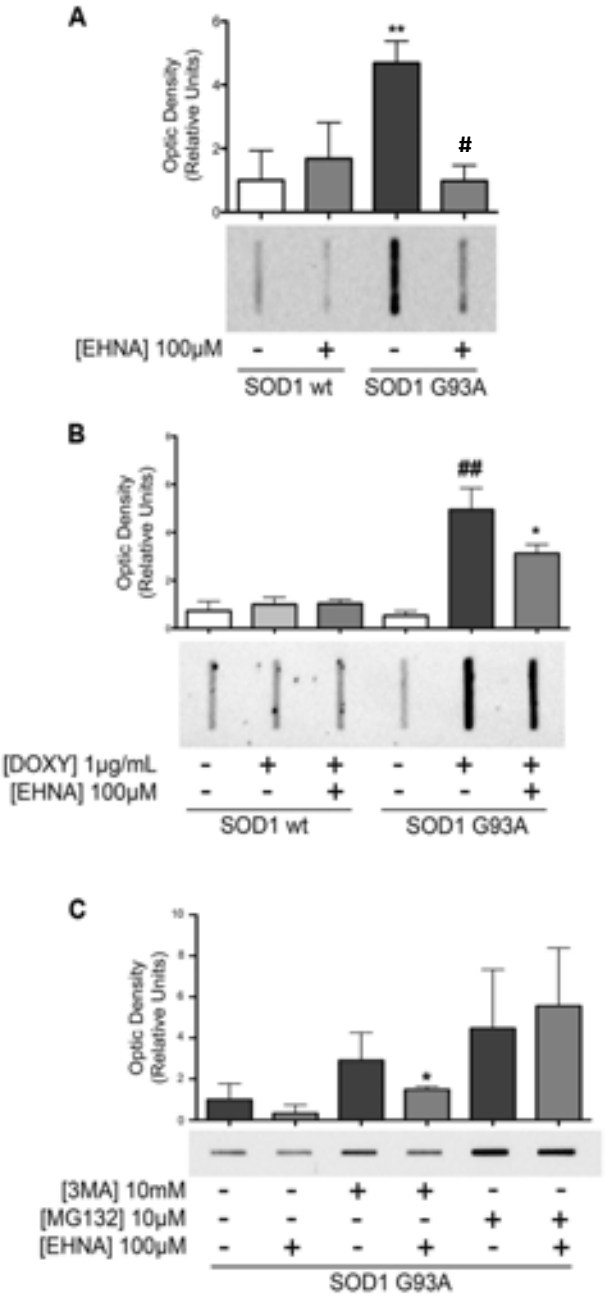

Figure 30 - Effects of dynein inhibition on SOD1 insoluble fraction.

(A) NSC34 expressing SOD1 wt and G93A treated with DMSO or 100 μM EHNA for last 48h. FRA shows SOD1G93A accumulation and SOD1G93A reduction after 100 μM EHNA treatment; (**=p<0.01 vs. SOD1wt; ##=p<0.01 vs. SOD1G93A). (B) NSC34 stably transfected with SOD1 wt or G93A induced with doxycycline and treated with DMSO or 100 μM EHNA for last 48h. FRA shows SOD1G93A accumulation and SOD1G93A reduction after 100 μM EHNA treatment; (##=p<0.01 vs. SOD1wt; *=p<0.5 vs. SOD1G93A). (C) NSC34 expressing SOD1 G93A treated with DMSO, 100 M EHNA and/or 10 mM 3-MA last 48h and 10 M MG132 for last 16 hours. FRA shows SOD1G93A accumulation after 10 mM 3-MA and 10 μM MG132 treatment. 100 μM EHNA treatment counteracts 10 mM 3-MA activity but not 10 M MG132 activity; (*=p<0.5 vs. SOD1G93A 3-MA). Histograms represent densitometric analysis of three replicates for each sample.

-

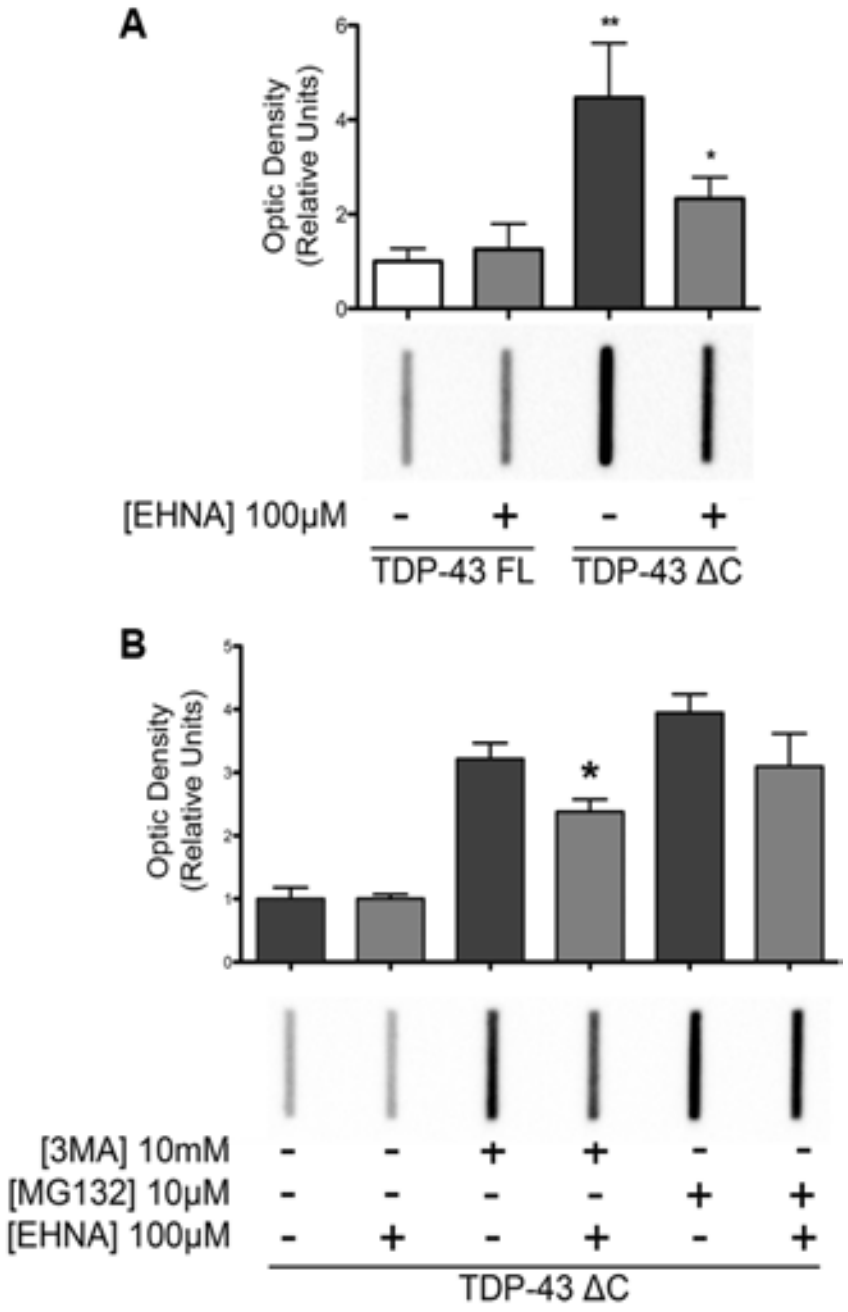

Figure 31 - Effects of dynein inhibition on TDP43 insoluble fraction.

(A) NSC34 expressing FL and ΔC TDP-43 treated with DMSO or 100 μM EHNA for last 48h. FRA shows ΔC TDP-43 accumulation and ΔC TDP-43 reduction after 100 μM EHNA treatment; (**=p<0.01 vs. FL TDP-43; *=p<0.05 vs. ΔC TDP-43 DMSO); (B) NSC34 expressing ΔC TDP-43 treated with DMSO, 100 μM EHNA and/or 3-MA last 48h and 10 μM MG132 for last 16 hours. FRA shows ΔC TDP-43 accumulation after 10 mM 3-MA and 10 μM MG132 treatment. 100 μM EHNA treatment counteracts 10 mM 3-MA activity but not 10 μM MG132 activity. Histograms represent densitometric analysis of three replicates for each sample; (*=p<0.05 vs. ΔC TDP-43 3-MA).

-

HSPB8 pro-degradative effect on C9ORF72 ALS cell model

We then investigated whether HSB8 may also act on aggregate-prone dipeptides produced by RAN translation in patients with C9ORF72 exanucleotide expansion. Interestingly, these long dipeptides, generated by ATG independent (RAN) translation of all three lecture frames of sense and anti-sense mRNA, seem to have no function in the cell, but were found accumulated in neuronal cells of C9ORF72 expanded carriers. This clearly shows that C9ORF72-related poly-dipeptideds are sticky and prone to form aggregates as well as the misfolded proteins involved in motor neuronal and neuronal diseases. Then, we first transfected the NSC34 cell with plasmid encoding for 66 GGGGCC repeats without ATG, without a stop codon and tagged with one peptide-tag per frame (polyGA-HA; polyGP-Myc; polyGR-FLAG) in order to evaluate the production of RAN translated dipeptide. FRA (Fig. 32 A) shows that in our cells polyGP-Myc peptide is detectable as retained on cellulose acetate membrane, indicating that RAN translation polyGP dipeptide was produced and was prone to aggregate. Unfortunately, we detected only polyGP dipeptide. Accordingly, to study the PQC processing of all C9ORF72 dipeptide, we decided to use synthetic cDNAs encoding for 100 repeats of poly-GA, poly-GP, poly-GR, poly-PR and poly-PA with a start codon, avoiding GGGGCC repeats (Yamakawa et al., 2015). FRA (Fig. 32 B) shows that all dipeptides are retained on cellulose acetate membrane and perturbation of PQC degradative pathway increases the retained dipeptide levels. In particular, polyGP accumulation is drastically worsened by MG132 and 3MA treatment. We next used polyGP construct to investigate if HSPB8 plays its pro-degradative action also on C9ORF72 dipeptides. In FRA in Fig. 33 A-B, we observed that HSPB8 silencing

significantly increases the retained PBS insoluble polyGP species and HSPB8 over-expression drastically reduces polyGP aggregation. These data show that polyGP dipeptide is recognized by HSPB8 as other MNDs related proteins here studied. HSPB8 pro-degradative action is also confirmed on total soluble polyGP in WB (Fig. 33 C). We then evaluated the HSPB8 effect on other C9ORF72 dipeptides. By FRA (Fig. 33 D), we evaluated the PBS insoluble levels that are significantly reduced by HSPB8 over-expressions and also in this case confirmed by WB analysis (Fig. 33 E). Collectively, these data confirm that all C9ORF72 dipeptides can be managed by PQC and in particular can be recognized by HSPB8 to route dipeptides to autophagy.

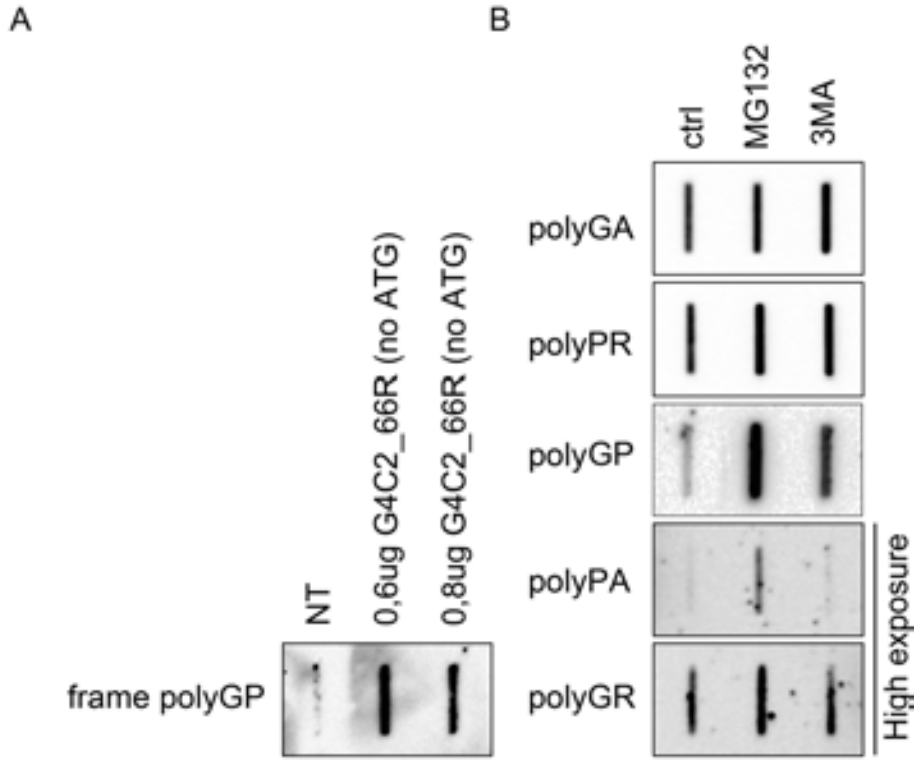

Figure 32 - dipeptide models of C9ORF72 exanucleotide expantion.

A) NSC34 cells transfected with 0,6 ug or 0,8 ug G4C2 66 repeats plasmid. FRA shows PBS insoluble fraction of polyGP frame detected with anti-myc TAG. B) NSC34 cells transfected with synthetic poly (GA, PR, GP, PA or GR) with 100 repeats and treated with MG132 or 3MA. FRA shows PBS insoluble fraction of different dipeptide.

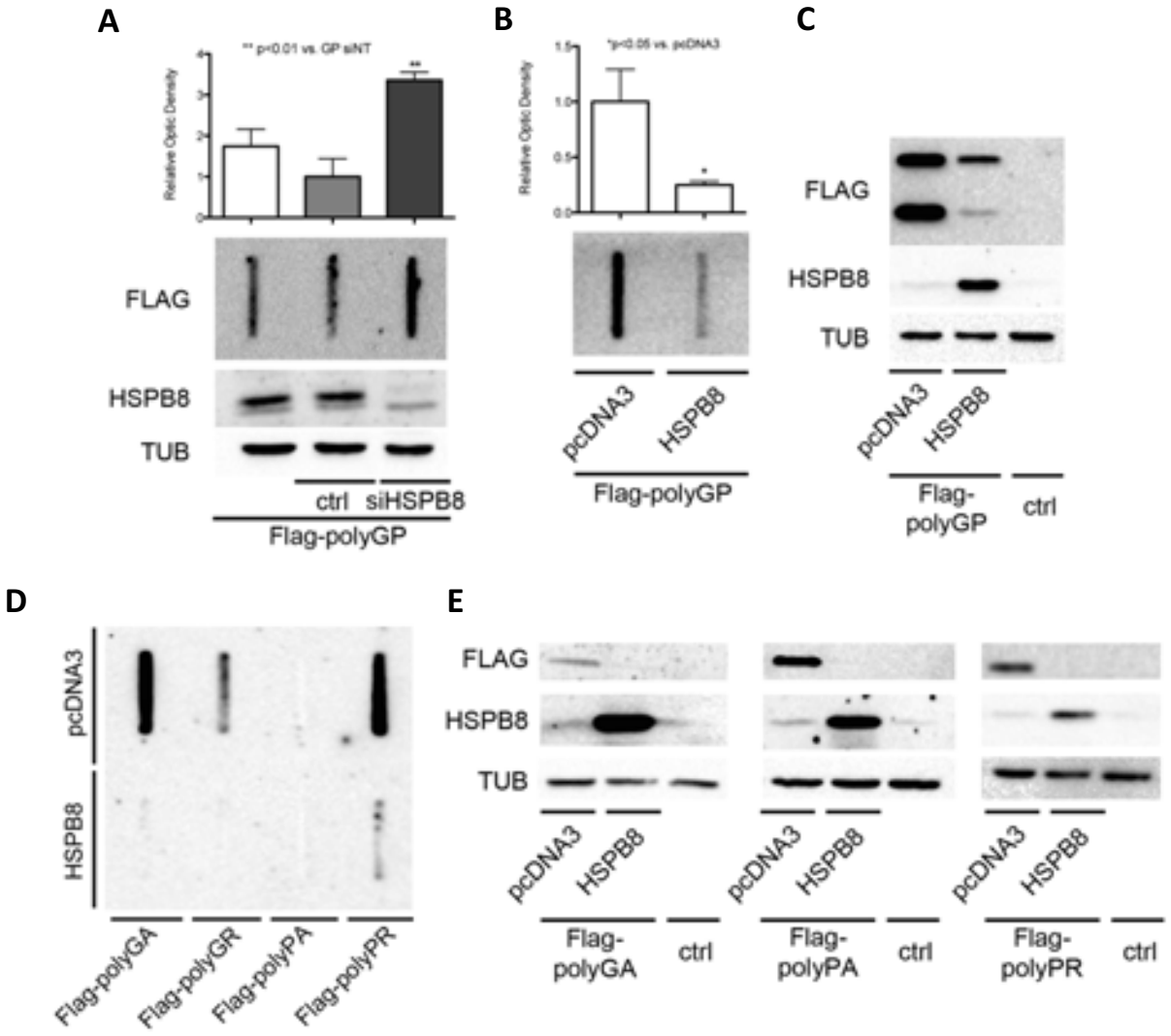

Figure 33 - HSPB8 pro-degradative effect on polydipeptide produced by C9ORF72 exanucleotide expantion.

NSC34 cells transfected with synthetic poly (GP, GA, GR, PA and PR) with 100 repeats, HSPB8 plasmid or HSPB8 siRNA. A) FRA shows PBS insoluble polyGP levels (upper panel), histograms represent the densitometric analysis of three replicates for each sample (**=p<0.01 vs ctrl), WB (lower panel) shows polyGP FLAG tagged and HSPB8 protein levels, α-tubulin was used as loading control; B) FRA shows PBS insoluble polyGP levels (upper panel), histograms represent the densitometric analysis of three replicates for each sample (*=p<0.05 vs pcDNA3); C) WB shows polyGP FLAG tagged and HSPB8 protein level, α-tubulin was used as loading control. D) FRA shows PBS insoluble poly (GA, GR, PA and PR); E) WB shows poly (GA, GR, PA and PR) FLAG tagged and HSPB8 protein levels, α-tubulin was used as loading control.

EHNA effect on C9ORF72 ALS cell model

As autophagy clearly manages ARpolyQ, SOD1 and TDP-43, it may also manage C9ORF72 dipeptides. We then tested if dynein inhibition perturbs dipeptides concentration at MTOC and consequently the aggregation process. The NSC34 cells have been transfected with polyGP construct and treated with EHNA. We then performed FRA to evaluate the PBS insoluble fraction of polyGP dipeptide. Fig. 34 shows that, as occurs for other misfolded proteins related to MNDs, EHNA drastically reduces the level of PBS insoluble species of polyGP also when autophagy is blocked by 3-MA treatment. The EHNA effect is counteracted only by proteasome inhibition with MG132.

Collectively, these data clearly show that dynein transport inhibition reduces the C9ORF72 dipeptide aggregation by disrupting the concentration at MTOC and routing C9ORF72 dipeptides to proteasome degradation.

-

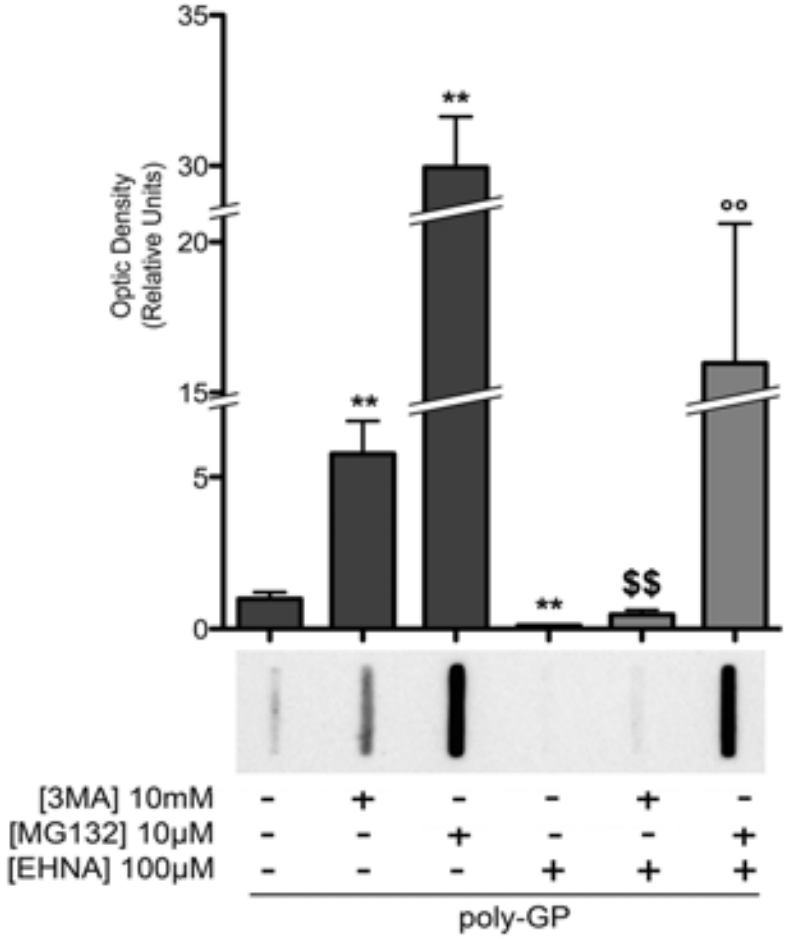

Figure 34 - Effects of dynein inhibition on poly-GP insoluble fraction.

NSC34 cells expressing poly-GP (100 repeat) treated with 10 mM 3MA and/or 100 μM EHNA for last 48 hours and/or 10 μM MG132 for last 16 hours. FRA shows poly-GP insoluble fraction; histograms represent densitometric analysis of three replicates for each sample (**=p<0.01 vs. not treated; $$=p<0.01 vs. 3MA; °°p<0.01 vs. MG132).

-

DISCUSSION

Misfolded proteins responsible for Kennedy's disease (or SBMA) and ALS are managed by PQC system to facilitate their re-folding, to prevent their aggregation and to promote their degradation. It has been proven that autophagy and UPS degradative PQC pathways are impaired in MNDs. Indeed, the ubiquitinated misfolded proteins accumulating into the inclusions might be degraded by UPS. Autophagy also contributes to counteract neurodegeneration and autophagic flux blockage may worsen the neurodegenerative process; in fact autophagic vacuoles are known to accumulate in affected motor neurons (Crippa et al., 2010b; McCray & Taylor, 2008; Nixon et al., 2005; Anglade et al., 1997). It has been confirmed that increased autophagy activity is beneficial for SBMA and ALS cell models preventing inclusions (Rusmini et al., 2013; Crippa et al., 2010b; Gurney et al., 1994). In ad dition, also HSP90 chemical inhibition promotes AR degradation by dissociation of client proteins from the/a cytoplasmic chaperone. This allows the recognition and degradation of misfolded proteins by the proteasome. Both UPS and autophagy play an essential role in SBMA and ALS pathogenesis; in this thesis we investigated their activation and regulation in affected tissue in order to better understand these mechanisms and identify new potential therapeutic targets.

First of all, we analysed the role of the PQC response in skeletal muscles and in spinal cords in mice expressing mutant ARpolyQ as primary degenerated tissues in SBMA. Indeed, Lieberman et al., 2014 showed that in the peripheral tissues the mutant AR is an important contributor to SBMA pathology in mice. In their study they showed that the suppressions of mutant AR in peripheral tissues rescued deficits in muscles, reversed ARpolyQ induced alterations in muscle gene expression, and extended

lifespan of the SBMA male mice (Lieberman et al., 2014). These mice carried AR113Q mutation and developed motoneuronal phenotype and were analysed at the pre-symptomatic stage and at the symptomatic stage. Previous studies have established that AR113Q male mice show symptoms by 24 weeks of age. Also from this age they show muscle atrophy but not motor neurons degeneration (Chua et al., 2014; Lieberman & Robins, 2008; Yu et al., 2006b). As controls, we used normal male mice and age-matched non symptomatic AR113Q female mice. We observed that expression levels of the AR mRNA in muscles and spinal cords of symptomatic mice were equal, suggesting that the absence of either positive or negative selection of muscle and motor neuronal cells was directly mediated by ARpolyQ at this stages of disease. We then analysed whether the autophagic pathway alterations were present in our AR113Q mice. Indeed, previous observation demonstrated that AR mediated toxicity in skeletal muscles is sufficient to cause motor neuron disease comparable with the toxicity exerted by the polyQ expanded protein (Monks et al., 2007). Also, it has already been reported that the autophagy master regulator TFEB is up-regulated in muscles of SBMA mice and patients (Chua et al., 2014). These changes in autophagy have been correlated with enhanced responsiveness to physiological stimuli. This study showed that autophagy regulation was compromised, confirmed by the increasing of the p62-SQSTM1 and LC3-II autophagic markers. They postulate that autophagy may contribute to the SBMA pathogenesis, including muscle atrophy. Also, they proved that enhanced autophagic response to exercise was implicated in SBMA and it is to be considered in the evaluation of the benefits of exercise observed in clinical trials (Chua et al., 2014). Here, we found that the gene expression of Beclin-1,

ATG10, p62/SQSTM1, LC3 autophagic markers was increased in the muscles of symptomatic AR113Q male mice. We also found either p62/SQSTM1 stabilization or LC3 reduction in the overall levels of the corresponding coded proteins. Interestingly, both p62/SQSTM1 and LC3 proteins are normally cleared by activated autophagy. Notably, the increased turnover of total LC3 protein was accompanied by an increased LC3-II/LC3-I ratio. Collectively, these data strongly suggest that autophagy activation is sustained by a regular flux in the atrophic skeletal muscles of symptomatic AR113Q male mice. This confirmed that autophagy is activated in SBMA muscle as show by Chua et al., 2014, but suggests that autophagy activation has a protective in muscles.

On these observations, we proved that the HSPB8-mediated PQC machinery is also activated in the muscles of symptomatic AR113Q male mice. Indeed, HSPB8 protein and mRNA levels were up-regulated in skeletal muscles of symptomatic AR113Q male mice. In addition, also the HSPB8 co-chaperone BAG3 was greatly up-regulated. Thus, the entire HSPB8-mediated autophagic machinery seems to be stimulated by the presence of mutant ARpolyQ in the skeletal muscle of SBMA affected mice. These data are consistent with the results of study on muscles of fALS (G93A-SOD1) mice (Crippa et al., 2013a; Crippa et al., 2013b). In this previous study, we clearly proved that misfolded mutant SOD1 activates autophagy in muscle of fALS mice. Indeed, we found that HSPB8 mRNA and protein levels were highly induced in transgenic G93A-SOD1 female and male mice. Likewise, BAG3, BAG1 mRNA and protein levels were higher in male and female G93A-SOD1 mice than in the control mice. Interestingly, the BAG3:BAG1 ratio was increased, confirming that G93A-SOD1 promotes the autophagy activation. In addition, autophagy activation was confirmed by the increased levels of

p62-SQSTM1 and LC3 mRNA and protein levels. As we found in SBMA mice, also in fALS mice muscle we observed a potent activation of autophagy if compared to spinal cord, suggesting that muscle tissue is efficiently protected by autophagy from misfolded proteins toxicity (Crippa et al., 2013a). Moreover, the levels of the muscle-specific small heat shock protein HSPB2 and HSPB3 (den Engelsman et al., 2009) were found to be up-regulated in the same animals. Moreover, the BAG3:BAG1 ratio (both at mRNA and protein levels) was increased, suggesting that misfolded proteins are preferentially routed to autophagy rather than to UPS (Carra et al., 2013; Gamerdinger et al., 2011). We then analysed the spinal cord of the same animals; we did not detect variation in the mRNA levels of all autophagic genes observed, only the relative BAG3:BAG1 ratio was found increased in symptomatic AR113Q male mice. This is the only observation that suggests the autophagy activation, instead of the UPS pathway, in the spinal cords of affected mice. This may show that motor neurons are not highly affected at this stage of the disease, or possibly the lack of variation is due to the fact that the large fraction of AR-negative cells (interneurons, glial cells, etc.) in the spinal cord "diluted" the mild variations of the mRNA levels present in AR-positive cells. Therefore, all data here found proves that the presence of mutant ARpolyQ in muscle cells activates autophagy, possibly to remove toxic misfolded species. In this context HSPB8-mediated PQC machinery seems to be involved in agreement with its pro-autophagic activity.

Next, we analysed how the inhibition of the dynein-mediated retrograde transport of misfolded proteins to MTOC may affect misfolded proteins intracellular aggregation and clearance. Previous data show that HSPB8 exhibits its pro-autophagic activity in

complex with BAG3 and HSC70/CHIP complex. Indeed, misfolded proteins interact with HSPB8/BAG3/HSC70/CHIP complex for their ubiquitination and p62 mediated insertion into the nascent autophagosome at MTOC (Crippa et al., 2010a; Arndt et al., 2010; Crippa et al., 2010b). This process requires the activity of 14-3-3 proteins that connect BAG3 and dynein to allow complex transport to MTOC (Xu et al., 2013; Jia et al.,). Given this evidence, dynein inhibition should cause the increased accumulation of insoluble and aggregated misfolded ARpolyQ. Conversely, we found that, in motor neuron cells, the depletion or chemical inhibition of dynein decreases the insoluble and aggregate fractions of misfolded ARpolyQ. Also, the inhibition of dynein mediated transport with EHNA, a typical cytoplasmic mechanism, in PC12/AR.Q112 SBMA inducible model, characterized by inclusions localized in the nuclei, was able to counteract insoluble misfolded ARpolyQ accumulation, even when this occurs at nuclear level (Walcott & Merry, 2002). This strongly suggests that the total ARpolyQ clearance may have been decreased by the treatment. Therefore, the inhibition of dynein transport of misfolded ARpolyQ species, by preventing their concentration at the MTOC, counteracts their aggregation, enhancing their solubility. As expected, dynein inhibition resulted in autophagy impairment. This is probably due to the fact that dynein is essential to the transport of autophagosomes to lysosomes and to facilitate their fusion into autophago-lysosomes. Indeed, we proved that in this condition autophagy is impaired and LC3-II, that decores autophagosomes of large size, accumulates in the cell cytoplasm altering the autophagic flux. As a consequence, also p62/SQSTM1 oligomerizes into the p62-bodies. These data suggest that, contrary to what had been predicted, the inhibition of dynein-mediated transport in cells in

which autophagy is impaired prevents the formation of ARpolyQ aggregated species, possibly by preventing the concentration of the misfolded species at the MTOC, where aggresomes are formed. Interestingly, we also observed the up-regulation of the HSC70 co-chaperone BAG1 and Lamp2a, which are involved, respectively, in the UPS and CMA degradations of clients bound by HSC70 (Kettern et al., 2011; Bejarano & Cuervo, 2010; Gamerdinger et al., 2009; Rohde et al., 2008; Alberti et al., 2002; Demand et al., 2001; Lüders et al., 2000). In basal conditions, the narrow barrel-shape of UPS may not properly digest dimeric and/or oligomeric forms of misfolded ARpolyQ. As a consequence, these species could be targeted for degradation to autophagy in a dynein-dependent manner. Then, the inhibition of the transport of the misfolded ARpolyQ proteins might delay their association into aggregates, maintaining the protein into a monomeric (or small oligomeric) form that may be efficiently digested by the UPS. Thus, when misfolded proteins cannot be efficiently transported to the aggresome and autophagosomes for proper disposal, the cells up-regulate a chaperone system that does not require an active transport of clients, such as the BAG1-mediated binding of HSC70 clients, which can be efficiently directed to the proteasome via the UBL domain of BAG1 or to the lysosomes via interaction of BAG1-HSC70 with Lamp2a. This explains why the dynein inhibition resulted in an enhanced clearance of misfolded proteins preventing their accumulation into insoluble aggregates. The effect of BAG1 protein over-expression is congruent with the data obtained using EHNA on SBMA cells, which suggest that the pro-degradative activity responsible for ARpolyQ clearance is exerted more on its insoluble misfolded fraction than on the entire pool of the protein also largely folded in the cells.

We also evaluated the effects of EHNA on misfolded proteins responsible for ALS. In accord with the previous data on SBMA models, dynein transport impairments significantly reduced the misfolded and aggregate fraction of mutant SOD1, TDP-43 and polyGP dipeptide. In addition, both the pro-degradative activity of BAG1 and the effects of dynein inhibition were counteracted by the blockage of proteasome with a selective inhibitor MG132, but not by autophagic flux blockage with 3-MA. These data suggest that by preventing the HSPB8/BAG3(14-3-3) dynein-directed accumulation of misfolded proteins at the MTOC, where their concentration may favour oligomerization and aggregation, the cells allow an optimized BAG1 intervention on the monomeric misfolded species facilitating the high selectivity/low capacity action of the UPS for their degradation. Therefore, the increased expression of Lamp2a indicates that, when autophagic clearance is prevented (inhibition of transport), BAG1 may not only re-route misfolded substrates to proteasome, but may also enhance the CMA activity. Unfortunately, no CMA selective inhibitors were available to deeply investigate the possible contribution of CMA in BAG1 pro-degradative effect. Collectively, these data extended the previous observation showing that nocodazole treatment inhibits aggresome formation of mutant hungtintin and ARpolyQ by microtubule disruption (Webb et al., 2004; García-Mata et al., 1999; Johnston, 1998). In addition, these studies showed that a reduced aggregation correlates with an increased toxicity of misfolded proteins analysed, supporting at least the initial protective role of aggregates (Simeoni, 2000; Saudou et al., 1998; Klement et al., 1998). In this study, thanks to a more specific approach to block misfolded protein concentration at MTOC, we observed that the neuronal cells respond to the toxicity of

the monomeric mutant misfolded proteins by enhancing the UPS routing via BAG1. This suggests that the alteration of equilibrium of protein routing to PQC may affect the accumulation of neurotoxic species, rather than the impairment or overwhelming of a single degradative pathway.

These data apparently contrast with the observations obtained in transgenic mice carrying missense point mutations in the cytoplasmic dynein heavy chain. Indeed, in heterozygous mice a motor neuron degeneration was found without accumulation of proteinaceous material, while homozygous mice showed also accumulation of Lewy-like inclusion bodies (Hafezparast et al., 2003). In addition, mutation in the p150Glued subunit of dynactin (DCTN1), responsible for cytoplasmic dynein activation, causes specific motor neuron loss, with the formation of p150Glued protein aggregates (Kuźma-Kozakiewicz et al., 2011; Levy et al., 2006; Puls et al., 2003) (see also (Schiavo et al., 2013) for extensively review on dynein mutations in humans and mice). However several mice in which dynein/dynactin functions were altered (either because of dynein mutations (Legs at odd angles (Loa)) (El-kadi et al., 2010; Kieran et al., 2005), or because of neuron specific expression of Bicaudal D2 N-terminus (BICD2-N) (Teuling et al., 2008)), when they were crossed with tg G93A SOD1 mice, showed the reduction of ALS-like phenotype and improved lifespan. So, the ALS-like phenotype of these double transgenic mice was also bettered in comparison to the fALS mice expressing the mutant SOD1 (Cortes et al., 2014; Teuling et al., 2008; Kieran et al., 2005).

On the basis of the data here presented, dynein may contribute to prevent the toxic effects of mutant misfolded proteins on motor neurons by significantly inhibiting

misfolded proteins transport at the the MTOC where aggregation may block autophagic flux, while dynein mutations per se are deleterious to motor neurons.

In conclusion, in this work we contributed to show the new mechanisms involved in misfolded proteins response in MNDs. Data here reported in the first part of this work clearly confirm the HSPB8 pro-degradative activity and they underline that HSPB8-mediated PQC response is present in muscle tissue at the symptomatic stage of disease. Therefore, the modification of the expression of specific genes encoding for proteins involved in this response, may provide muscle-specific biomarkers which could allow to follow the progression of disease in SBMA mice and in patients.

Data presented in the second part of this work confirmed the HSPB8 pro-degradative activity in SBMA and in fALS motor neuronal cell models and show the primary role of dynein mediated transport in the autophagy and in the aggregate formation process. Moreover, when autophagy is overwhelmed dynein inhibition strongly suggests that the PQC may prevent aggregation by routing the misfolded protein to UPS or CMA.

REFERENCES

Adachi, H., Katsuno, M., Waza, M., Minamiyama, M., … Sobue, G., **2009**. Heat shock proteins in neurodegenerative diseases: pathogenic roles and therapeutic implications. *Int. J. Hyperthermia*, 25(8), pp.647–54 DOI:10.3109/02656730903315823.

Adachi, H., Waza, M., Tokui, K., Katsuno, M., … Sobue, G., **2007**. CHIP Overexpression Reduces Mutant Androgen Receptor Protein and Ameliorates Phenotypes of the Spinal and Bulbar Muscular Atrophy Transgenic Mouse Model. *J. Neurosci.*, 27(19), pp.5115–5126 DOI:10.1523/JNEUROSCI.1242-07.2007.

Alberti, S., Demand, J., Esser, C., Emmerich, N., … Hohfeld, J., **2002**. Ubiquitylation of BAG-1 suggests a novel regulatory mechanism during the sorting of chaperone substrates to the proteasome. *J. Biol. Chem.*, 277(48), pp.45920–7 DOI:10.1074/jbc.M204196200.

Allen, S., Heath, P.R., Kirby, J., Wharton, S.B., … Shaw, P.J., **2003**. Analysis of the cytosolic proteome in a cell culture model of familial amyotrophic lateral sclerosis reveals alterations to the proteasome, antioxidant defenses, and nitric oxide synthetic pathways. *J. Biol. Chem.*, 278(8), pp.6371–83 DOI:10.1074/jbc.M209915200.

Anglade, P., Vyas, S., Javoy-Agid, F., Herrero, M.T., … Agid, Y., **1997**. Apoptosis and autophagy in nigral neurons of patients with Parkinson's disease. *Histol. Histopathol.*, 12(1), pp.25–31.

Arai, T., Hasegawa, M., Akiyama, H., Ikeda, K., … Oda, T., **2006**. TDP-43 is a component of ubiquitin-positive tau-negative inclusions in frontotemporal lobar degeneration and amyotrophic lateral sclerosis. *Biochem. Biophys. Res. Commun.*, 351(3), pp.602–11 DOI:10.1016/j.bbrc.2006.10.093.

Arndt, V., Dick, N., Tawo, R., Dreiseidler, M., … Höhfeld, J., **2010**. Chaperone-assisted selective autophagy is essential for muscle maintenance. *Curr. Biol.*, 20(2), pp.143–8 DOI:10.1016/j.cub.2009.11.022.

Atsuta, N., Watanabe, H., Ito, M., Banno, H., … Sobue, G., **2006**. Natural history of spinal and bulbar muscular atrophy (SBMA): A study of 223 Japanese patients. *Brain*, 129(6), pp.1446–1455 DOI:10.1093/brain/awl096.

Ayala, Y.M., Misteli, T. & Baralle, F.E., **2008a**. TDP-43 regulates retinoblastoma protein phosphorylation through the repression of cyclin-dependent kinase 6 expression. *Proc. Natl. Acad. Sci. U. S. A.*, 105(10), pp.3785–3789 DOI:10.1073/pnas.0800546105.

Ayala, Y.M., Zago, P., D'Ambrogio, A., Xu, Y.-F., … Baralle, F.E., **2008b**. Structural determinants of the cellular localization and shuttling of TDP-43. *J. Cell Sci.*, 121(22), pp.3778–3785 DOI:10.1242/jcs.038950.

Badadani, M., Nalbandian, A., Watts, G.D., Vesa, J., … Kimonis, V.E., **2010**. VCP associated inclusion body myopathy and paget disease of bone knock-in mouse model exhibits tissue pathology typical of human disease. *PLoS One*, 5(10), p.e13183 DOI:10.1371/journal.pone.0013183.

Battaglia, F., Le Galudec, V., Cossee, M., Tranchant, C., … Echaniz-Laguna, A., **2003**. Kennedy's Disease Initially Manifesting as an Endocrine Disorder. *J. Clin. Neuromuscul. Dis.*, 4(4), pp.165–7.

Bejarano, E. & Cuervo, A.M., **2010**. Chaperone-mediated autophagy. *Proc. Am. Thorac. Soc.*, 7(1), pp.29–39 DOI:10.1513/pats.200909-102JS.

Bence, N.F., Sampat, R.M. & Kopito, R.R., **2001**. Impairment of the ubiquitin-proteasome system by protein aggregation. *Science*, 292(5521), pp.1552–5 DOI:10.1126/science.292.5521.1552.

Bilsland, L.G., Sahai, E., Kelly, G., Golding, M., … Schiavo, G., **2010**. Deficits in axonal transport precede ALS symptoms in vivo. *Proc. Natl. Acad. Sci. U. S. A.*, 107(47), pp.20523–8 DOI:10.1073/pnas.1006869107.

Brinkmann, A.O., **2001**. Molecular basis of androgen insensitivity. *Mol. Cell. Endocrinol.*, 179(1-2), pp.105–9.

Bunton-Stasyshyn, R.K.A., Saccon, R.A., Fratta, P. & Fisher, E.M.C., **2014**. SOD1 Function and Its Implications for Amyotrophic Lateral Sclerosis Pathology: New and Renascent Themes. *Neuroscientist*, 21(5), pp.1–11 DOI:10.1177/1073858414561795.

Byström, R., Andersen, P.M., Gröbner, G. & Oliveberg, M., **2010**. SOD1 mutations targeting surface hydrogen bonds promote amyotrophic lateral sclerosis without reducing apo-state stability. *J. Biol. Chem.*, 285(25), pp.19544–52 DOI:10.1074/jbc.M109.086074.

Carra, S., Crippa, V., Rusmini, P., Boncoraglio, A., … Poletti, A., **2012**. Alteration of protein folding and degradation in motor neuron diseases: Implications and protective functions of small heat shock proteins. *Prog. Neurobiol.*, 97(2), pp.83–100 DOI:10.1016/j.pneurobio.2011.09.009.

Carra, S., Rusmini, P., Crippa, V., Giorgetti, E., … Poletti, A., **2013**. Different anti-aggregation and pro- degradative functions of the members of the mammalian sHSP family in neurological disorders. *… R. …*, 368(1617), p.20110409 DOI:10.1098/rstb.2011.0409.

Carra, S., Sivilotti, M., Zobel, a. T.C., Lambert, H. & Landry, J., **2005**. HspB8, a small heat shock protein mutated in human neuromuscular disorders, has in vivo chaperone activity in cultured cells. *Hum. Mol. Genet.*, 14(12), pp.1659–1669 DOI:10.1093/hmg/ddi174.

Cashman, N.R., Durham, H.D., Blusztajn, J.K., Oda, K., … Antel, J.P., **1992**. Neuroblastoma x spinal cord (NSC) hybrid cell lines resemble developing motor neurons. *Dev. Dyn.*, 194(3), pp.209–221 DOI:10.1002/aja.1001940306.

Chang, C.S., Kokontis, J. & Liao, S.T., **1988**. Molecular cloning of human and rat complementary DNA encoding androgen receptors. *Science*, 240(4850), pp.324–6.

Chevalier-Larsen, E.S., O'Brien, C.J., Wang, H., Jenkins, S.C., … Merry, D.E., **2004**. Castration restores function and neurofilament alterations of aged symptomatic males in a transgenic mouse model of spinal and bulbar muscular atrophy. *J. Neurosci.*, 24(20), pp.4778–86 DOI:10.1523/JNEUROSCI.0808-04.2004.

Chiò, A., Borghero, G., Restagno, G., Mora, G., … Sabatelli, M., **2012**. Clinical characteristics of patients with familial amyotrophic lateral sclerosis carrying the pathogenic GGGGCC hexanucleotide repeat expansion of C9ORF72. *Brain*, 135(Pt 3), pp.784–93 DOI:10.1093/brain/awr366.

Chua, J.P., Reddy, S.L., Merry, D.E., Adachi, H., … Lieberman, A.P., **2014**. Transcriptional activation of TFEB/ZKSCAN3 target genes underlies enhanced autophagy in spinobulbar muscular atrophy. *Hum. Mol. Genet.*, 23(5), pp.1376–86 DOI:10.1093/hmg/ddt527.

Corson, L.B., Strain, J.J., Culotta, V.C. & Cleveland, D.W., **1998**. Chaperone-facilitated copper binding is a property common to several classes of familial amyotrophic lateral sclerosis-linked superoxide dismutase mutants. *Proc. Natl. Acad. Sci. U. S. A.*, 95(11), pp.6361–6.

Cortes, C.J., Ling, S.-C., Guo, L.T., Hung, G., … La Spada, A.R., **2014**. Muscle expression of mutant androgen receptor accounts for systemic and motor neuron disease phenotypes in spinal and bulbar muscular atrophy. *Neuron*, 82(2), pp.295–307 DOI:10.1016/j.neuron.2014.03.001.

Crippa, V., Boncoraglio, A., Galbiati, M., Aggarwal, T., … Poletti, A., **2013a**. Differential autophagy power in the spinal cord and muscle of transgenic ALS mice. *Front. Cell. Neurosci.*, 7(November), p.234 DOI:10.3389/fncel.2013.00234.

Crippa, V., Carra, S., Rusmini, P., Sau, D., … Poletti, A., **2010a**. A role of small heat shock protein B8 (HspB8) in the autophagic removal of misfolded proteins responsible for neurodegenerative diseases. *Autophagy*, 6(7), pp.958–960 DOI:10.4161/auto.6.7.13042.

Crippa, V., Galbiati, M., Boncoraglio, A., Rusmini, P., … Poletti, A., **2013b**. Motoneuronal and muscle-selective removal of ALS-related misfolded proteins. *Biochem. Soc. Trans.*, 41(6), pp.1598–604 DOI:10.1042/BST20130118.

Crippa, V., Sau, D., Rusmini, P., Boncoraglio, A., … Poletti, A., **2010b**. The small heat shock protein B8 (HspB8) promotes autophagic removal of misfolded proteins involved in amyotrophic lateral sclerosis (ALS). *Hum. Mol. Genet.*, 19(17), pp.3440–3456 DOI:10.1093/hmg/ddq257.

DeJesus-Hernandez, M., Mackenzie, I.R., Boeve, B.F., Boxer, A.L., … Rademakers, R., **2011**. Expanded GGGGCC hexanucleotide repeat in noncoding region of C9ORF72 causes chromosome 9p-linked FTD and ALS. *Neuron*, 72(2), pp.245–56 DOI:10.1016/j.neuron.2011.09.011.

Demand, J., Alberti, S., Patterson, C., Höhfeld, J. & Demand J, Alberti S, Patterson C, H.J., **2001**. Cooperation of a ubiquitin domain protein and an E3 ubiquitin ligase during chaperone/proteasome coupling. *Curr. Biol.*, 11(20), pp.1569–1577 DOI:10.1016/S0960-9822(01)00487-0.

Deng, H.-X., Zhai, H., Bigio, E.H., Yan, J., … Siddique, T., **2010**. FUS-immunoreactive inclusions are a common feature in sporadic and non-SOD1 familial amyotrophic lateral sclerosis. *Ann. Neurol.*, 67(6), pp.739–48 DOI:10.1002/ana.22051.

Doi, H., Adachi, H., Katsuno, M., Minamiyama, M., … Sobue, G., **2013**. p62/SQSTM1 differentially removes the toxic mutant androgen receptor via autophagy and inclusion formation in a spinal and bulbar muscular atrophy mouse model. *J. Neurosci.*, 33(18), pp.7710–27 DOI:10.1523/JNEUROSCI.3021-12.2013.

Dompierre, J.P., Godin, J.D., Charrin, B.C., Cordelières, F.P., … Saudou, F., **2007**. Histone deacetylase 6 inhibition compensates for the transport deficit in Huntington's disease by increasing tubulin acetylation. *J. Neurosci.*, 27(13), pp.3571–83 DOI:10.1523/JNEUROSCI.0037-07.2007.

Dossena, M., Bedini, G., Rusmini, P., Giorgetti, E., … Poletti, A., **2014**. Human adipose-derived mesenchymal stem cells as a new model of spinal and bulbar muscular atrophy. *PLoS One*, 9(11), p.e112746 DOI:10.1371/journal.pone.0112746.

Dul, J.L., Davis, D.P., Williamson, E.K., Stevens, F.J. & Argon, Y., **2001**. Hsp70 and antifibrillogenic peptides promote degradation and inhibit intracellular aggregation of amyloidogenic light chains. *J. Cell Biol.*, 152(4), pp.705–16.

Durham, H.D., Dahrouge, S. & Cashman, N.R., **1993**. Evaluation of the spinal cord neuron X neuroblastoma hybrid cell line NSC-34 as a model for neurotoxicity testing. *Neurotoxicology*, 14(4), pp.387–95.

Eisen, A., Schulzer, M., MacNeil, M., Pant, B. & Mak, E., **1993**. Duration of amyotrophic lateral sclerosis is age dependent. *Muscle Nerve*, 16(1), pp.27–32 DOI:10.1002/mus.880160107.

El-kadi, A.M., Bros-facer, V., Deng, W., Philpott, A., … Moore, A.L., **2010**. The Legs at odd angles (Loa) Mutation in Cytoplasmic Dynein Ameliorates Mitochondrial Function in SOD1 G93A Mouse Model for Motor Neuron Disease * □. , 285(24), pp.18627–18639 DOI:10.1074/jbc.M110.129320.

den Engelsman, J., Boros, S., Dankers, P.Y.W., Kamps, B., … Boelens, W.C., **2009**. The small heat-shock proteins HSPB2 and HSPB3 form well-defined heterooligomers in a unique 3 to 1 subunit ratio. *J. Mol. Biol.*, 393(5), pp.1022–32 DOI:10.1016/j.jmb.2009.08.052.

van Es, M. a, Veldink, J.H., Saris, C.G.J., Blauw, H.M., … van den Berg, L.H., **2009**. Genome-wide association study identifies 19p13.3 (UNC13A) and 9p21.2 as susceptibility loci for sporadic amyotrophic lateral sclerosis. *Nat. Genet.*, 41(10), pp.1083–1087 DOI:10.1038/ng.442.

Fan, H.C., Ho, L.I., Chi, C.S., Chen, S.J., … Harn, H.J., **2014**. Polyglutamine (PolyQ) diseases: Genetics to treatments. *Cell Transplant.*, 23(4-5), pp.441–458 DOI:10.3727/096368914X678454.

Ferri, A., Cozzolino, M., Crosio, C., Nencini, M., … Carrì, M.T., **2006**. Familial ALS-superoxide dismutases associate with mitochondria and shift their redox potentials. *Proc. Natl. Acad. Sci. U. S. A.*, 103(37), pp.13860–13865 DOI:10.1073/pnas.0605814103.

Figlewicz, D.A. & Orrell, R.W., **2003**. The genetics of motor neuron diseases. *Amyotroph. Lateral Scler. Other Motor Neuron Disord.*, 4(4), pp.225–31.

Fontaine, J.-M., Sun, X., Hoppe, A.D., Simon, S., … Benndorf, R., **2006**. Abnormal small heat shock protein interactions involving neuropathy-associated HSP22 (HSPB8) mutants. *FASEB J.*, 20(12), pp.2168–70 DOI:10.1096/fj.06-5911fje.

Furukawa, Y. & O'Halloran, T. V, **2005**. Amyotrophic lateral sclerosis mutations have the greatest destabilizing effect on the apo- and reduced form of SOD1, leading to unfolding and oxidative aggregation. *J. Biol. Chem.*, 280(17), pp.17266–74 DOI:10.1074/jbc.M500482200.

Gamerdinger, M., Carra, S. & Behl, C., **2011**. Emerging roles of molecular chaperones and co-chaperones in selective autophagy: focus on BAG proteins. *J. Mol. Med. (Berl).*, 89(12), pp.1175–82 DOI:10.1007/s00109-011-0795-6.

Gamerdinger, M., Hajieva, P., Kaya, a M., Wolfrum, U., … Behl, C., **2009**. Protein quality control during aging involves recruitment of the macroautophagy pathway by BAG3. *EMBO J.*, 28(7), pp.889–901 DOI:10.1038/emboj.2009.29.

García-Mata, R., Bebök, Z., Sorscher, E.J. & Sztul, E.S., **1999**. Characterization and dynamics of aggresome formation by a cytosolic GFP-chimera. *J. Cell Biol.*, 146(6), pp.1239–54.

Gendron, T.F., van Blitterswijk, M., Bieniek, K.F., Daughrity, L.M., … Boylan, K.B., **2015**. Cerebellar c9RAN proteins associate with clinical and neuropathological characteristics of C9ORF72 repeat expansion carriers. *Acta Neuropathol.*, DOI:10.1007/s00401-015-1474-4.

Gendron, T.F., Rademakers, R. & Petrucelli, L., **2013**. TARDBP mutation analysis in TDP-43 proteinopathies and deciphering the toxicity of mutant TDP-43. *J. Alzheimers. Dis.*, 33 Suppl 1, pp.S35–45 DOI:10.3233/JAD-2012-129036.

Giorgetti, E., Rusmini, P., Crippa, V., Cristofani, R., … Poletti, A., **2015**. Synergic prodegradative activity of Bicalutamide and trehalose on the mutant androgen receptor responsible for spinal and bulbar muscular atrophy. *Hum. Mol. Genet.*, 24(1), pp.64–65 DOI:10.1093/hmg/ddu419.

Grunseich, C., Kats, I.R., Bott, L.C., Rinaldi, C., … Fischbeck, K.H., **2014a**. Early onset and novel features in a spinal and bulbar muscular atrophy patient with a 68 CAG repeat. *Neuromuscul. Disord.*, 24(11), pp.978–981 DOI:10.1016/j.nmd.2014.06.441.

Grunseich, C., Zukosky, K., Kats, I.R., Ghosh, L., … Fischbeck, K.H., **2014b**. Stem cell-derived motor neurons from spinal and bulbar muscular atrophy patients. *Neurobiol. Dis.*, 70, pp.12–20 DOI:10.1016/j.nbd.2014.05.038.

Gurney, M.E., Pu, H., Chiu, a Y., Dal Canto, M.C., … Deng, H.X., **1994**. Motor neuron degeneration in mice that express a human Cu,Zn superoxide dismutase mutation. *Science*, 264(5166), pp.1772–1775 DOI:10.1126/science.8209258.

Hafezparast, M., Klocke, R., Ruhrberg, C., Marquardt, A., … Fisher, E.M.C., **2003**. Mutations in dynein link motor neuron degeneration to defects in retrograde transport. *Science*, 300(5620), pp.808–12 DOI:10.1126/science.1083129.

Harding, A.E., Thomas, P.K., Baraitser, M., Bradbury, P.G., … Ponsford, J.R., **1982**. X-linked recessive bulbospinal neuronopathy: a report of ten cases. *J. Neurol. Neurosurg. Psychiatry*, 45(11), pp.1012–9.

Iguchi, Y., Katsuno, M., Ikenaka, K., Ishigaki, S. & Sobue, G., **2013**. Amyotrophic lateral sclerosis: An update on recent genetic insights. *J. Neurol.*, 260(11), pp.2917–2927 DOI:10.1007/s00415-013-7112-y.

Irobi, J., Almeida-Souza, L., Asselbergh, B., De Winter, V., … Timmerman, V., **2010**. Mutant HSPB8 causes motor neuron-specific neurite degeneration. *Hum. Mol. Genet.*, 19(16), pp.3254–65 DOI:10.1093/hmg/ddq234.

Jahreiss, L., Menzies, F.M. & Rubinsztein, D.C., **2008**. The Itinerary of Autophagosomes: From Peripheral Formation to Kiss-and-Run Fusion with Lysosomes. *Traffic*, 9(4), pp.574–587 DOI:10.1111/j.1600-0854.2008.00701.x.

Jia, B., Wu, Y. & Zhou, Y., 14-3-3 and aggresome formation: implications in neurodegenerative diseases. *Prion*, 8(2).

Jochum, T., Ritz, M.E., Schuster, C., Funderburk, S.F., … Cato, A.C.B., **2012**. Toxic and non-toxic aggregates from the SBMA and normal forms of androgen receptor have distinct oligomeric structures. *Biochim. Biophys. Acta*, 1822(6), pp.1070–8 DOI:10.1016/j.bbadis.2012.02.006.

Johnson, J.O., Mandrioli, J., Benatar, M., Abramzon, Y., … Traynor, B.J., **2010**. Exome sequencing reveals VCP mutations as a cause of familial ALS. *Neuron*, 68(5), pp.857–64 DOI:10.1016/j.neuron.2010.11.036.

Johnson, J.O., Pioro, E.P., Boehringer, A., Chia, R., … Traynor, B.J., **2014**. Mutations in the Matrin 3 gene cause familial amyotrophic lateral sclerosis. *Nat. Neurosci.*, 17(5), pp.664–6 DOI:10.1038/nn.3688.

Johnston, J. a., Illing, M.E. & Kopito, R.R., **2002**. Cytoplasmic dynein/dynactin mediates the assembly of aggresomes. *Cell Motil. Cytoskeleton*, 53(1), pp.26–38 DOI:10.1002/cm.10057.

Johnston, J.A., **1998**. Aggresomes: A Cellular Response to Misfolded Proteins. *J. Cell Biol.*, 143(7), pp.1883–1898 DOI:10.1083/jcb.143.7.1883.

Ju, J.-S., Fuentealba, R.A., Miller, S.E., Jackson, E., … Weihl, C.C., **2009**. Valosin-containing protein (VCP) is required for autophagy and is disrupted in VCP disease. *J. Cell Biol.*, 187(6), pp.875–888 DOI:10.1083/jcb.200908115.

Katsuno, M., Adachi, H., Kume, A., Li, M., … Sobue, G., **2002**. Testosterone reduction prevents phenotypic expression in a transgenic mouse model of spinal and bulbar muscular atrophy. *Neuron*, 35(5), pp.843–54.

Katsuno, M., Tanaka, F., Adachi, H., Banno, H., … Sobue, G., **2012**. Pathogenesis and therapy of spinal and bulbar muscular atrophy (SBMA). *Prog. Neurobiol.*, 99(3), pp.246–56 DOI:10.1016/j.pneurobio.2012.05.007.

Kaushik, S. & Cuervo, A.M., **2012**. Chaperone-mediated autophagy: a unique way to enter the lysosome world. *Trends Cell Biol.*, 22(8), pp.407–17 DOI:10.1016/j.tcb.2012.05.006.

Kawahara, H., **1897**. A family of progressive bulbar palsy. *Aichi Med. J.*, 16, pp.3–4.

Kennedy, W.R., Alter, M. & Sung, J.H., **1968**. Progressive proximal spinal and bulbar muscular atrophy of late onset. A sex-linked recessive trait. *Neurology*, 18(7).

Kettern, N., Rogon, C., Limmer, A., Schild, H. & Höhfeld, J., **2011**. The Hsc/Hsp70 co-chaperone network controls antigen aggregation and presentation during maturation of professional antigen presenting cells. *PLoS One*, 6(1), p.e16398 DOI:10.1371/journal.pone.0016398.

Kieran, D., Hafezparast, M., Bohnert, S., Dick, J.R.T., … Greensmith, L., **2005**. A mutation in dynein rescues axonal transport defects and extends the life span of ALS mice. , 169(4), pp.561–567 DOI:10.1083/jcb.200501085.

Klement, I.A., Skinner, P.J., Kaytor, M.D., Yi, H., … Orr, H.T., **1998**. Ataxin-1 Nuclear Localization and Aggregation. *Cell*, 95(1), pp.41–53 DOI:10.1016/S0092-8674(00)81781-X.

Kolb, S.J., Snyder, P.J., Poi, E.J., Renard, E.A., … Prior, T.W., **2010**. Mutant small heat shock protein B3 causes motor neuropathy: utility of a candidate gene approach. *Neurology*, 74(6), pp.502–6 DOI:10.1212/WNL.0b013e3181cef84a.

Kondo, N., Katsuno, M., Adachi, H., Minamiyama, M., … Sobue, G., **2013**. Heat shock factor-1 influences pathological lesion distribution of polyglutamine-induced neurodegeneration. *Nat. Commun.*, 4, p.1405 DOI:10.1038/ncomms2417.

Koyama, S., Arawaka, S., Chang-Hong, R., Wada, M., … Kato, T., **2006**. Alteration of familial ALS-linked mutant SOD1 solubility with disease progression: its modulation by the proteasome and Hsp70. *Biochem. Biophys. Res. Commun.*, 343(3), pp.719–30 DOI:10.1016/j.bbrc.2006.02.170.

Kraft, C., Peter, M. & Hofmann, K., **2010**. Selective autophagy: ubiquitin-mediated recognition and beyond. *Nat. Cell Biol.*, 12(9), pp.836–41 DOI:10.1038/ncb0910-836.

Kuźma-Kozakiewicz, M., Usarek, E., Ludolph, A.C. & Barańczyk-Kuźma, A., **2011**. Mice with mutation in dynein heavy chain 1 do not share the same tau expression pattern with mice with SOD1-related motor neuron disease. *Neurochem. Res.*, 36(6), pp.978–85 DOI:10.1007/s11064-011-0436-z.

Kwiatkowski, T.J., Bosco, D.A., Leclerc, A.L., Tamrazian, E., … Brown, R.H., **2009**. Mutations in the FUS/TLS gene on chromosome 16 cause familial amyotrophic lateral sclerosis. *Science*, 323(5918), pp.1205–8 DOI:10.1126/science.1166066.

Lagier-Tourenne, C., Polymenidou, M., Hutt, K.R., Vu, A.Q., … Yeo, G.W., **2012**. Divergent roles of ALS-linked proteins FUS/TLS and TDP-43 intersect in processing long pre-mRNAs. *Nat. Neurosci.*, 15(11), pp.1488–97 DOI:10.1038/nn.3230.

LaMonte, B.H., Wallace, K.E., Holloway, B.A., Shelly, S.S., … Holzbaur, E.L.F., **2002**. Disruption of dynein/dynactin inhibits axonal transport in motor neurons causing late-onset progressive degeneration. *Neuron*, 34(5), pp.715–27.

Lattante, S., Ciura, S., Rouleau, G.A. & Kabashi, E., **2015**. Defining the genetic connection linking amyotrophic lateral sclerosis (ALS) with frontotemporal dementia (FTD). *Trends Genet.*, 31(5), pp.263–273 DOI:10.1016/j.tig.2015.03.005.

Levy, J.R., Sumner, C.J., Caviston, J.P., Tokito, M.K., … Holzbaur, E.L.F., **2006**. A motor neuron disease-associated mutation in p150Glued perturbs dynactin function and induces protein aggregation. *J. Cell Biol.*, 172(5), pp.733–45 DOI:10.1083/jcb.200511068.

Li, M., Nakagomi, Y., Kobayashi, Y., Merry, D.E., … Sobue, G., **1998**. Nonneural nuclear inclusions of androgen receptor protein in spinal and bulbar muscular atrophy. *Am. J. Pathol.*, 153(3), pp.695–701 DOI:10.1016/S0002-9440(10)65612-X.

Li, W., Li, J. & Bao, J., **2012**. Microautophagy: lesser-known self-eating. *Cell. Mol. Life Sci.*, 69(7), pp.1125–1136 DOI:10.1007/s00018-011-0865-5.

Lieberman, A.P. & Robins, D.M., **2008**. The androgen receptor's CAG/glutamine tract in mouse models of neurological disease and cancer. *J. Alzheimers. Dis.*, 14(2), pp.247–55.

Lieberman, A.P., Yu, Z., Murray, S., Peralta, R., … Hung, G., **2014**. Peripheral androgen receptor gene suppression rescues disease in mouse models of spinal and bulbar muscular atrophy. *Cell Rep.*, 7(3), pp.774–84 DOI:10.1016/j.celrep.2014.02.008.

Ling, S.-C., Polymenidou, M. & Cleveland, D.W.W., **2013**. Converging mechanisms in ALS and FTD: disrupted RNA and protein homeostasis. *Neuron*, 79(3), pp.416–38 DOI:10.1016/j.neuron.2013.07.033.

Locatelli, D., Terao, M., Fratelli, M., Zanetti, A., … Garattini, E., **2012**. Human axonal survival of motor neuron (a-SMN) protein stimulates axon growth, cell motility, C-C motif ligand 2 (CCL2), and insulin-like growth factor-1 (IGF1) production. *J. Biol. Chem.*, 287(31), pp.25782–94 DOI:10.1074/jbc.M112.362830.

Lubahn, D.B., Joseph, D.R., Sullivan, P.M., Willard, H.F., … Wilson, E.M., **1988**. Cloning of human androgen receptor complementary DNA and localization to the X chromosome. *Science*, 240(4850), pp.327–30.

Lüders, J., Demand, J. & Höhfeld, J., **2000**. The ubiquitin-related BAG-1 provides a link between the molecular chaperones Hsc70/Hsp70 and the proteasome. *J. Biol. Chem.*, 275(7), pp.4613–4617 DOI:10.1074/jbc.275.7.4613.

Majoor-Krakauer, D., Willems, P.J. & Hofman, A., **2003**. Genetic epidemiology of amyotrophic lateral sclerosis. *Clin. Genet.*, 63(2), pp.83–101.

Malik, B., Nirmalananthan, N., Bilsland, L.G., La Spada, A.R., … Greensmith, L., **2011**. Absence of disturbed axonal transport in spinal and bulbar muscular atrophy. *Hum. Mol. Genet.*, 20(9), pp.1776–1786 DOI:10.1093/hmg/ddr061.

Mariotti, C., Castellotti, B., Pareyson, D., Testa, D., … Donato, S.D., **2000**. Phenotypic manifestations associated with CAG-repeat expansion in the androgen receptor gene in male patients and heterozygous females: a clinical and molecular study of 30 families. *Neuromuscul. Disord.*, 10(6), pp.391–7.

Marron, T.U., Guerini, V., Rusmini, P., Sau, D., … Poletti, A., **2005**. Androgen-induced neurite outgrowth is mediated by neuritin in motor neurones. *J. Neurochem.*, 92(1), pp.10–20 DOI:10.1111/j.1471-4159.2004.02836.x.

Maruyama, H., Morino, H., Ito, H., Izumi, Y., … Kawakami, H., **2010**. Mutations of optineurin in amyotrophic lateral sclerosis. *Nature*, 465(7295), pp.223–6 DOI:10.1038/nature08971.

Matsumoto, A., **1997**. Hormonally induced neuronal plasticity in the adult motoneurons. *Brain Res. Bull.*, 44(4), pp.539–47.

Matsumoto, A., Micevych, P.E. & Arnold, A.P., **1988**. Androgen regulates synaptic input to motoneurons of the adult rat spinal cord. *J. Neurosci.*, 8(11), pp.4168–76.

Matsumoto, T., Sakari, M., Okada, M., Yokoyama, A., … Kato, S., **2013**. The Androgen Receptor in Health and Disease. *Annu. Rev. Physiol.*, 75(1), pp.201–224 DOI:10.1146/annurev-physiol-030212-183656.

McCray, B.A. & Taylor, J.P., **2008**. The role of autophagy in age-related neurodegeneration. *Neurosignals.*, 16(1), pp.75–84 DOI:10.1159/000109761.

Menzies, F.M., Fleming, A. & Rubinsztein, D.C., **2015**. Compromised autophagy and neurodegenerative diseases. *Nat. Rev. Neurosci.*, 16(6), pp.345–357 DOI:10.1038/nrn3961.

Meyer, H., Bug, M. & Bremer, S., **2012**. Emerging functions of the VCP/p97 AAA-ATPase in the ubiquitin system. *Nat. Cell Biol.*, 14(2), pp.117–23 DOI:10.1038/ncb2407.

Miller, J., Arrasate, M., Brooks, E., Libeu, C.P., … Finkbeiner, S., **2011**. Identifying polyglutamine protein species in situ that best predict neurodegeneration. *Nat. Chem. Biol.*, 7(12), pp.925–34 DOI:10.1038/nchembio.694.

Monks, D.A., Johansen, J.A., Mo, K., Rao, P., … Jordan, C.L., **2007**. Overexpression of wild-type androgen receptor in muscle recapitulates polyglutamine disease. *Proc. Natl. Acad. Sci. U. S. A.*, 104(46), pp.18259–64 DOI:10.1073/pnas.0705501104.

Moore, J.K., Sept, D. & Cooper, J.A., **2009**. Neurodegeneration mutations in dynactin impair dynein-dependent nuclear migration. *Proc. Natl. Acad. Sci.*, 106(13), pp.5147–5152 DOI:10.1073/pnas.0810828106.

Mori, K., Weng, S.-M., Arzberger, T., May, S., … Edbauer, D., **2013**. The C9orf72 GGGGCC repeat is translated into aggregating dipeptide-repeat proteins in FTLD/ALS. *Science*, 339(6125), pp.1335–8 DOI:10.1126/science.1232927.

Muchowski, P.J. & Wacker, J.L., **2005**. Modulation of neurodegeneration by molecular chaperones. *Nat. Rev. Neurosci.*, 6(1), pp.11–22 DOI:10.1038/nrn1587.

Muñoz-Moreno, R., Barrado-Gil, L., Galindo, I. & Alonso, C., **2015**. Analysis of HDAC6 and BAG3-aggresome pathways in African swine fever viral factory formation. *Viruses*, 7(4), pp.1823–31 DOI:10.3390/v7041823.

Nagashima, T., Seko, K., Hirose, K., Mannen, T., … Morimatsu, Y., **1988**. Familial bulbo-spinal muscular atrophy associated with testicular atrophy and sensory neuropathy (Kennedy-Alter-Sung syndrome). Autopsy case report of two brothers. *J. Neurol. Sci.*, 87(2-3), pp.141–52.

Neumann, M., Sampathu, D.M., Kwong, L.K., Truax, A.C., … Lee, V.M.-Y., **2006**. Ubiquitinated TDP-43 in frontotemporal lobar degeneration and amyotrophic lateral sclerosis. *Science*, 314(5796), pp.130–3 DOI:10.1126/science.1134108.

Neuschmid-Kaspar, F., Gast, A., Peterziel, H., Schneikert, J., … Cato, A.C.B., **1996**. CAG-repeat expansion in androgen receptor in Kennedy's disease is not a loss of function mutation. *Mol. Cell. Endocrinol.*, 117(2), pp.149–156 DOI:10.1016/0303-7207(95)03741-1.

Nihei, Y., Ito, D., Okada, Y., Akamatsu, W., … Suzuki, N., **2013**. Enhanced Aggregation of Androgen Receptor in Induced Pluripotent Stem Cell-derived Neurons from Spinal and Bulbar Muscular Atrophy. *J. Biol. Chem.*, 288(12), pp.8043–8052 DOI:10.1074/jbc.M112.408211.

Nixon, R.A., Wegiel, J., Kumar, A., Yu, W.H., … Cuervo, A.M., **2005**. Extensive involvement of autophagy in Alzheimer disease: an immuno-electron microscopy study. *J. Neuropathol. Exp. Neurol.*, 64(2), pp.113–22.

Nollen, E. a a, Kabakov, A.E., Brunsting, J.F., Kanon, B., … Kampinga, H.H., **2001**. Modulation of in Vivo HSP70 Chaperone Activity by Hip and Bag-1. *J. Biol. Chem.*, 276(7), pp.4677–4682 DOI:10.1074/jbc.M009745200.

Nollen, E. a. a., Brunsting, J.F., Song, J., Kampinga, H.H. & Morimoto, R.I., **2000**. Bag1 Functions In Vivo as a Negative Regulator of Hsp70 Chaperone Activity. *Mol. Cell. Biol.*, 20(3), pp.1083–1088 DOI:10.1128/MCB.20.3.1083-1088.2000.

Onesto, E., Rusmini, P., Crippa, V., Ferri, N., … Poletti, A., **2011**. Muscle cells and motoneurons differentially remove mutant SOD1 causing familial amyotrophic lateral sclerosis. *J. Neurochem.*, 118(2), pp.266–280 DOI:10.1111/j.1471-4159.2011.07298.x.

Orsini, M., Oliveira, A.B., Nascimento, O.J.M., Reis, C.H.M., … Smidt, B., **2015**. Amyotrophic lateral sclerosis: new perpectives and update. *Neurol. Int.*, 7(2), DOI:10.4081/ni.2015.5885.

Osawa, T., Mizuno, Y., Fujita, Y., Takatama, M., … Okamoto, K., **2011**. Optineurin in neurodegenerative diseases. *Neuropathology*, 31(6), pp.569–74 DOI:10.1111/j.1440-1789.2011.01199.x.

Palazzolo, I., Stack, C., Kong, L., Musaro, A., … Pennuto, M., **2009**. Overexpression of IGF-1 in Muscle Attenuates Disease in a Mouse Model of Spinal and Bulbar Muscular Atrophy. *Neuron*, 63(3), pp.316–328 DOI:10.1016/j.neuron.2009.07.019.

Pardo, C.A., Xu, Z., Borchelt, D.R., Price, D.L., … Cleveland, D.W., **1994**. Superoxide dismutase is an abundant component in cell bodies, dendrites, and axons of motor neurons and in a subset of other neurons. *Proc. Natl. Acad. Sci. U. S. A.*, 92(4), pp.954–8.

Parodi, S. & Pennuto, M., **2011**. Neurotoxic effects of androgens in spinal and bulbar muscular atrophy. *Front. Neuroendocrinol.*, 32(4), pp.416–425 DOI:10.1016/j.yfrne.2011.06.003.

Pasinelli, P. & Brown, R.H., **2006**. Molecular biology of amyotrophic lateral sclerosis: insights from genetics. *Nat. Rev. Neurosci.*, 7(9), pp.710–723 DOI:10.1038/nrn1971.

Piccioni, F., Pinton, P., Simeoni, S., Pozzi, P., … Poletti, A., **2002**. Androgen receptor with elongated polyglutamine tract forms aggregates that alter axonal trafficking and mitochondrial distribution in motor neuronal processes. *FASEB J.*, 16(11), pp.1418–20 DOI:10.1096/fj.01-1035fje.

Pokrishevsky, E., Grad, L.I., Yousefi, M., Wang, J., … Cashman, N.R., **2012**. Aberrant localization of FUS and TDP43 is associated with misfolding of SOD1 in amyotrophic lateral sclerosis. *PLoS One*, 7(4), p.e35050 DOI:10.1371/journal.pone.0035050.

Poletti, A., **2004**. The polyglutamine tract of androgen receptor: From functions to dysfunctions in motor neurons. *Front. Neuroendocrinol.*, 25(1), pp.1–26 DOI:10.1016/j.yfrne.2004.03.001.

Poletti, A., Rampoldi, A., Piccioni, F., Volpi, S., … Martini, L., **2001**. 5Alpha-reductase type 2 and androgen receptor expression in gonadotropin releasing hormone GT1-1 cells. *J. Neuroendocrinol.*, 13(4), pp.353–7.

Pozzi, P., Bendotti, C., Simeoni, S., Piccioni, F., … Poletti, A., **2003**. Androgen 5-alpha-reductase type 2 is highly expressed and active in rat spinal cord motor neurones. *J. Neuroendocrinol.*, 15(9), pp.882–7.

Pratt, W.B., Morishima, Y., Gestwicki, J.E., Lieberman, A.P. & Osawa, Y., **2014**. A model in which heat shock protein 90 targets protein-folding clefts: rationale for a new approach to neuroprotective treatment of protein folding diseases. *Exp. Biol. Med. (Maywood).*, 239(11), pp.1405–13 DOI:10.1177/1535370214539444.

Puls, I., Jonnakuty, C., LaMonte, B.H., Holzbaur, E.L.F., … Fischbeck, K.H., **2003**. Mutant dynactin in motor neuron disease. *Nat. Genet.*, 33(4), pp.455–6 DOI:10.1038/ng1123.

Ravikumar, B., Acevedo-Arozena, A., Imarisio, S., Berger, Z., … Rubinsztein, D.C., **2005**. Dynein mutations impair autophagic clearance of aggregate-prone proteins. *Nat. Genet.*, 37(7), pp.771–776 DOI:10.1038/ng1591.

Reddi, A.R. & Culotta, V.C., **2013**. SOD1 integrates signals from oxygen and glucose to repress respiration. *Cell*, 152(1-2), pp.224–35 DOI:10.1016/j.cell.2012.11.046.

Renton, A.E., Majounie, E., Waite, A., Simón-Sánchez, J., … Traynor, B.J., **2011**. A hexanucleotide repeat expansion in C9ORF72 is the cause of chromosome 9p21-linked ALS-FTD. *Neuron*, 72(2), pp.257–68 DOI:10.1016/j.neuron.2011.09.010.

Rinaldi, C., Bott, L.C., Chen, K., Harmison, G.G., … Fischbeck, K.H., **2012**. Insulinlike growth factor (IGF)-1 administration ameliorates disease manifestations in a mouse model of spinal and bulbar muscular atrophy. *Mol. Med.*, 18, pp.1261–8 DOI:10.2119/molmed.2012.00271.

Rocchi, A. & Pennuto, M., **2013**. New routes to therapy for spinal and bulbar muscular atrophy. *J. Mol. Neurosci.*, 50(3), pp.514–23 DOI:10.1007/s12031-013-9978-7.

Rodriguez, J.A., Shaw, B.F., Durazo, A., Sohn, S.H., … Valentine, J.S., **2005**. Destabilization of apoprotein is insufficient to explain Cu,Zn-superoxide dismutase-linked ALS pathogenesis. *Proc. Natl. Acad. Sci. U. S. A.*, 102(30), pp.10516–21 DOI:10.1073/pnas.0502515102.

Rohde, G., Kermer, P., Reed, J.C., Bähr, M. & Weishaupt, J.H., **2008**. Neuron-specific overexpression of the co-chaperone Bcl-2-associated athanogene-1 in superoxide dismutase 1(G93A)-transgenic mice. *Neuroscience*, 157(4), pp.844–9 DOI:10.1016/j.neuroscience.2008.09.055.

Roselli, C.E., Handa, R.J. & Resko, J.A., **1989**. Quantitative distribution of nuclear androgen receptors in microdissected areas of the rat brain. *Neuroendocrinology*, 49(5), pp.449–53.

Rosen, D.R., Siddique, T., Patterson, D., Figlewicz, D.A., … Deng, H.X., **1993**. Mutations in Cu/Zn superoxide dismutase gene are associated with familial amyotrophic lateral sclerosis. *Nature*, 362(6415), pp.59–62 DOI:10.1038/362059a0.

Rusmini, P., Bolzoni, E., Crippa, V., Onesto, E., … Poletti, A., **2010**. Proteasomal and autophagic degradative activities in spinal and bulbar muscular atrophy. *Neurobiol. Dis.*, 40(2), pp.361–369 DOI:10.1016/j.nbd.2010.06.016.

Rusmini, P., Crippa, V. & Giorgetti, E., **2013**. Clearance of the mutant androgen receptor in motoneuronal models of spinal and bulbar muscular atrophy. *Neurobiol. …*.

Rusmini, P., Polanco, M.J., Cristofani, R., Cicardi, M.E., … Poletti, A., **2015**. Aberrant Autophagic Response in The Muscle of A Knock-in Mouse Model of Spinal and Bulbar Muscular Atrophy. *Sci. Rep.*, 5(October), p.15174 DOI:10.1038/srep15174.

Rusmini, P., Sau, D., Crippa, V., Palazzolo, I., … Poletti, A., **2007**. Aggregation and proteasome: the case of elongated polyglutamine aggregation in spinal and bulbar muscular atrophy. *Neurobiol. Aging*, 28(7), pp.1099–111 DOI:10.1016/j.neurobiolaging.2006.05.015.

Rusmini, P., Simonini, F., Crippa, V., Bolzoni, E., … Poletti, A., **2011**. 17-AAG increases autophagic removal of mutant androgen receptor in spinal and bulbar muscular atrophy. *Neurobiol. Dis.*, 41(1), pp.83–95 DOI:10.1016/j.nbd.2010.08.023.

Saccon, R.A., Bunton-Stasyshyn, R.K.A., Fisher, E.M.C. & Fratta, P., **2013**. Is SOD1 loss of function involved in amyotrophic lateral sclerosis? *Brain*, 136(Pt 8), pp.2342–58 DOI:10.1093/brain/awt097.

Sahlender, D.A., Roberts, R.C., Arden, S.D., Spudich, G., … Buss, F., **2005**. Optineurin links myosin VI to the Golgi complex and is involved in Golgi organization and exocytosis. *J. Cell Biol.*, 169(2), pp.285–95 DOI:10.1083/jcb.200501162.

Sarkar, S., Davies, J.E., Huang, Z., Tunnacliffe, A. & Rubinsztein, D.C., **2007**. Trehalose, a novel mTOR-independent autophagy enhancer, accelerates the clearance of mutant huntingtin and ??-synuclein. *J. Biol. Chem.*, 282(8), pp.5641–5652 DOI:10.1074/jbc.M609532200.

Sau, D., De Biasi, S., Vitellaro-Zuccarello, L., Riso, P., … Poletti, A., **2007**. Mutation of SOD1 in ALS: A gain of a loss of function. *Hum. Mol. Genet.*, 16(13), pp.1604–1618 DOI:10.1093/hmg/ddm110.

Sau, D., Rusmini, P., Crippa, V., Onesto, E., … Poletti, A., **2011**. Dysregulation of axonal transport and motorneuron diseases. *Biol. Cell*, 103(2), pp.87–107 DOI:10.1042/BC20100093.

Saudou, F., Finkbeiner, S., Devys, D. & Greenberg, M.E., **1998**. Huntingtin Acts in the Nucleus to Induce Apoptosis but Death Does Not Correlate with the Formation of Intranuclear Inclusions. *Cell*, 95(1), pp.55–66 DOI:10.1016/S0092-8674(00)81782-1.

Schiavo, G., Greensmith, L., Hafezparast, M. & Fisher, E.M.C., **2013**. Cytoplasmic dynein heavy chain: the servant of many masters. *Trends Neurosci.*, 36(11), pp.641–51 DOI:10.1016/j.tins.2013.08.001.

Scoto, M., Rossor, A.M., Harms, M.B., Cirak, S., … Muntoni, F., **2015**. Novel mutations expand the clinical spectrum of DYNC1H1-associated spinal muscular atrophy. *Neurology*, 84(7), pp.668–79 DOI:10.1212/WNL.0000000000001269.

Seelaar, H., Klijnsma, K.Y., de Koning, I., van der Lugt, A., … van Swieten, J.C., **2010**. Frequency of ubiquitin and FUS-positive, TDP-43-negative frontotemporal lobar degeneration. *J. Neurol.*, 257(5), pp.747–53 DOI:10.1007/s00415-009-5404-z.

Sha, Y., Pandit, L., Zeng, S. & Eissa, N.T., **2009**. A critical role for CHIP in the aggresome pathway. *Mol. Cell. Biol.*, 29(1), pp.116–28 DOI:10.1128/MCB.00829-08.

Shaw, B.F. & Valentine, J.S., **2007**. How do ALS-associated mutations in superoxide dismutase 1 promote aggregation of the protein? *Trends Biochem. Sci.*, 32(2), pp.78–85 DOI:10.1016/j.tibs.2006.12.005.

Simeoni, S., **2000**. Motoneuronal cell death is not correlated with aggregate formation of androgen receptors containing an elongated polyglutamine tract. *Hum. Mol. Genet.*, 9(1), pp.133–144 DOI:10.1093/hmg/9.1.133.

Sorarù, G., D'Ascenzo, C., Polo, A., Palmieri, A., … Angelini, C., **2008**. Spinal and bulbar muscular atrophy: skeletal muscle pathology in male patients and heterozygous females. *J. Neurol. Sci.*, 264(1-2), pp.100–5 DOI:10.1016/j.jns.2007.08.012.

La Spada, A.R. & Taylor, J.P., **2010**. Repeat expansion disease: progress and puzzles in disease pathogenesis. *Nat. Rev. Genet.*, 11(4), pp.247–58 DOI:10.1038/nrg2748.

La Spada, A.R., Wilson, E.M., Lubahn, D.B., Harding, A.E., … La Spada E. M.; Lubahn, D. B.; Harding, A. E.; Fischbeck, K. H., A.R.. W., **1991**. Androgen receptor gene mutations in X-linked spinal and bulbar muscular atrophy. *Nature*, 352(6330), pp.77–79 DOI:10.1038/352077a0.

Strickland, A. V, Schabhüttl, M., Offenbacher, H., Synofzik, M., … Auer-Grumbach, M., **2015**. Mutation screen reveals novel variants and expands the phenotypes associated with DYNC1H1. *J. Neurol.*, 262(9), pp.2124–34 DOI:10.1007/s00415-015-7727-2.

Sugiyama, Y., Suzuki, A., Kishikawa, M., Akutsu, R., … Ohno, S., **2000**. Muscle develops a specific form of small heat shock protein complex composed of MKBP/HSPB2 and HSPB3 during myogenic differentiation. *J. Biol. Chem.*, 275(2), pp.1095–104.

Suzuki, K., Katsuno, M., Banno, H., Takeuchi, Y., … Sobue, G., **2008**. CAG repeat size correlates to electrophysiological motor and sensory phenotypes in SBMA. *Brain*, 131(Pt 1), pp.229–39 DOI:10.1093/brain/awm289.

Swarup, V. & Julien, J.P., **2011**. ALS pathogenesis: Recent insights from genetics and mouse models. *Prog. Neuro-Psychopharmacology Biol. Psychiatry*, 35(2), pp.363–369 DOI:10.1016/j.pnpbp.2010.08.006.

Tanaka, M., Machida, Y., Niu, S., Ikeda, T., … Nukina, N., **2004**. Trehalose alleviates polyglutamine-mediated pathology in a mouse model of Huntington disease. *Nat. Med.*, 10(2), pp.148–154 DOI:10.1038/nm985.

Taylor, J.P., Tanaka, F., Robitschek, J., Sandoval, C.M., … Fischbeck, K.H., **2003**. Aggresomes protect cells by enhancing the degradation of toxic polyglutamine-containing protein. *Hum. Mol. Genet.*, 12(7), pp.749–57.

Teuchert, M., Fischer, D., Schwalenstoecker, B., Habisch, H.J., … Ludolph, a. C., **2006**. A dynein mutation attenuates motor neuron degeneration in SOD1 G93A mice. *Exp. Neurol.*, 198(1), pp.271–274 DOI:10.1016/j.expneurol.2005.12.005.

Teuling, E., van Dis, V., Wulf, P.S., Haasdijk, E.D., … Jaarsma, D., **2008**. A novel mouse model with impaired dynein/dynactin function develops amyotrophic lateral sclerosis (ALS)-like features in motor neurons and improves lifespan in SOD1-ALS mice. *Hum. Mol. Genet.*, 17(18), pp.2849–2862 DOI:10.1093/hmg/ddn182.

Tortarolo, M., Crossthwaite, A.J., Conforti, L., Spencer, J.P., … Rattray, M., **2004**. Expression of SOD1 G93A or wild-type SOD1 in primary cultures of astrocytes down-regulates the glutamate transporter GLT-1: lack of involvement of oxidative stress. *J Neurochem*, 88(2), pp.481–493 DOI:10.1046/j.1471-4159.2003.02208.x.

Tortelli, R., Conforti, F.L., Cortese, R., D'Errico, E., … Simone, I.L., **2013**. Amyotrophic lateral sclerosis: A new missense mutation in the SOD1 gene. *Neurobiol. Aging*, 34(6), pp.1709.e3–1709.e5 DOI:10.1016/j.neurobiolaging.2012.10.027.

Trapman, J., Klaassen, P., Kuiper, G.G., van der Korput, J.A., … Brinkmann, A.O., **1988**. Cloning, structure and expression of a cDNA encoding the human androgen receptor. *Biochem. Biophys. Res. Commun.*, 153(1), pp.241–8.

Walcott, J.L. & Merry, D.E., **2002**. Ligand promotes intranuclear inclusions in a novel cell model of spinal and bulbar muscular atrophy. *J. Biol. Chem.*, 277(52), pp.50855–9 DOI:10.1074/jbc.M209466200.

Wang, Q., Johnson, J.L., Agar, N.Y.R. & Agar, J.N., **2008**. Protein aggregation and protein instability govern familial amyotrophic lateral sclerosis patient survival. *PLoS Biol.*, 6(7), p.e170 DOI:10.1371/journal.pbio.0060170.

Watts, G.D.J., Wymer, J., Kovach, M.J., Mehta, S.G., … Kimonis, V.E., **2004**. Inclusion body myopathy associated with Paget disease of bone and frontotemporal dementia is caused by mutant valosin-containing protein. *Nat. Genet.*, 36(4), pp.377–81 DOI:10.1038/ng1332.

Webb, J.L., Ravikumar, B. & Rubinsztein, D.C., **2004**. Microtubule disruption inhibits autophagosome-lysosome fusion: implications for studying the roles of aggresomes in polyglutamine diseases. *Int. J. Biochem. Cell Biol.*, 36(12), pp.2541–50 DOI:10.1016/j.biocel.2004.02.003.

Wegorzewska, I., Bell, S., Cairns, N.J., Miller, T.M. & Baloh, R.H., **2009**. TDP-43 mutant transgenic mice develop features of ALS and frontotemporal lobar degeneration. *Proc. Natl. Acad. Sci. U. S. A.*, 106(44), pp.18809–14 DOI:10.1073/pnas.0908767106.

Williamson, T.L. & Cleveland, D.W., **1999**. Slowing of axonal transport is a very early event in the toxicity of ALS-linked SOD1 mutants to motor neurons. *Nat. Neurosci.*, 2(1), pp.50–6 DOI:10.1038/4553.

Wils, H., Kleinberger, G., Janssens, J., Pereson, S., … Kumar-Singh, S., **2010**. TDP-43 transgenic mice develop spastic paralysis and neuronal inclusions characteristic of ALS and frontotemporal lobar degeneration. *Proc. Natl. Acad. Sci. U. S. A.*, 107(8), pp.3858–63 DOI:10.1073/pnas.0912417107.

Wyttenbach, A., **2004**. Role of heat shock proteins during polyglutamine neurodegeneration: mechanisms and hypothesis. *J. Mol. Neurosci.*, 23(1-2), pp.69–96 DOI:10.1385/JMN:23:1-2:069.

Xu, Z., Graham, K., Foote, M., Liang, F., … Zhou, Y., **2013**. 14-3-3 Protein Targets Misfolded Chaperone-Associated Proteins To Aggresomes. *J. Cell Sci.*, 126(Pt 18), pp.4173–86 DOI:10.1242/jcs.126102.

Yamakawa, M., Ito, D., Honda, T., Kubo, K. -i., … Suzuki, N., **2015**. Characterization of the dipeptide repeat protein in the molecular pathogenesis of c9FTD/ALS. *Hum. Mol. Genet.*, 24(6), pp.1630–1645 DOI:10.1093/hmg/ddu576.

Yu, Z., Dadgar, N., Albertelli, M., Gruis, K., … Lieberman, A.P., **2006a**. Androgen-dependent pathology demonstrates myopathic contribution to the Kennedy disease phenotype in a mouse knock-in model. *J. Clin. Invest.*, 116(10), pp.2663–72 DOI:10.1172/JCI28773.

Yu, Z., Dadgar, N., Albertelli, M., Scheller, A., … Lieberman, A.P., **2006b**. Abnormalities of germ cell maturation and sertoli cell cytoskeleton in androgen receptor 113 CAG knock-in mice reveal toxic effects of the mutant protein. *Am. J. Pathol.*, 168(1), pp.195–204 DOI:10.2353/ajpath.2006.050619.

Zhang, X., Chen, S., Song, L., Tang, Y., … Le, W., **2014**. MTOR-independent, autophagic enhancer trehalose prolongs motor neuron survival and ameliorates the autophagic flux defect in a mouse model of amyotrophic lateral sclerosis. *Autophagy*, 10(4), pp.588–602 DOI:10.4161/auto.27710.